

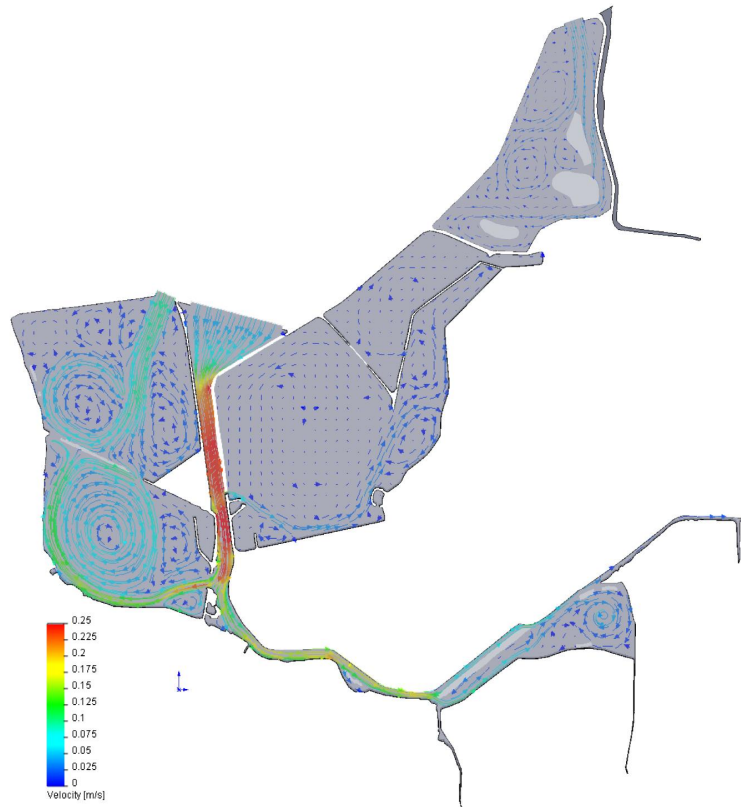
# **APPENDIX G**

## *Tidal Hydraulics Analysis*



# Tidal Hydraulics Analysis of the Otay River Estuary Restoration Plan

by  
Scott A. Jenkins, Ph. D. & Joseph Wasyl



Submitted by:  
Dr. Scott A Jenkins Consulting  
14765 Kalapana St.  
Poway, CA 92064

Submitted to:  
Poseidon Water LLC  
5780 Fleet Street, Suite 140  
Carlsbad, CA 92008

Draft: 23 September 2014

## Table of Contents

<b>ABSTRACT.....</b>	<b>3</b>
<b>1.0) Introduction.....</b>	<b>7</b>
<b>2.0) Technical Approach.....</b>	<b>16</b>
2.1 Tidal Hydraulics Model Physics.....	18
<b>3.0) Model Initialization.....</b>	<b>25</b>
3.1 San Diego Bay Circulation.....	26
3.2 San Diego Bay Tidal Regime .....	26
3.3 San Diego Bay Water Quality .....	31
3.4 Sea Level Rise Effects on San Diego Bay Water Levels .....	35
3.5 Model Calibration.....	42
<b>4.0) Tidal Hydraulics of the Existing Otay River Floodplain .....</b>	<b>44</b>
4.1 Tidal Current Simulations .....	44
4.2 Hydroperiod Simulations.....	49
<b>5.0) Analysis of the Intertidal Alternative.....</b>	<b>51</b>
5.1 Bathymetric Input for the Intertidal Alternative .....	51
5.2 Tidal Inundation Simulations of the Intertidal Alternative .....	54
5.3 Residence Time of the Intertidal Alternative .....	66
<b>6.0) Analysis of the Subtidal Alternative .....</b>	<b>68</b>
6.1 Bathymetric Input for the Subtidal Alternative .....	68
6.2 Tidal Inundation Simulations of the Subtidal Alternative .....	71
6.3 Residence Time of the Subtidal Alternative .....	83
<b>7.0) Summary and Conclusion.....</b>	<b>85</b>
<b>REFERENCES.....</b>	<b>90</b>

**ABSTRACT:** This study employs a well-tested and peer-reviewed hydrodynamic model to evaluate the tidal hydraulics the Intertidal Alternative and the Subtidal Alternative for the Otay River Estuary Restoration Project (ORERP). Both alternatives involve restoration of a portion of the Otay River Floodplain Site and Pond 15 Site to native habitat by lowering the existing ground elevations in the Otay River Floodplain Site and using the excavated soils from the Otay River Floodplain Site as fill material in the Pond 15 Site.

The model, analysis methods, and supporting data bases used herein are the same as those utilized in the Environmental Impact Report/Environmental Impact Statement (EIR/EIS) for the San Dieguito Wetland Restoration Project, (EIR/EIS, 2000), and for the preparation of the San Dieguito Wetlands Restoration Project, Final Restoration Plan, (SCE, 2005). The analysis is based on updated bathymetry provided by Wetlands Research Associates (WRA) and latest updates to San Diego Bay tides for the 1983-2001 tidal epoch supported by Otay Sonde tidal elevation measurements at the mouth of the Otay River. The computer models used in this study are 2-dimensional finite element types, built from some well-studied and proven computational methods and numerical architecture that have been successful in predicting shallow water tidal propagation. Monitoring data for the newly completed San Dieguito Lagoon Restoration Project was used to calibrate tidal hydraulics model. San Dieguito Lagoon was selected as a calibration proxy for the restoration alternatives because of morphologic similarities: in particular, both the San Dieguito and restoration sites have a long “goose-neck” feeder channel connecting source water to interior tidal basins of comparable acreage and distance from the source water. Habitat surveys conducted during the San Dieguito Lagoon Restoration Project by Josselyn & Whelchel (1999), and then later updated by vegetation surveys in the lower Otay River flood plain by Josselyn (2012), were used to develop functional relationships between habitat breaks and amounts of time for wetting and drying (hydroperiod functions). The hydroperiod functions were calculated by the model for both present and future extremes of sea level in the year 2050 from estimates of both maximum and minimum sea level rise. These relationships were used to transpose tidal hydraulics model output into calculations of acreage of various wetland habitat types created by the two restoration alternatives.

The elevation breaks (zonation) between the different wetland habitat types from the modeled hydroperiod curves are summarized below in Tables ES-1 and ES-2 for the Intertidal Alternative; and in Tables ES-3 and ES-4 for the Subtidal Alternative. The elevations for the habitat breaks in these tables are applied to the KTUA grading designs and yield the acreages of habitat creation listed in Table ES-5 for the Intertidal Alternative at present sea level, and at 2050 sea levels in Table ES-6. The companion set of habitat creation acres for the Subtidal Alternative are listed in Table ES-7 at present sea level, and in Table ES-8 at 2050 sea levels. Comparing Tables ES-5 and ES-7, it is apparent that the Intertidal Alternative creates an additional 1.37 acres of habitat in 2018 than does the Subtidal Alternative. For all possible sea level scenarios, the elevation limit of subtidal habitat in the floodplain basin of both restoration alternatives is limited by existing bars, hummocks and other channel bottom features at the inlet and inside the branch channel into this basin. These channel bottom features create an inlet sill at 0.0 ft NAVD 88. However, if sea level were to rise by 2 ft. according to the maximum sea level rise prediction in 2050, the available tidal range is not sufficient to prevent a rise in subtidal elevations in Pond # 15 of either restoration alternative. This amount of sea level rise will raise the elevations of the

zonation of all habitat types. This upward displacement of wetland zonation is largest for the linear superposition scenario of sea level rise, because the spectral correction scenario predicts a larger tidal range of about 1.0 ft. Under the 24 in. spectral sea level rise scenario at 2050, intertidal wetland habitat would begin at an elevation of between -0.25 ft. and -0.20 ft NAVD, and the mud flat habitat would reside about 0.4 ft. to 0.5 ft. lower than under the linear superposition scenario; while the low marsh habitat would reside about 0.25 ft. lower than under the linear superposition scenario. Therefore there are some apparent differences between the habitat mix predictions of these two sea-level rise prediction methods; although both give the same estimate of the maximum elevation of high salt marsh wetland zonation in both of the proposed basins of the restoration alternatives.

From model simulations of tidal currents throughout complete spring-neap tidal cycles, it is concluded that both source water inlets to the tidal basins of the Intertidal and Subtidal Alternatives are stable and immune to closure or restriction by sedimentation under dry weather tidal exchange. (Wet-weather conditions are addressed in a companion study, Everest, 2014). Inlet sedimentation due to influxes of wave driven long-shore transport of sand (as occurs on the open coast), does not occur in the fetch limited environment of South San Diego Bay. The mouth of the Otay River that supplies source water to the floodplain tidal basin is in a dynamic steady-state equilibrium that is neither depositional nor erosional; while the inlet to Pond 15 will remain in a non-equilibrium stationary state (as-built) in the absence of a local sediment sources or adequate fluid forcing by waves and currents that might otherwise import sediment from more distant sources.

**Table ES-1:** Elevations of Upper Limits of Habitat Breaks Intertidal Plan Floodplain Basin

Elevation of Habitat Breaks (Units of ft. NAVD 88)	@ Present Sea Level	@ 4.68 in. linear Sea Level Rise	@ 24 in. linear Sea Level Rise	@ 24 in. spectral Sea Level Rise
Sub-tidal	0.00 ft.	0.00 ft.	0.25 ft.	0.00 ft.
Frequently Flooded Mud Flat	2.40 ft.	3.40 ft.	4.50 ft.	4.10 ft.
Frequently Exposed Mud Flat	2.70 ft.	3.70 ft.	4.85 ft.	4.45 ft.
Low Marsh	4.30 ft.	4.90 ft.	6.55 ft.	6.25 ft.
Mid Marsh	6.30 ft.	6.80 ft.	8.55 ft.	8.50 ft.
High Marsh	7.55 ft.	8.05 ft.	9.71 ft.	9.71 ft.

**Table ES-2:** Elevations of Upper Limits of Habitat Breaks in the Intertidal Plan Pond 15 Basin

Elevation of Habitat Breaks (Units of ft. NAVD 88)	@ Present Sea Level	@ 4.68 in. linear Sea Level Rise	@ 24 in. linear Sea Level Rise	@ 24 in. spectral Sea Level Rise
Sub-tidal	-1.65 ft.	-1.70 ft.	0.25 ft.	-0.25 ft.
Frequently Flooded Mud Flat	2.40 ft.	2.50 ft.	4.50 ft.	4.10 ft.
Frequently Exposed Mud Flat	2.70 ft.	2.85 ft.	4.85 ft.	4.45 ft.
Low Marsh	4.30 ft.	4.50 ft.	6.50 ft.	6.25 ft.
Mid Marsh	6.30 ft.	6.55 ft.	8.55 ft.	8.50 ft.
High Marsh	7.50 ft.	7.90ft.	9.72 ft.	9.72 ft.

**Table ES-3:** Elevations of Upper Limits of Habitat Breaks in the Subtidal Plan Floodplain Basin

Elevation of Habitat Breaks (Units of ft. NAVD 88)	@ Present Sea Level	@ 4.68 in. linear Sea Level Rise	@ 24 in. linear Sea Level Rise	@ 24 in. spectral Sea Level Rise
Sub-tidal	0.00 ft.	0.00 ft.	0.25 ft.	0.00 ft.
Frequently Flooded Mud Flat	2.38 ft.	3.40 ft.	4.50 ft.	4.15 ft.
Frequently Exposed Mud Flat	2.70 ft.	3.70 ft.	4.85 ft.	4.50 ft.
Low Marsh	4.30 ft.	4.90 ft.	6.52 ft.	6.25 ft.
Mid Marsh	6.27 ft.	6.80 ft.	8.55 ft.	8.50 ft.
High Marsh	7.55 ft.	8.10 ft.	9.71 ft.	9.71 ft.

**Table ES-4:** Elevations of Upper Limits of Habitat Breaks in the Subtidal Plan Pond 15 Basin

Elevation of Habitat Breaks (Units of ft. NAVD 88)	@ Present Sea Level	@ 4.68 in. linear Sea Level Rise	@ 24 in. linear Sea Level Rise	@ 24 in. spectral Sea Level Rise
Sub-tidal	-1.65 ft.	-1.70 ft.	0.25 ft.	-0.20 ft.
Frequently Flooded Mud Flat	2.35 ft.	2.50 ft.	4.50 ft.	4.15 ft.
Frequently Exposed Mud Flat	2.70 ft.	2.85 ft.	4.85 ft.	4.50 ft.
Low Marsh	4.30 ft.	4.50 ft.	6.50 ft.	6.25 ft.
Mid Marsh	6.30 ft.	6.55 ft.	8.55 ft.	8.50 ft.
High Marsh	7.50 ft.	7.90ft.	9.72 ft.	9.72 ft.

**Table ES-5:** Intertidal Alternative Predicted Habitat Distribution, acres 2018

Vegetation Community to be Created	Otay River Floodplain Site Acres	Pond 15 Site
SubTidal	0.00	9.53
Mudflat – Frequently Flooded	4.45	16.36
Mudflat – Frequently Exposed	0.70	1.57
Low Marsh	10.34	15.73
Mid Marsh	10.99	34.47
High Marsh	3.23	5.61
Total Marsh	29.26	80.68
Transitional	0.45	2.59
<b>Total Created Habitat</b>	<b>29.71</b>	<b>83.27</b>

**Table ES-6:** Intertidal Alternative Predicted Habitat Distribution, acres 2050

<b>Vegetation Community to be Created</b>	<b>Otay River Floodplain Site Acres</b>	<b>Pond 15 Site</b>
SubTidal	0	9.35
Mudflat – Frequently Flooded	8.84	17.06
Mudflat – Frequently Exposed	2.21	1.85
Low Marsh	7.91	17.32
Mid Marsh	10.36	35.38
High Marsh	0.52	2.87
<b>Total Created Habitat</b>	<b>29.84</b>	<b>83.83</b>

**Table ES-7:** Subtidal Alternative Predicted Habitat Distribution, acres, 2018

<b>Vegetation Community to be Created</b>	<b>Otay River Floodplain Site Acres</b>	<b>Pond 15 Site</b>
Subtidal	4.48	9.17
Mudflat – Frequently Flooded	5.26	14.70
Mudflat – Frequently Exposed	1.79	1.32
Low Marsh	8.64	11.77
Mid Marsh	7.90	33.25
High Marsh	1.64	11.78
Total Salt Marsh	29.71	82.00
Transitional	0.45	2.15
<b>Total Created Habitat</b>	<b>29.26</b>	<b>79.85</b>

**Table ES-8:** Subtidal Alternative Predicted Habitat Distribution, acres, 2050

<b>Vegetation Community to be Created</b>	<b>Otay River Floodplain Site Acres</b>	<b>Pond 15 Site</b>
Subtidal	4.48	9.0
Mudflat – Frequently Flooded	110.01	15.28
Mudflat – Frequently Exposed	1.70	1.58
Low Marsh	5.43	12.68
Mid Marsh	6.71	41.20
High Marsh	0.52	3.06
<b>Total Created Habitat</b>	<b>29.85</b>	<b>82.80</b>

## Tidal Hydraulics Analysis of the Otay River Estuary Restoration Plan

by: Scott A. Jenkins, Ph. D. and Joseph Wasyl

### 1) Introduction:

The Otay River Estuary Restoration Project (ORERP) is a partnership between Poseidon Water (Channelside) L.P. (Poseidon), the U.S. Fish and Wildlife Service (Service or USFWS), and San Diego Bay National Wildlife Refuge (Refuge). The ORERP project involves the creation, restoration, and enhancement of coastal wetlands to benefit native fish, wildlife, and plant species and to provide habitat for migratory seabirds and shorebirds and salt marsh-dependent species within the South San Diego Bay Unit of the Refuge (Figure 1).

There are two restoration alternatives considered in this study: *The Intertidal Plan*, and *The Sub-tidal Plan*. Both alternatives involve restoration of the two noncontiguous sites outlined in red in Figure 2, including the Otay River Floodplain Site (identified in Figure 3) and the Pond 15 Site, as labeled in Figure 1. The approximately 78-acre Otay River Floodplain Site is located west of Interstate 5 (I-5) between Main Street to the north and Palm Avenue to the south (cf Figures 2 & 3). The approximately 90-acre Pond 15 Site is located approximately 0.75 miles north of the Otay River Floodplain Site and directly south of the Chula Vista Marina (cf Figure 1).

Both alternatives involve restoration of a portion of the Otay River Floodplain Site and Pond 15 Site to native habitat by lowering the existing ground elevations in the Otay River Floodplain Site and using the excavated soils from the Otay River Floodplain Site as fill material in the Pond 15 Site. Both alternatives would impact identical footprints on the two noncontiguous sites shown in Figure 2, with the variance relating to the habitat implemented within this site boundary. Both alternatives would permanently impact approximately 34 acres on the 78-acre Otay River Floodplain Site. The remaining 60 acres of the Otay River Floodplain Site east of Nestor Creek include soil contamination from prior agricultural use as well as cultural resources which would be avoided under both alternatives. Under both restoration alternatives, 88 acres of the approximately 90-acre Pond 15 Site would be permanently impacted by proposed habitat restoration. Under both restoration alternatives the Otay River Floodplain Site would be excavated to a range of elevations and then vegetated to create tidally influenced wetlands communities. The excavated materials from the Otay River Floodplain Site would be transferred to the Pond 15 Site to raise to the appropriate elevations to support a range of wetlands that would also be tidally influenced once an approximately 200 foot wide portion of the levee separating the Pond 15 Site from San Diego Bay is removed. Neither restoration alternative would require dredging the Otay River from the Otay River Floodplain Site to the San Diego Bay.

The Intertidal Alternative would involve lowering the elevation and contouring the Otay River Floodplain Site to create approximately 30 acres of tidally-influenced habitat, as shown in Figure 4. The grading design shown in Figure 4 is designed to achieve approximately 17% intertidal mudflat and, through increasing elevations on the site, 83% intertidal salt marsh habitat. The Intertidal Alternative would also involve raising the elevation and contouring the Pond 15



**Figure 1:** The Otay River Estuary Restoration Project Site in south San Diego Bay, CA.

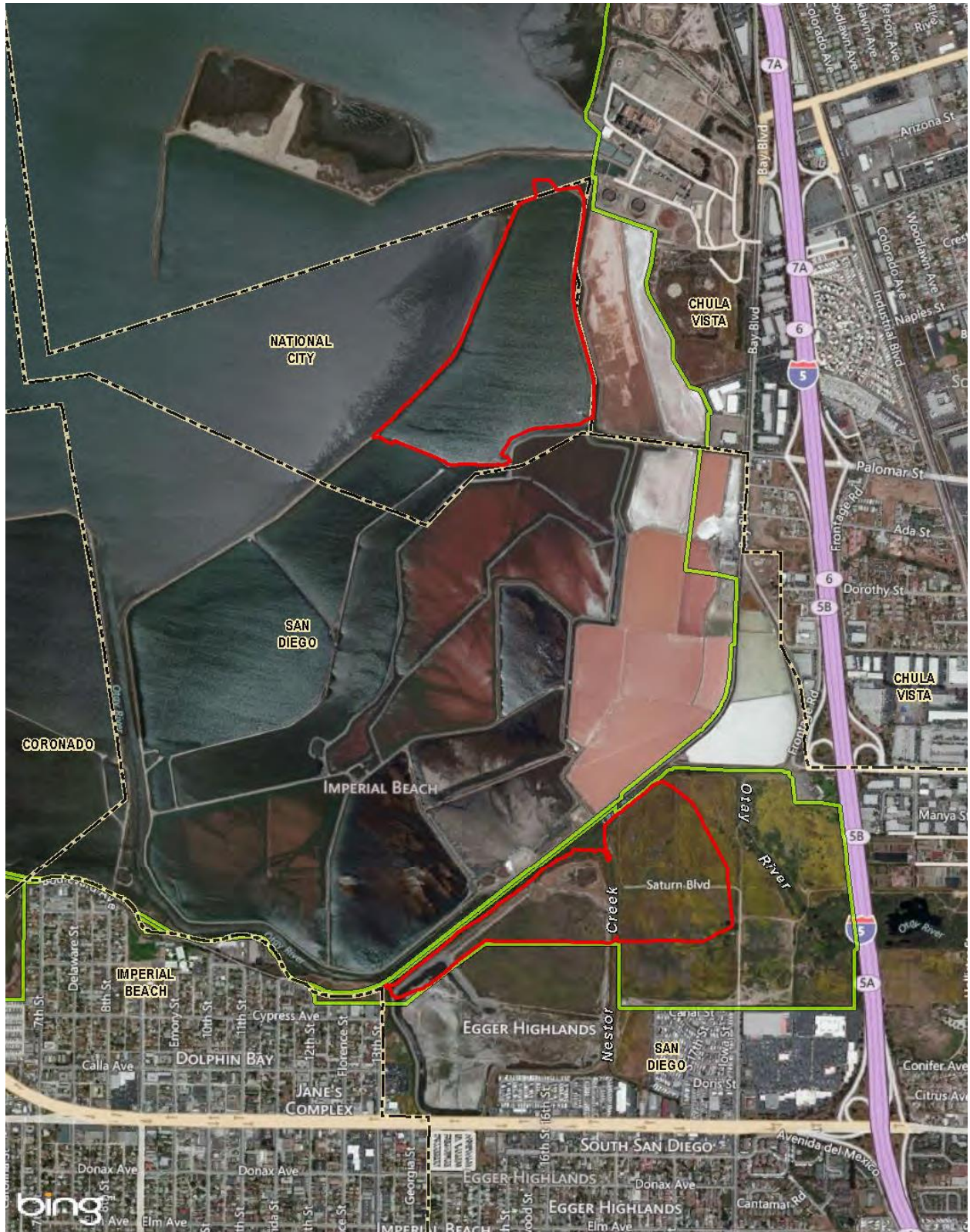


**Figure 2:** Noncontiguous restoration sites outlined in red.

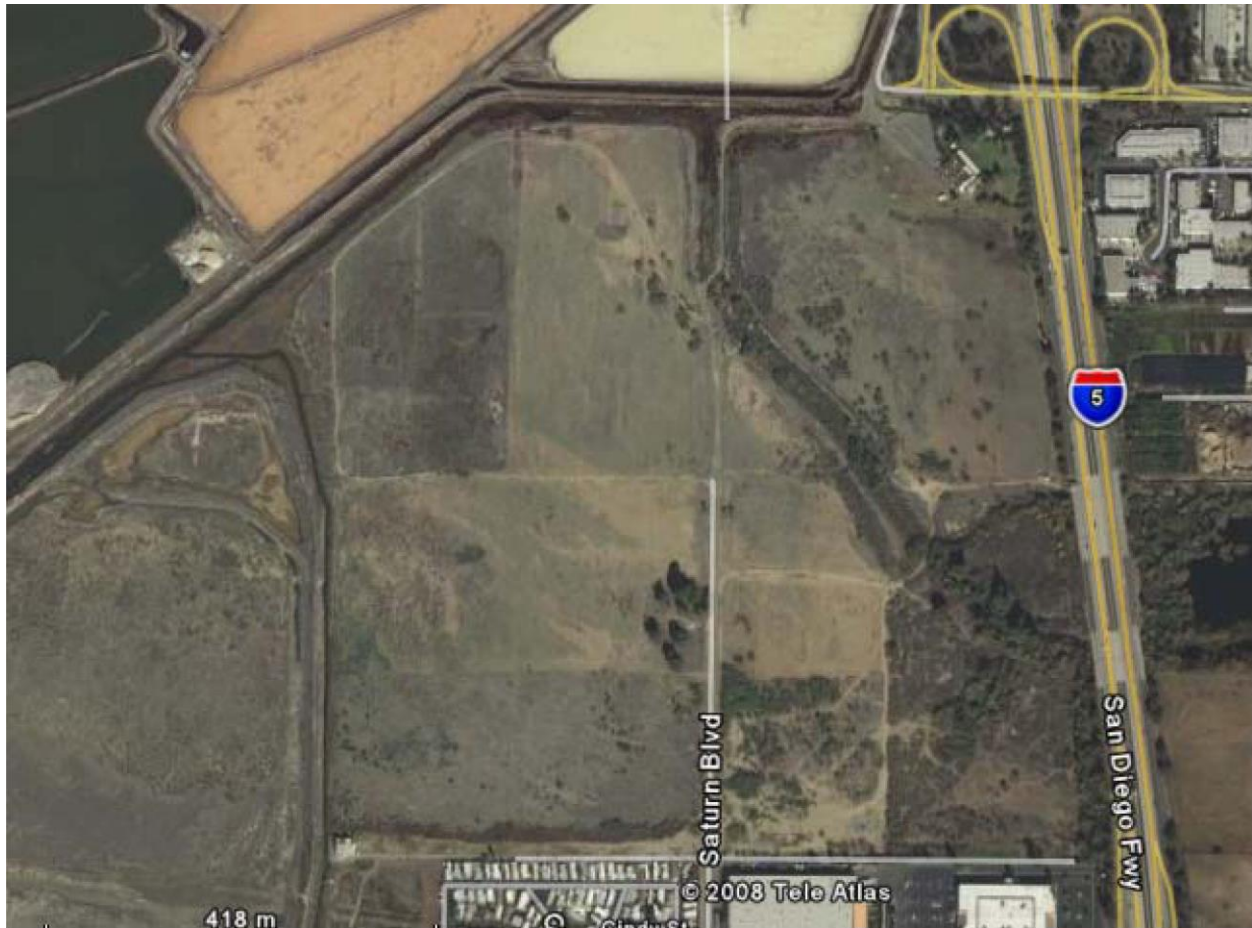


**Figure 2:** Otay River floodplain, site of the wetland restoration alternatives.

Site as shown in Figure 5, with grading contours intended to create approximately 11% subtidal channel, 22% intertidal mudflat and 67% intertidal salt marsh habitat. Both sites would be planted with a mix of native wetland vegetation that would mature into low marsh, mid marsh, and high marsh vegetative communities. The intertidal areas and the unvegetated mudflat would provide foraging habitat for adult and juvenile fish which form the basis of the food chain that would benefit larger fish, birds and other species on and off the site. Construction of the Intertidal Alternative would require excavation of approximately 320,000 cubic yards of soils at the Otay River Floodplain Site to lower the elevation to the necessary contours to establish a subtidal wetland on the site. The majority of the soil would be beneficially used as fill and cover within Pond 15 to raise the ground to elevations suitable to support coastal salt marsh habitat and nesting areas. The excavated material would also be disposed of on-site as fill for dikes, levees, and upland habitat creation.

The Subtidal Alternative would involve lowering the Otay River Floodplain Site and Pond 15 Site to an elevation lower than that proposed under the Intertidal Alternative to create a subtidal channel within the Otay River Floodplain Site. Under the Subtidal Alternative, the subtidal zone would be surrounded by mudflat and increasing elevations of salt marsh. The Subtidal Alternative would involve lowering the elevation and contouring the Otay River Floodplain Site. Here, the proposed grading plan for the Subtidal Alternative (Figure 6) is intended to create approximately 15% subtidal channel, 24% intertidal mudflat and 61% intertidal salt marsh mudflat. The grading plan of the Subtidal Alternative at the Pond 15 Site would involve raising the elevation and contouring the Pond 15 Site to create approximately 11% subtidal channel, 20% intertidal mudflat and 69% intertidal salt marsh mudflat as shown in Figure 7. Again, both excavated and fill sites would be planted with a mix of immature plants that would mature into low marsh, mid marsh, and high marsh vegetative communities. The subtidal areas would provide spawning and foraging habitat, and the unvegetated mudflat would provide foraging habitat for adult and juvenile fish during high tides. Combined, the habitat would provide habitat for the basis of the food chain that would benefit larger fish, birds and other species on and off the site. Construction of the Subtidal Alternative would require excavation of approximately 370,000 cubic yards of soils at the Otay River Floodplain Site to lower the elevation the necessary contours to establish a subtidal wetland on the site. In addition, between 50,000 and 60,000 cubic yards of soil would be excavated from Pond 15. The majority of the soil would be beneficially used as fill and cover within Pond 15 to raise the ground to elevations suitable to support coastal salt marsh habitat and nesting areas. The excavated material would also be disposed of on-site as fill for dikes, levees, and upland habitat creation.

The Intertidal Preferred Alternative would require fewer truck trips or a shorter construction window for either the conveyor belt or pipeline haul methods, due to the decreased amount of soil that would need to be hauled to Pond 15 as compared to the Subtidal Alternative. This in turn results in less air quality and greenhouse gas emissions, less construction traffic, and generally less environmental impacts related to construction.

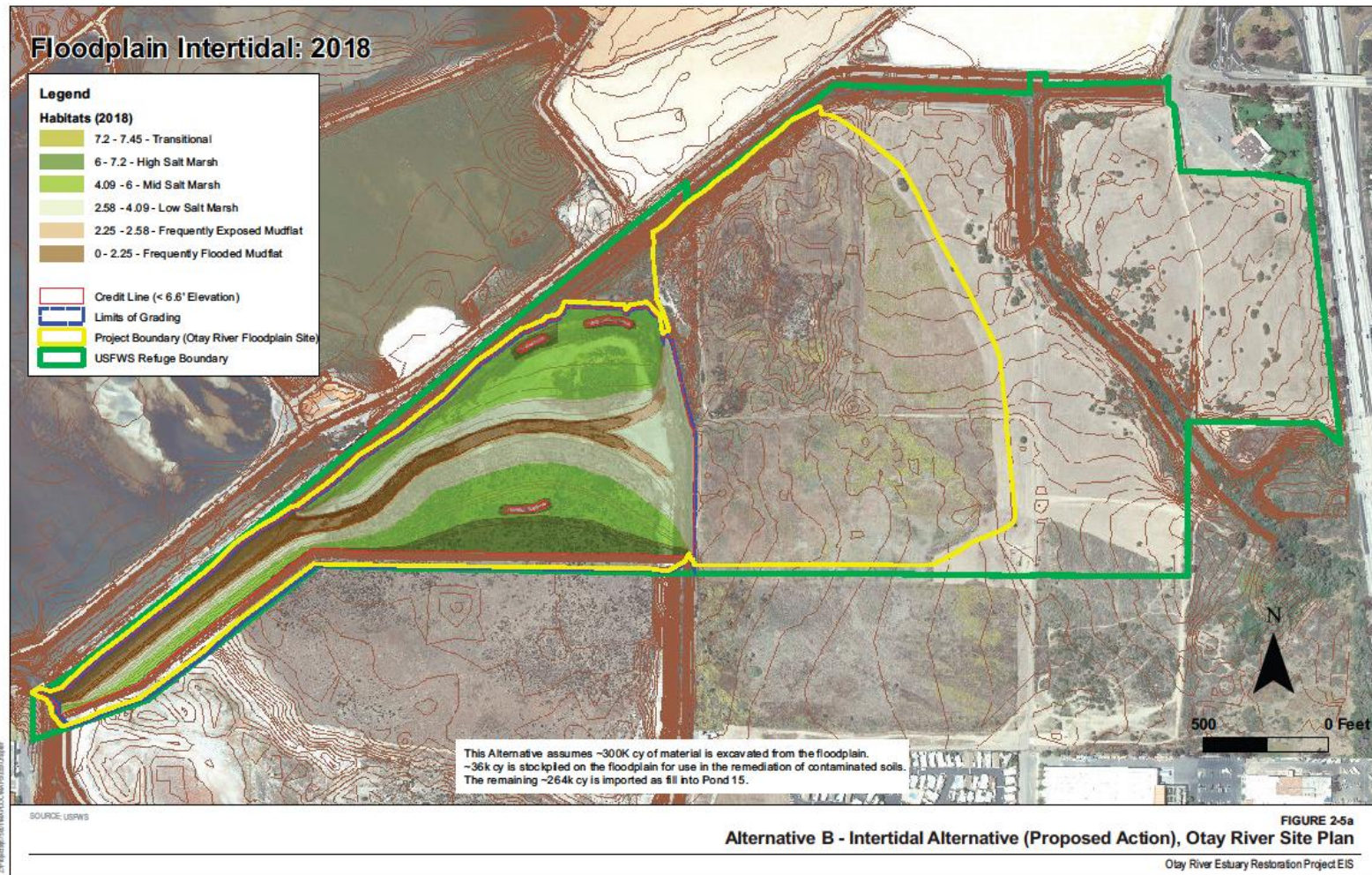


**Figure 4:** Grading plan for the Otay River Floodplain Tidal Basin under the Intertidal Alternative.

**Figure 5: Pond 15 grading plan under the Intertidal Alternative.**

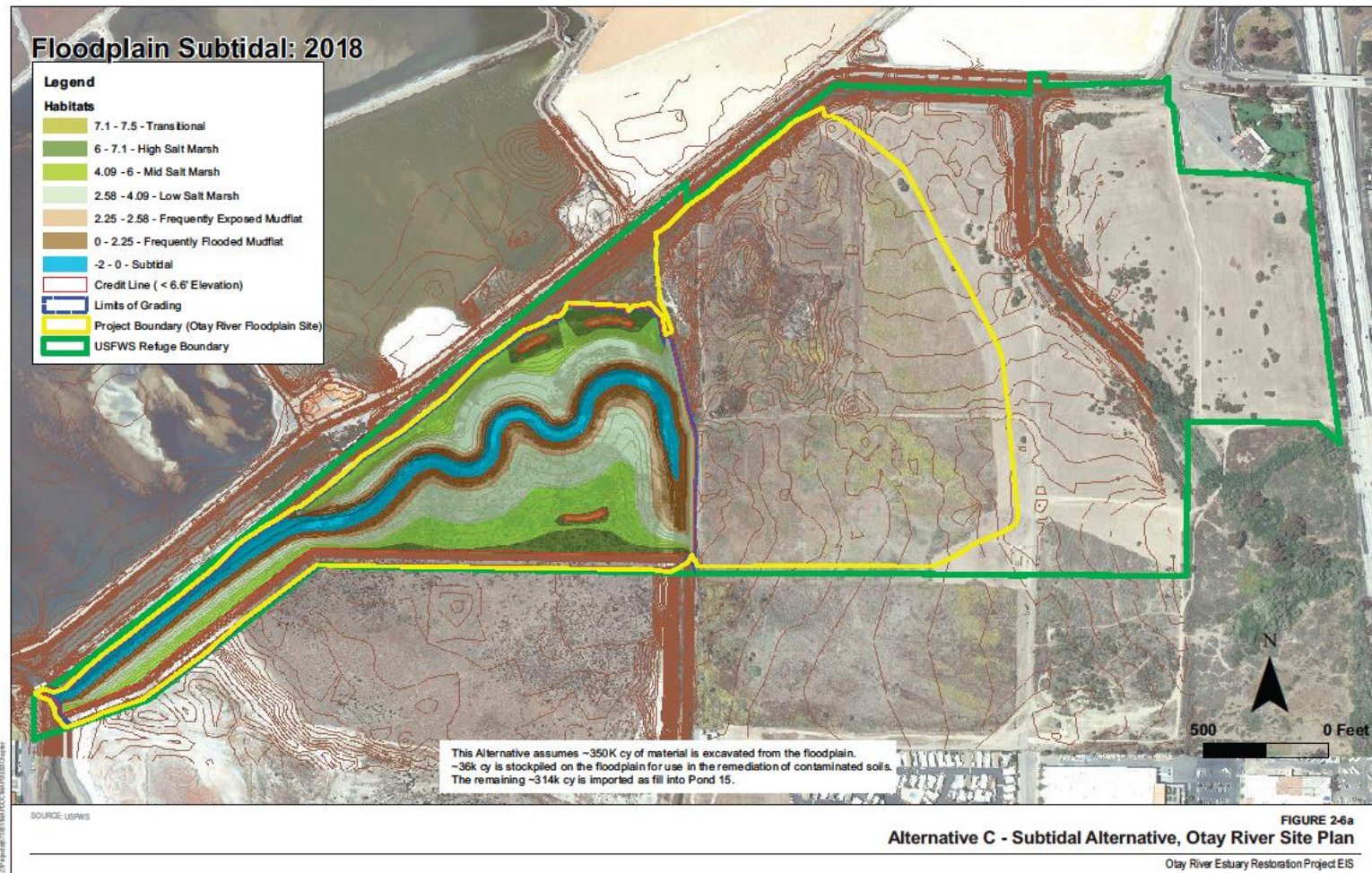


**Figure 6:** Grading plan for the Otay River Floodplain Tidal Basin under the Subtidal Alternative

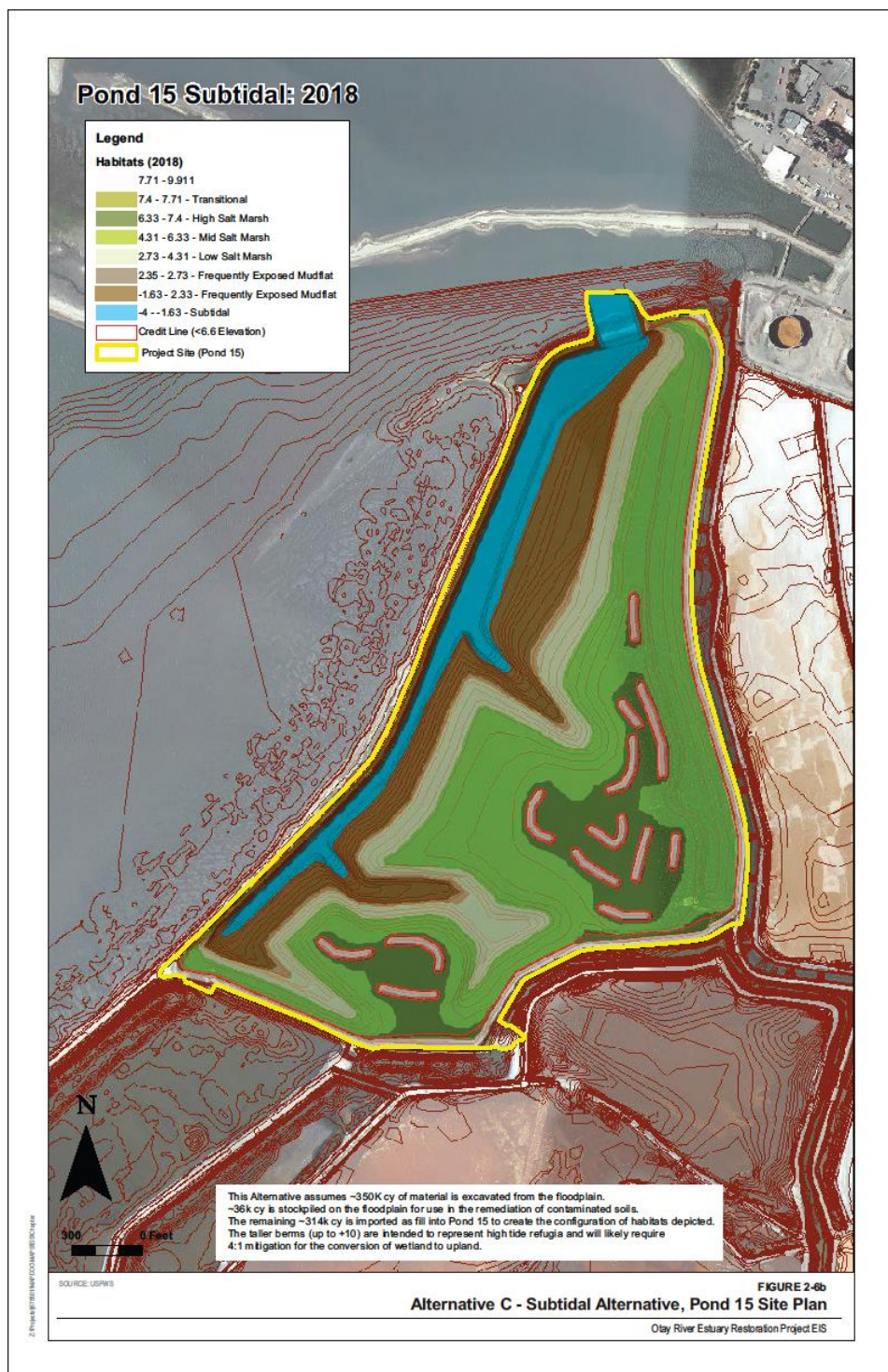


**Figure 7: Pond 15 grading plan under the Subtidal Alternative**

The objective of this study is to perform hydrodynamic simulation of the tidal exchange that would occur in each of these restoration alternatives, and make quantitative evaluation of the acreages of each habitat type that would be created. The hydrodynamic simulations will also assess the velocities of tidal flows and the stability and potential maintenance requirements of the approximately 7,000 ft long river channel that connects the new tidal basin in the Otay River Floodplain with south San Diego Bay.

## **2.0) Technical Approach**

This study employs a well-tested and peer-reviewed hydrodynamic model to evaluate the tidal hydraulics the Intertidal Alternative and the Subtidal Alternative based on updated bathymetry provided by Wetlands Research Associates (WRA) and latest updates to San Diego Bay tides for the 1983-2001 tidal epoch. The computer models used in this study are finite element types. The tidal hydraulics model is the research model, *TIDE\_FEM*, [Inman & Jenkins, 1996] and the littoral transport model is *TIDE\_FEM/SEDXPORT*. *TIDE\_FEM* was built from some well-studied and proven computational methods and numerical architecture that have been successful in predicting shallow water tidal propagation in Massachusetts Bay [Connor & Wang, 1974] and estuaries in Rhode Island, [Wang, 1975 ], and have been reviewed in basic text books [Weiyan, 1992] and symposia on the subject, e.g., Gallagher (1981). A discussion of the physics of *TIDE\_FEM* is given in Jenkins and Wasyl (2003 & 2005).

In its most recent version, the *TIDE\_FEM/TIDE\_FEM/SEDXPORT* modeling system has been integrated into the Navy's Coastal Water Clarity Model and the Littoral Remote Sensing Simulator (LRSS) (see Hammond, et al., 1995). The *TIDE\_FEM/SEDXPORT* code has been validated in mid-to-inner shelf waters (see Hammond, et al., 1995; Schoonmaker, et al., 1994). A detailed description of the architecture and codes of the *TIDE\_FEM/SEDXPORT* is given in Jenkins and Wasyl (2005) that is available on-line at the University of California digital library at: <http://repositories.cdlib.org/sio/techreport/58/>.

Validation of the *TIDE\_FEM/SEDXPORT* code was shown by three independent methods: 1) direct measurement of suspended particle transport and particle size distributions by means of a laser particle sizer; 2) measurements of water column optical properties; and, 3) comparison of computed stratified plume dispersion patterns with LANDSAT imagery. Besides being validated in coastal waters of Southern California, the *TIDE\_FEM/SEDXPORT* modeling system has been extensively peer reviewed. Although some of the early peer review was confidential and occurred inside the Office of Naval Research and the Naval Research Laboratory, the following is a listing of 5 independent peer review episodes of *TIDE\_FEM/SEDXPORT* that were conducted by 9 independent experts and can be found in the public records of the State Water Resources Control Board, the California Coastal Commission and the City of Huntington Beach.

1997- Reviewing Agency: State Water Resources Control Board

Project: NPDES 316 a/b Permit renewal, Scripps Beach, Carlsbad, CA

Reviewer: Dr. Andrew Lissner, SAIC, La Jolla, CA

- 1998- Reviewing Agency: California Coastal Commission  
 Project: Coastal Development Permit, San Dieguito Lagoon Restoration  
 Reviewers: Prof. Ashish Mehta, University of Florida, Gainesville;  
 Prof. Paul Komar, Oregon State University, Corvallis;  
 Prof. Peter Goodwin, University of Idaho, Moscow
- 2000- Reviewing Agency: California Coastal Commission  
 Project: Coastal Development Permit, Crystal Cove Development  
 Reviewers: Prof. Robert Wiegel, University of California, Berkeley;  
 Dr. Ron Noble, Noble Engineers, Irvine, CA
- 2002- Reviewing Agency: California Coastal Commission  
 Project: Coastal Development Permit, Dana Point Headland Reserve  
 Reviewers: Prof. Robert Wiegel, University of California, Berkeley;  
 Dr. Richard Seymour, University of California, San Diego
- 2003- Reviewing Agency: City of Huntington Beach  
 Project: EIR Certification, Poseidon Desalination Project  
 Reviewer: Prof. Stanley Grant, University of California, Irvine

The model, analysis methods, and supporting data bases used herein are the same as those utilized in the Environmental Impact Report/Environmental Impact Statement (EIR/EIS) for the San Dieguito Wetland Restoration Project, (EIR/EIS, 2000), and for the preparation of the San Dieguito Wetlands Restoration Project, Final Restoration Plan, (SCE, 2005). Monitoring data for the newly completed San Dieguito Lagoon Restoration Project was also used to calibrate tidal hydraulics model. San Dieguito Lagoon was selected as a proxy for the restoration alternatives because of morphologic similarities: in particular, both restoration sites have a long “goose-neck” feeder channel connecting source water to interior tidal basins of comparable acreage and distance from the source water. Habitat surveys conducted during the San Dieguito Lagoon Restoration Project by Josselyn & Whelchel (1999), and then later updated by vegetation surveys in the lower Otay River flood plain by Josselyn (2012), were used to develop functional relationships between habitat breaks and amounts of time for wetting and drying (hydroperiod functions). These relationships were used to transpose tidal hydraulics model output into calculations of acreage of various wetland habitat types created by the two restoration alternatives.

**2.1 Tidal Hydraulics Model Physics:** The tidal hydraulics are treated herein as a vertically well-mixed, two-dimensional, homogeneous flow because of a number of factors, including: the shallow depths in both the existing Otay River; the episodic and usually infrequent river flow events; and the enormous complexity of attempting to model a continuously stratified, brackish system. Salinity measurements from 1994-1997 by Boland (1998) suggest that this is not an unrealistic approximation. These salinity measurements indicate fairly uniform seawater salinities exist in the estuary most of the time, with relatively brief periods of fresh water dominance when high river flow rates prevent saline intrusion, e.g., the February 1995 flood series. Consequently, the lower Otay River is a tidally dominated system throughout most any given long-term period of record.

A finite element approach was adapted in preference to more common finite difference shallow water tidal models, e.g., Leendertse (1970), Abbott et al (1973), etc. Finite difference models employ rectangular grids which would be difficult to adapt to the complex geometry of the systems of channels of the Otay. It is believed that large errors would accumulate from attempting to approximate the irregular boundaries of the Otay system with orthogonal segments. On the other hand, finite element methods allow the computational problem to be contained within a domain bounded by a continuous contour surface, such as the  $S_f$  contours stored within the *bathym* file.

A finite element tidal hydraulics model, **TIDE\_FEM**, [Inman and Jenkins, 1996] was employed to evaluate the tidal hydraulics of the existing conditions. **TIDE\_FEM** was built from some well-studied and proven computational methods and numerical architecture that have done well in predicting shallow water tidal propagation in Massachusetts Bay [Connor and Wang, 1974] and estuaries in Rhode Island, [Wang, 1975], and have been reviewed in basic text books [Weiyan, 1992] and symposia on the subject, e.g., Gallagher (1981).

**TIDE\_FEM** employs a variant of the vertically integrated equations for shallow water tidal propagation after Connor and Wang (1975). These are based upon the Boussinesq approximations with Chezy friction and Manning's roughness. The finite element discretization is based upon the commonly used *Galerkin weighted residual method* to specify integral functionals that are minimized in each finite element domain using a variational scheme, see Gallagher (1981). Time integration is based upon the simple *trapezoidal rule* [Gallagher, 1981]. The computational architecture of **TIDE\_FEM** is adapted from Wang (1975), whereby a transformation from a **global** coordinate system to a **natural** coordinate system based on the unit triangle is used to reduce the weighted residuals to a set of order-one ordinary differential equations with constant coefficients. These coefficients (*influence coefficients*) are posed in terms of a *shape function* derived from the natural coordinates of each nodal point. The resulting systems of equations are assembled and coded as banded matrices and subsequently solved by *Cholesky's method*, see Oden and Oliveira (1973 and Boas (1966).

We adapt the California coordinates as our **global** coordinate system ( $x, y$ ) to which the nodes are referenced, with  $x$  (easting) and  $y$  (northing). The vertical coordinate  $z$  is fixed at 0.0 ft NGVD and is positive upward. The local depth relative to 0.0 ft NGVD is  $h$  and the mean surface elevation about 0.0 ft NGVD is  $\eta$ . The total depth of water at any node is  $H = h + \eta$ . The vertically averaged xy-components of velocity are  $(\bar{u}, \bar{v})$ . The continuity and momentum equations may be written from Connor and Wang, (1974), as:

$$\begin{aligned}
\frac{\partial}{\partial t} \rho H + \frac{\partial}{\partial x} q_x + \frac{\partial}{\partial y} q_y &= 0 \\
\frac{\partial}{\partial t} q_x + \frac{\partial}{\partial x} \bar{u} q_x + \frac{\partial}{\partial y} \bar{u} q_y &= B_x + \frac{\partial}{\partial x} (F_{xx} - F_p) + \frac{\partial}{\partial x} F_{yx} \\
\frac{\partial}{\partial t} q_y + \frac{\partial}{\partial x} \bar{v} q_x + \frac{\partial}{\partial y} \bar{v} q_y &= B_y + \frac{\partial}{\partial y} (F_{yy} - F_p) + \frac{\partial}{\partial y} F_{xy}
\end{aligned} \tag{1}$$

Here  $q_x, q_y$  are mass flux components

$$q_x = \rho \int_{-h}^{\eta} \bar{u} dz \tag{2}$$

$$q_y = \rho \int_{-h}^{\eta} \bar{v} dz \tag{3}$$

and  $q_I$  is the mass flux through the ocean inlet due to water surface elevation changes in the estuary:

$$q_I = \rho \frac{\partial}{\partial t} \left( \frac{\partial s}{\partial \eta} \right) \tag{4}$$

$F_p$  is the pressure force resultant and  $F_{xx}, F_{xy}, F_{yy}$  are "equivalent" internal stress resultants due to turbulent and dispersive momentum fluxes

$$\begin{aligned}
F_p &= \int_{-h}^{\eta} p dz = \frac{\rho g H^2}{2} \\
F_{xx} &= 2\varepsilon \frac{\partial}{\partial x} q_x \\
F_{yy} &= 2\varepsilon \frac{\partial}{\partial y} q_y \\
F_{yx} &= F_{xy} = \varepsilon \left( \frac{\partial}{\partial y} q_y + \frac{\partial}{\partial x} q_x \right)
\end{aligned} \tag{5}$$

and  $\varepsilon$  is the eddy viscosity.  $B_x$  and  $B_y$  are the bottom stress components

$$\begin{aligned}
B_x &= \tau_x + \rho g H \frac{\partial h}{\partial x} \\
B_y &= \tau_y + \rho g H \frac{\partial h}{\partial y}
\end{aligned} \tag{6}$$

In Equation (6),  $\tau_x$  and  $\tau_y$  are the bottom shear stress components that are quasi-linearized by Chezy-based friction using Manning's roughness factor,  $n_0$ :

$$\begin{aligned}
\tau_x &= -\frac{g}{\rho H^2 C_z^2} q_x (q_x^2 + q_y^2)^{1/2} \\
\tau_y &= -\frac{g}{\rho H^2 C_z^2} q_y (q_x^2 + q_y^2)^{1/2}
\end{aligned} \tag{7}$$

where  $C_z$  is the Chezy coefficient calculated as:

$$C_z = \frac{1.49}{n_0} H^{1/6} \tag{8}$$

Boundary conditions are imposed at the locus of possible land/water boundaries,  $S_f$  in the *bathym* file and at the ocean inlet,  $S_o$ . Flux quantities normal to these contours are denoted with "n" subscripts and tangential fluxes are given "s" subscripts. At any point along a boundary contour, the normal and tangential mass fluxes are:

$$\begin{aligned}
q_n &= \int_{-h}^{\eta} \rho u_n dz = \alpha_{nx} q_x + \alpha_{ny} q_y \\
q_s &= \int_{-h}^{\eta} \rho u_s dz = -\alpha_{nx} q_x + \alpha_{ny} q_y \\
\alpha_{nx} &= \cos(n, x) \\
\alpha_{ny} &= \cos(n, y)
\end{aligned} \tag{9}$$

Components of momentum fluxes across a boundary are equivalent to internal force resultants according to:

$$\begin{aligned}
F_{nx} &= \alpha_{nx} (F_{xx} - F_p) + \alpha_{ny} F_{yx} \\
F_{ny} &= \alpha_{ny} (F_{yy} - F_p) + \alpha_{nx} F_{xy}
\end{aligned} \tag{10}$$

On land boundary contours, the flux components are prescribed

$$q_n = q_s = 0 \quad \text{on land} \tag{11}$$

On the ocean boundary, the normal boundary forces (due to sea surface elevation) are continuous with ocean values, and the mass exchange is limited by the storage capacity of the estuary.

Hence

$$F_{nm} = \bar{F}_{nm} \quad \text{and} \quad q_{nm} = q_I \quad \text{at inlet} \quad (12)$$

In the problem at hand  $\bar{F}_{nn}$  is prescribed at the inlet by the ocean tidal elevation,  $\eta_0$ , and the inlet sill depth,  $h_0$  according to

$$\bar{F}_{nm} = \frac{\rho g}{2} (\eta_0 + h_0)^2 \quad \text{on } S_0 \quad (13)$$

Ocean *tidal forcing functions*  $\eta_0$  were developed in Section 3. The ocean boundary condition as specified by Equation (12) places a dynamic boundary condition on the momentum equations and a kinematic boundary condition on the continuity equation that is constrained by the storage rating curve. Solutions are possible by specifying only the dynamic boundary condition, but then mass exchanges are controlled by the wetting and drying of individual grid cells with associated discretization and interpolation errors which threaten mass conservation. The technique of over specifying the ocean boundary condition with both a dynamic and kinematic condition is discussed in the book by Weiyan (1992).

The governing equations and the boundary conditions are cast as a set of integral functionals in a variational scheme, [Boas, 1966]. Within the domain of each element of the mesh,  $A_i$  the unknown solution to the governing equations is simulated by a set of *trial functions*  $(\hat{H}, \hat{q})$  having adjustable coefficients. The trial functions are substituted into the governing equations to form *residuals*,  $(R_H, R_q)$ . The residuals are modified by *weighting functions*,  $(\Delta H, \Delta q)$ . The coefficients of the trial functions are adjusted until the weighted residuals vanish. The solution condition on the weighted residuals then becomes:

$$\begin{aligned} \iint_{A_i} R_H \Delta H dA &= 0 \\ \iint_{A_i} R_q \Delta q dA &= 0 \end{aligned}$$

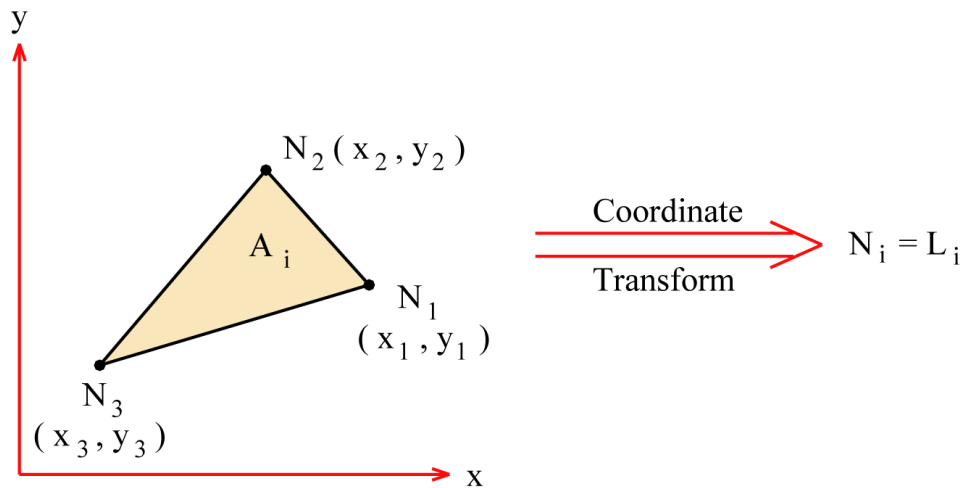
By the Galerkin method of weighted residuals, [Finlaysen, 1972], the weighting functions are set equal to nodal *shape functions*,  $\langle N \rangle$ , or:

$$\begin{aligned} \Delta H &\sim N_i \\ \Delta q &\sim N_j \end{aligned}$$

The shape function,  $\langle N \rangle$ , is a polynomial of degree which must be at least equivalent to the order of the highest derivative in the governing equations. The shape function also provides the mechanism to discretized the governing equations. The shape function polynomial is specified in terms of *global (California)* coordinates (Figure 8a) for the first nodal point,  $N_1$  of a generalized

## Specifying the Shape Function $\langle N \rangle$ for any 3-Node Triangular Element

a) Global (California) Coordinates

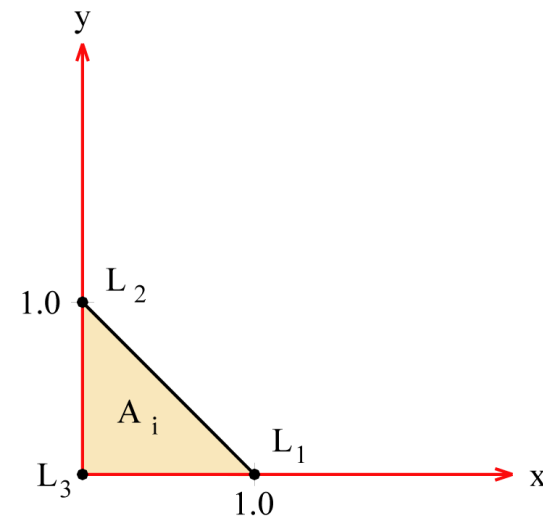


$$\langle N \rangle = (N_1, N_2, N_3)$$

$$N_1 = [(x_2 y_3 - x_3 y_2) + (y_2 - y_3)x + (x_3 - y_2)y] / 2 A_i$$

$$2 A_i = (x_1 - x_3)(y_2 - y_3) - (x_2 - x_3)(y_1 - y_3)$$

b) Natural Coordinates



$$x = L_1 x_1 + L_2 x_2 + L_3 x_3$$

$$y = L_1 y_1 + L_2 y_2 + L_3 y_3$$

$$L_1 + L_2 + L_3 = 1.0$$

**Figure 8:** Shape function polynomial and transform to natural coordinates for a generalized 3-node triangular element; (a) 3-node element in California coordinates; (b) 3-node element in natural coordinates.

3-node triangular element of area  $A_i$ . Wang (1975) obtained significant numerical efficiency in computing the weighted residuals when the shape functions of each nodal point,  $N_i$ , are transformed to a system of *natural* coordinates based upon the unit triangle, giving  $N_i \rightarrow L_i$ , see Figure 8b. The shape functions also permit semi-discretization of the governing equations when the trial functions are posed in the form:

$$\begin{aligned}\hat{H}(x, y, t) &= \sum_i H_i(t) N_i(x, y) \\ \hat{q}(x, y, t) &= \sum_j q_j(t) N_j(x, y)\end{aligned}\tag{14}$$

Discretization using the weighting and trial functions expressed in terms of the nodal shape functions allows the *distribution* of dependent variables over each element to be obtained from the values of the independent variables at discrete nodal points. However, the shape function at any given nodal point, say  $N_i$ , is a function of the independent variables of the two other nodal points which make up that particular 3-node triangular element. Consequently, the computations of the weighted residuals leads to a series of influence coefficient matrices defined

$$\begin{aligned}a_{ij} &= \frac{1}{A_i} \iint N_i N_j dA \\ s_{ij} &= \frac{1}{A_i} \iint N_i \frac{\partial N_j}{\partial x} dA \\ t_{ij} &= \frac{1}{A_i} \iint N_i \frac{\partial N_j}{\partial y} dA \\ g_{ijk} &= \frac{1}{A_i} \iint N_i N_j \frac{\partial N_k}{\partial x} dA \\ h_{ijk} &= \frac{1}{A_i} \iint N_i N_j \frac{\partial N_k}{\partial y} dA\end{aligned}\tag{15}$$

The influence coefficient matrices given by equation (15) are evaluated in both global and natural coordinates. Once the influence coefficients have been calculated for each 3-node element, the weighted residuals reduce to a set of order-one ordinary differential with constant coefficients. The continuity equation becomes:

$$\begin{aligned}
\sum \left( a_{ij} \frac{dH_i}{dt} \right) &= - \sum_i \sum_k \left[ g_{ijk} (H_i q_{xk} + H_k q_{xi}) + h_{ijk} (H_i q_{yk} + H_k q_{yi}) \right] \\
\sum \left( a_{ij} \frac{dq_{xj}}{dt} \right) &= - \sum_j \sum_k \left[ g_{ijk} (q_{xk} q_{xj}) + h_{ijk} (q_{yj} q_{xk}) \right] + N_i \sum_j N_j S_{jj} + g \sum_i s_{ij} H_i \\
\sum \left( a_{ij} \frac{dq_{yj}}{dt} \right) &= - \sum_j \sum_k \left[ g_{ijk} (q_{xj} q_{yk}) + h_{ijk} (q_{yj} q_{xk}) \right] + N_i \sum_j N_j S_{jj} + g \sum_i t_{ij} H_i
\end{aligned} \tag{16}$$

Equations (16) are essentially simple oscillator equations forced by the collection of algebraic terms appearing on the right hand side; and are therefore easily integrated over time. The time integration scheme used over each time step of the tidal forcing function is based upon the **trapezoidal rule**, see Gallagher (1981) or Conte and deBoor (1972). This scheme was chosen because it is known to be unconditionally stable, and in tidal propagation problems has not been known to introduce spurious phase differences or damping. It replaces time derivatives between two successive times,  $\Delta t = t_{n+1} - t_n$ , with a truncated Taylor series. For the water depth it would take on the form:

$$\begin{aligned}
\frac{dH}{dt} &= \eta(t) \\
H_{n+1} - H_n &= \frac{\Delta t}{2} (\eta_{n+1} + \eta_n) + E \Delta t \\
E &= \frac{1}{12} (\Delta t)^2 \left| \frac{d^2 \eta}{dt^2} \right|
\end{aligned} \tag{17}$$

To solve equation (17), iteration is required involving successive forward and backward substitutions.

The influence and friction slope coefficient matrices together with the trapezoidal rule reduce equations to a system of algebraic equations [Grotkop, 1973] which are solved by Cholesky's method per a numerical coding scheme by Wang (1975). For more details, refer to the TIDE\_FEM code in Appendix-I of Jenkins and Wasyl (1996), and Gallagher (1981) or Oden and Oliveira (1973).

### 3.0) Model Initialization

Tidal basin water levels and tidal currents are studied using numerical transport models that are run over a historic surrogate time period for which environmental forcing is well-known.

In all such *boundary value problems* input variables are divided between two general classes, forcing functions and boundary conditions. The primary forcing function is San Diego Bay water level variation. The important boundary conditions are basin and feeder channel bathymetry, sediment grain size, and river channel scour configurations. Input for San Diego Bay water level

variations are discussed below in Sections 3.1 and 3.2. The remaining variables are site specific and will be dealt with separately for the Intertidal Alternative in Section 4, and the Subtidal Alternative in Section 5.

**3.1) San Diego Bay Circulation:** Currents in San Diego Bay are predominately produced by tides (Wang et al. 1998). This tidal exchange between the ocean and the bay is a result of a phenomenon called “tidal pumping” (Chadwick, et al.. 1997). The “pumping” of water is due to the flow difference between the ebb and the flood flows. Being located at mid-latitude, tides and currents within the San Diego Bay are dominated by a mixed diurnal-semidiurnal component (Peeling 1975). Typical tidal current speeds range between 0.3-0.5 m/s near the inlet and 0.1 m/s to 0.2 m/s in the southern region of the bay. The phase propagation suggests that the tides behave almost as standing waves with typical lags between the mouth and the back portion of the bay of 10 min and an increase in tidal amplitude in the inner bay compared to the outer bay. The overall tidal prism for the bay is  $5.5 \times 10^7 \text{ m}^3$  and the tidal excursion is larger than the mouth with a value of 4.4 km (Chadwick and Largier 1999b). Chu, et al. (2012) measured mass exchange between San Diego Bay and the Pacific Ocean using a combination of flow measurements by acoustic Doppler current profiling and tracer measurements using a naturally occurring ultraviolet fluorescence tracer. They found that variations in exchange with tidal range could be isolated by separately evaluating the ebb and flood tidal transport budgets. The tracer transport during the ebb increased rapidly with tidal range, while during the flood tide, the transport increased more gradually. The resulting difference in tidal transport between the ebb and flood accounts for the exchange between the bay and ocean. For weak tides, the exchange tends to increase rapidly with increasing tidal range, while for stronger tides, the exchange is more constant.

**3.2 San Diego Bay Tidal Regime:** The flow of sea water into and out of the Otay River Channel, the South Bay salt ponds and the proposed restoration tidal basins are driven by the time variation in San Diego Bay water level. The nearest NOAA tide gage to the Otay River and South Bay salt ponds is located at the Navy Pier in San Diego Bay. This tide gage (NOAA #941-0170) was last leveled using the 1983-2001 tidal epoch. Elevations of tidal datums referred to NAVD 88 are given in the second column of Table 1.

Tidal data in Table 1 indicates that tidal ranges in San Diego Bay are greater than those found on the open coast. Mean diurnal tidal ranges are 5.72 ft as compared to 5.33 ft on the open coast, an increase of 0.39 ft of diurnal range in San Diego Bay. The extreme water level range is 11.23 ft in San Diego Bay as compared to 10.51 ft on the open coast, an increase of 0.72 ft of extreme range in the bay. All high water datum in the bay exceed those on the open coast and all the low water level datum are lower in the bay than on the open coast. This occurs because San Diego Bay is a resonant tidal system where higher harmonics of the K1 lunar-solar diurnal tidal constituent and the M2 principal lunar semi-diurnal tidal constituent are bathymetrical trapped in the bay, leading to a build-up in tidal amplitude. The tidal resonance of San Diego Bay provides additional tidal energy for forcing tidal inundation of the proposed tidal basins in the Otay River floodplain and in Salt Pond #15, and is an attribute of this site that increases the chance of achieving a sustainable functioning wetland restoration.

**TABLE 1: Tidal datums for SAN DIEGO BAY at NOAA #941-0170 Navy Pier:**

LENGTH OF DATA SERIES: 19 Years

TIME PERIOD: January 1983 - December 2001

TIDAL EPOCH: 1983-2001

HIGHEST WATER LEVEL (01/27/1983)	= 7.71 ft NAVD (8.1402 ft MLLW)
MEAN HIGHER HIGH WATER	<u>MHHW</u> = 5.292 ft NAVD (5.7253 ft MLLW)
MEAN HIGH WATER	<u>MHW</u> = 4.5507 ft NAVD (4.9838 ft MLLW)
MEAN TIDE LEVEL	<u>MTL</u> = 2.5264 ft NAVD (2.9595 ft MLLW)
MEAN SEA LEVEL	<u>MSL</u> = 2.5067 ft NAVD (2.9398 ft MLLW)
MEAN LOW WATER	<u>MLW</u> = 0.5020 ft NAVD (0.9351 ft MLLW)
North American Vertical Datum	<u>NAVD88</u> = 0.00 ft NAVD (0.4331 ft MLLW)
MEAN LOWER LOW WATER	<u>MLLW</u> = -0.4331 ft NAVD (0.000 ft MLLW)
LOWEST WATER LEVEL (12/17/1937)	= -3.5238 ft NAVD (-3.0907 MLLW ft)

In spite of the resonant tidal system in the deeper middle and outer portions of San Diego Bay, there is significant muting of the tidal range in the far southern portions of the Bay in the neighborhood of the mouth of the Otay River and the South Bay salt ponds. NOAA lists four other tide gages in San Diego Bay, including: Ballast Point, NOAA # 9410155; Sweetwater Channel, NOAA #9410136; North Island Navy Wharf, NOAA # 9410169; and US Coast Guard AirStation, NOAA #9410175. However no data is available (or exists) for any of these other four NOAA tide gages in The Bay. Tide information at other locations in The Bay are model predictions of the kind in the Wang et al, 1998 paper. However, the Southwest Wetland Interpretive Association (SWIA) has operated a self-recording water quality monitoring station since 2007 at the mouth of the Otay River at the location noted in yellow in Figure 1. This monitoring station (referred to as the Otay River Sonde) has recorded water level, salinity and dissolved oxygen at 15 minute intervals from December 2007 through December 2011. Figure 9 gives a comparison between the measured water levels at the NOAA #941-0170 Navy Pier tide gage versus the Otay River Sonde. Both monitoring stations give the same mean tidal level, but maximum water levels are slightly higher at the Otay River Sonde, and minimum water levels are significantly higher, indicating *low-tide muting* of the tides in the extreme South Bay. Lowest water levels recorded at the Otay River Sonde are -1.6108 ft. NAVD as compared with -3.5238 ft NAVD at the Navy Pier. This response is believed to be the result of bottom friction effects and additional resonances associated with the K1 and M2 barotropic tidal constituents flowing over the shallows of the *South Bay Shelf*. This hypothesis is supported by a spectral decomposition (distribution of tidal energy with frequency) of the water level measurements shown in Figure 10a. The principal spectral peaks show an enhanced second harmonic of the K1 lunar-solar diurnal tidal constituent at the mouth of the Otay River, indicating the effect of bottom friction over the shallow South Bay Shelf. There is also an enlarged resonant triad sub-harmonic (difference frequency) between the K1 lunar-solar diurnal tidal constituent and the M2 principal lunar semi-diurnal tidal constituent measured at the mouth of the Otay River, indicating

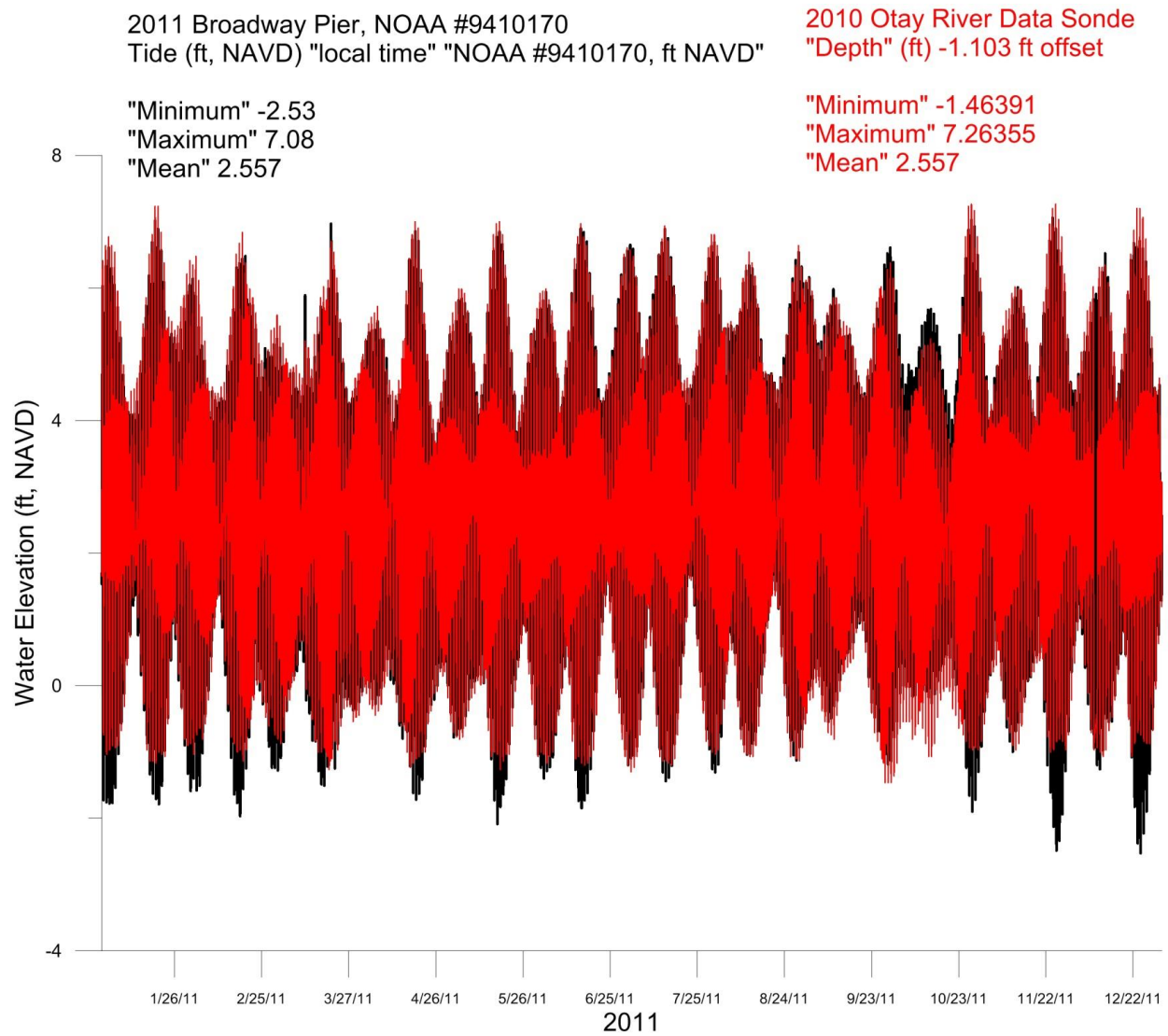


**Figure 9:** Comparison of mid-bay tides at the Navy Pier (black) versus south-bay tides at the mouth of the Otay River (red).

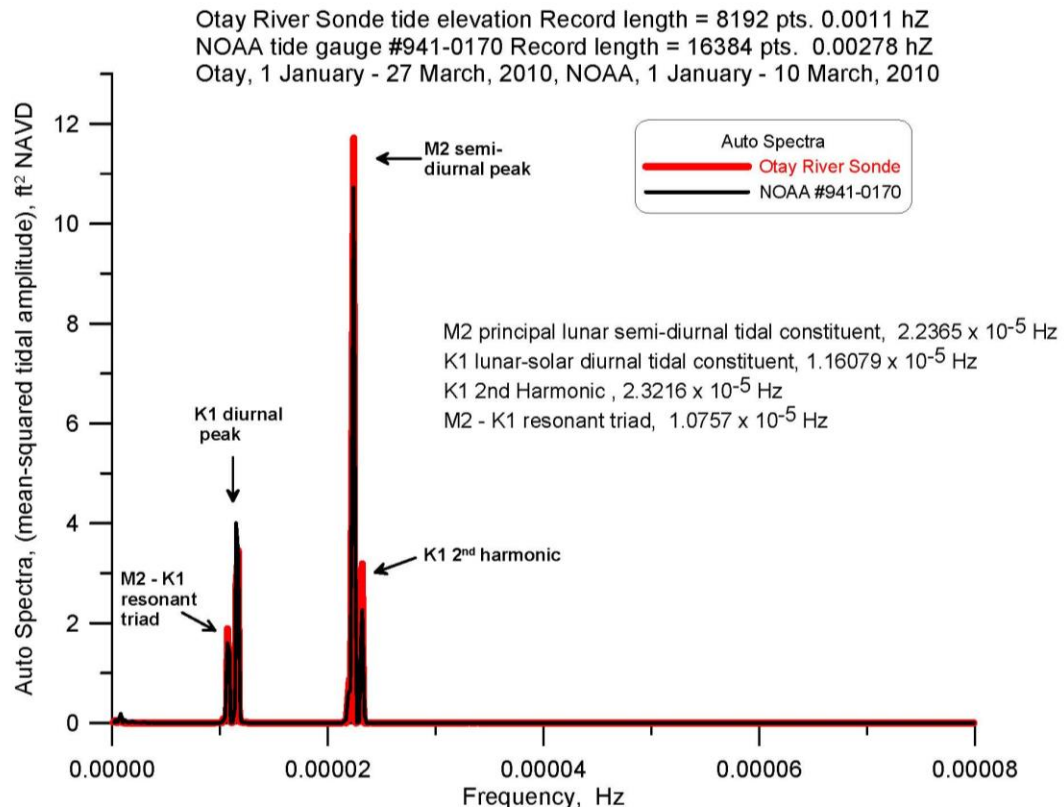


**Figure 10a:** Auto spectra (mean-squared tidal amplitude) of the Otay River Sonde measurements (red), versus the NOAA Navy Pier tidal record (black).

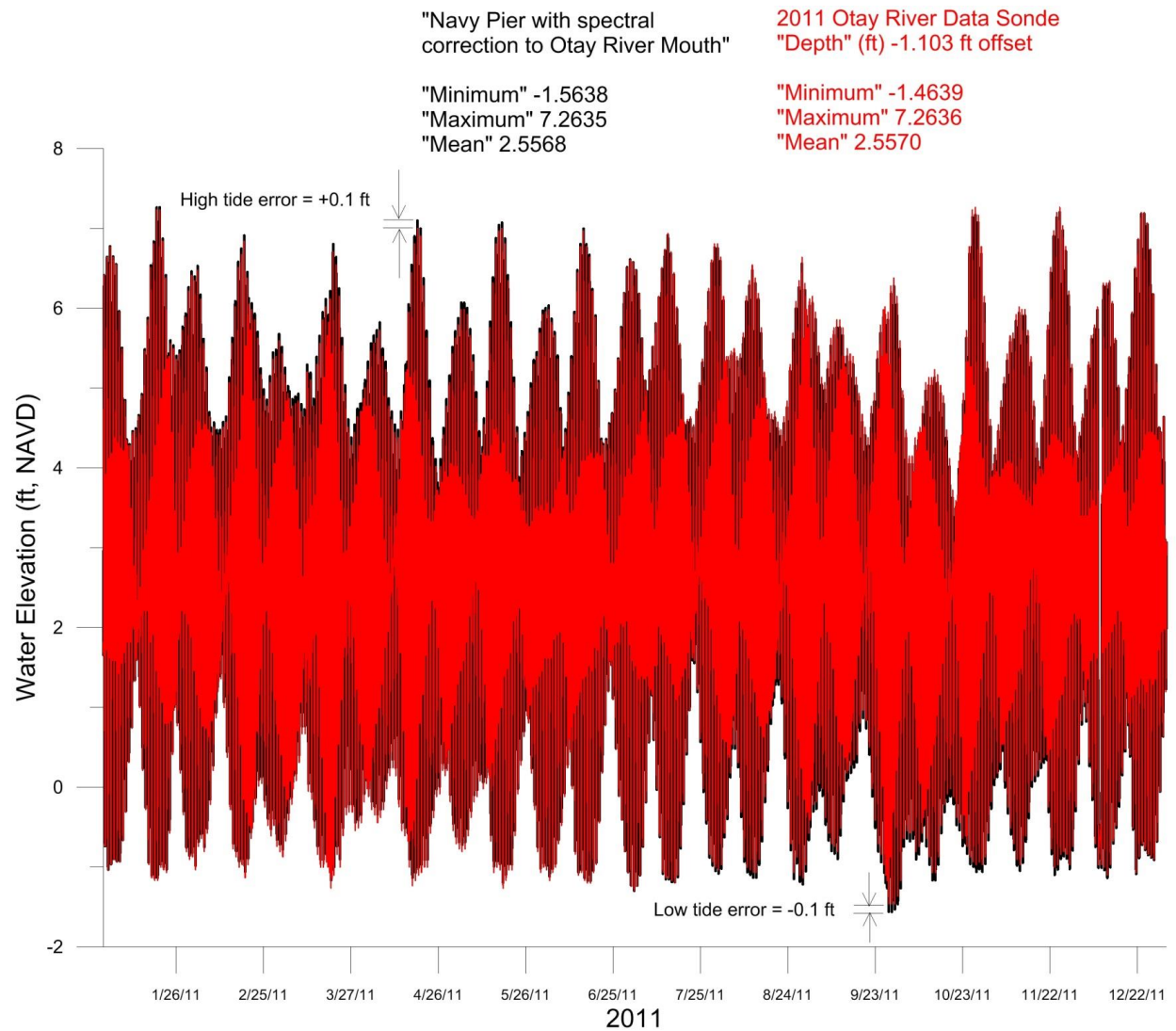


**Figure 10b:** Comparison of spectrally corrected Navy Pier tides (black) versus south-bay tides at the mouth of the Otay River (red). The spectral correction is made to transform Navy Pier tides to equivalent tides at the mouth of the Otay River. Transform error is  $\pm 0.1$  ft.

bathymetrically trapped tidal oscillations on the South Bay Shelf.

The importance of the tidal spectra in Figure 10a is that it permits the very long term tidal records at the Navy Pier to be converted into long term records of the tides at the mouth of the Otay River. The published NOAA tidal constituents for the Navy Pier are modified to conform to the spectral harmonics for the Otay River tides in Figure 10a, and then re-assembled in the time domain as shown Figure 10b. This process gives a long term tidal records (30 year in length) of the South Bay tides at the mouth of the Otay River to within an error of  $\pm 0.1$  ft. The analytic requirement for these long term South Bay tides is to have tidal forcing for the hydrodynamic models that captures the extremes of tidal inundation over many years. These extremes in tidal inundation are a determining factor in Nature's adaptations to upper and lower limits of wetland habitat, while the frequency of long term tidal inundation at various intermediate elevations determines the zonation of wetland habitat types.

**3.3) San Diego Bay Water Quality:** The quality of the water that enters the Otay River mouth is another important aspect to the quality and distribution of wetland habitat that can recruit in the Otay River Floodplain. The Otay River Sonde (noted in yellow in Figure 1) has recorded salinity and dissolved oxygen at 15 minute intervals from December 2007 through April 2010. Figure 11 gives the temporal variation of the salinity in parts per thousand (ppt) recorded by the Otay River Sonde, while Figure 12 gives the dissolved oxygen in mg/L. The maximum salinity reached during the dry, evaporative summer months is 42.57 ppt, while the minimum salinity during wet winter periods reaches as low as 0.2 ppt, but the average salinity is 33.52 ppt, identical to the average salinity recorded on the open coast at Scripps Pier. These salinity ranges are comparable to what has been measured in the San Dieguito Lagoon on the open coast by Boland (1998), and are suitable for sustaining a healthy functioning salt water wetland. The dissolved oxygen readings (DO) in Figure 12 show a maximum DO reached during the wet, winter months of 17.5 mg/L, while the minimum DO occurs during summer and can reach 0.0 mg/L. However, the average DO is 6.47 mg/L, about the same as found in nearshore waters along the open coast as measured at Scripps Pier. DO readings at the Otay River Sonde are roughly equivalent to what Boland (1998) reported for San Dieguito Lagoon. Percent departures from the mean for salinity and DO are compared in Figure 13 indicating that DO maximums occur when Otay River flooding occurs and the salinity is depressed to minimum values, and conversely, DO minimums occur during warm evaporative months in summer when south San Diego Bay waters turn hyper saline. Regardless, variability in salinity and dissolved oxygen at the Otay River Sonde are within normal limits of a healthy functioning salt water wetland.

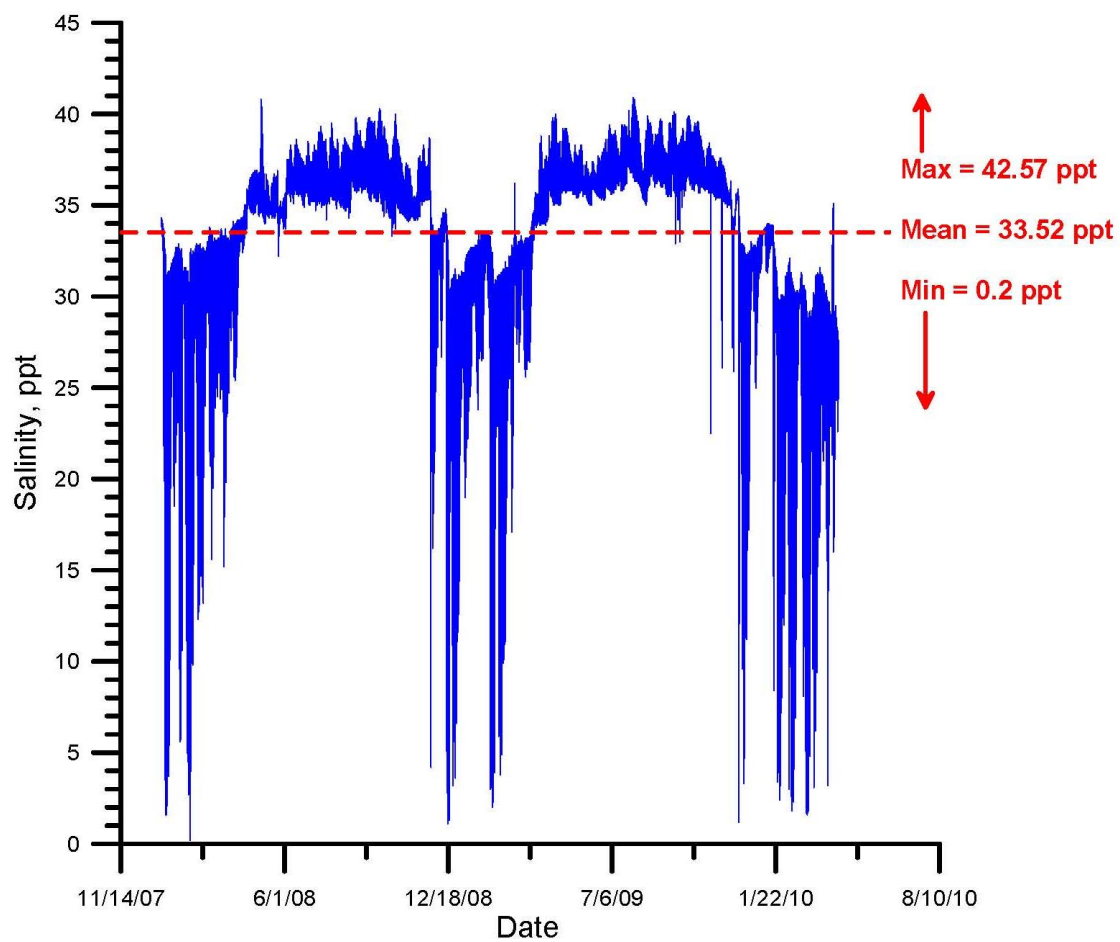


**Figure 11:** Salinity variation in south San Diego Bay at the Otay River mouth. Data from Otay River Sonde, 2007-2010.

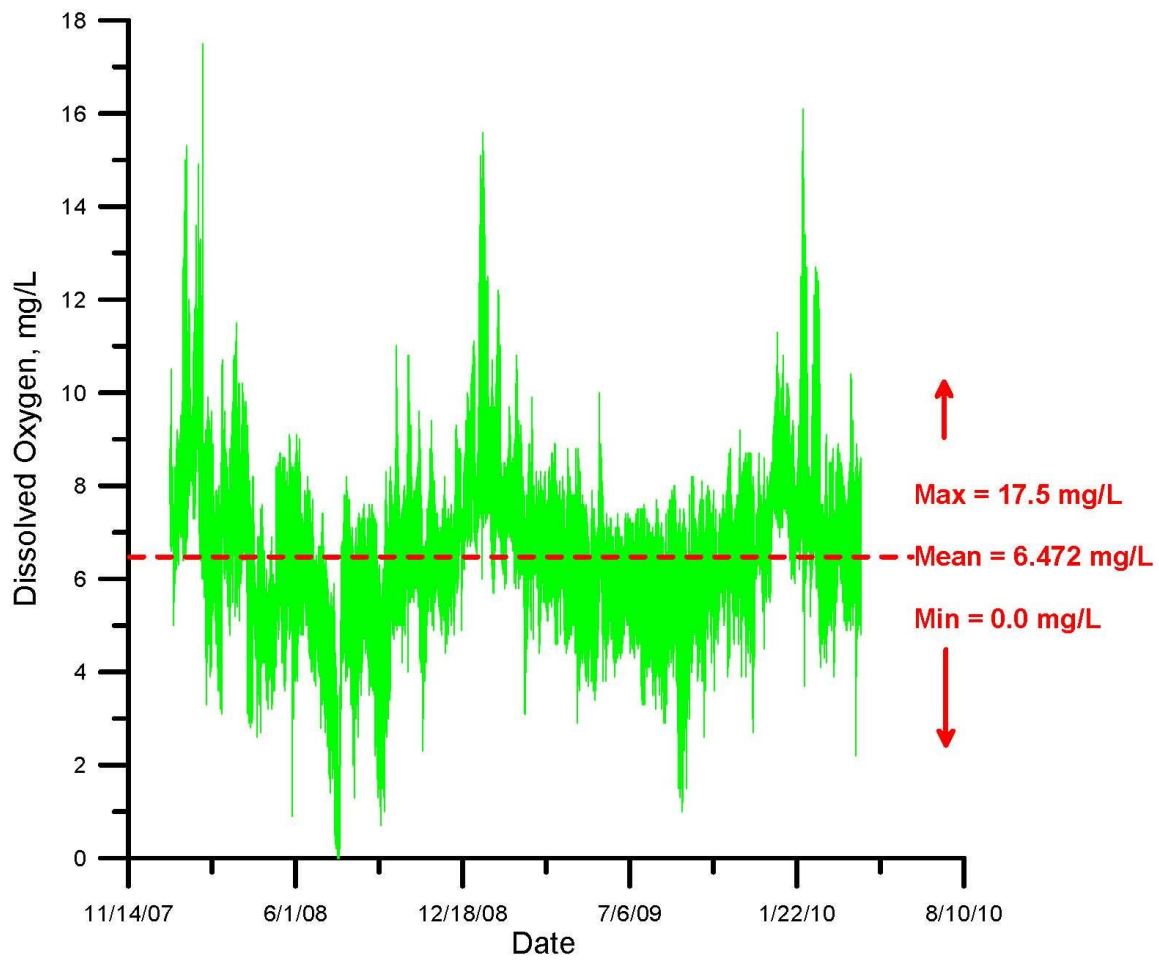


**Figure 12:** Dissolved Oxygen (DO) variation in south San Diego Bay at the Otay River mouth. Data from Otay River Sonde, 2007-2010.

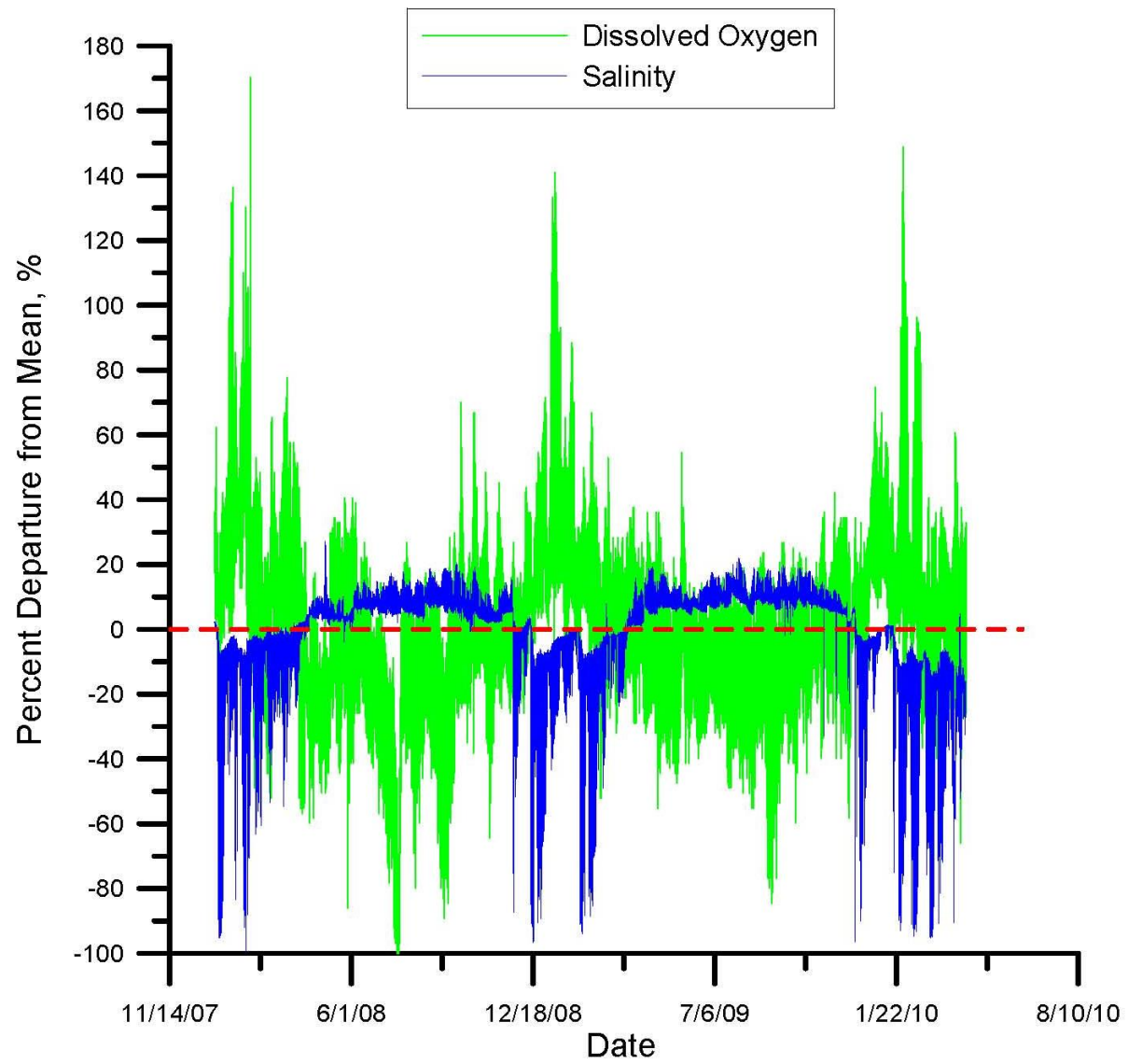


**Figure 13:** Variation in departure from the mean of salinity and dissolved oxygen at the Otay River mouth, from Otay Sonde data base, 2007-2010.

**3.4 Sea Level Rise Effects on San Diego Bay Water Levels:** Globally, oceans rose at an average rate of 0.7 inches (18 mm) per decade from 1961 to 2003.2 Local, or relative, sea level rise is affected by global sea level rise, as well as key additional factors such as El Nino events, circulation patterns, and land elevations changes. As shown in Figure 14, sea level rise has been documented in the San Diego Bay since 1906 with a rise of 0.8 inches (20.6mm) per decade over the past century.

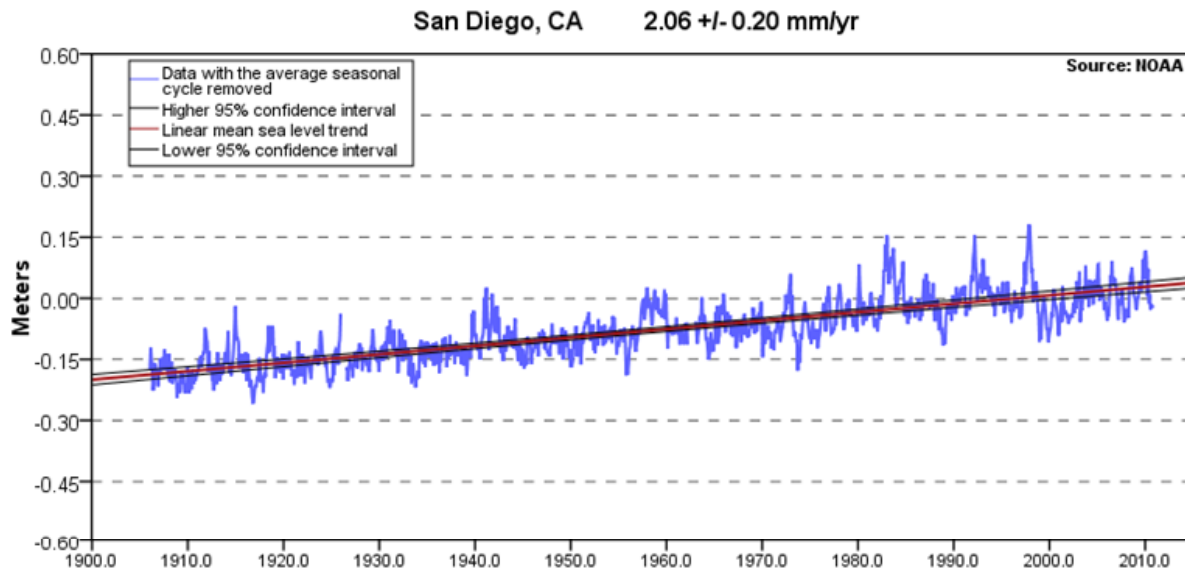


**Figure 14:** Observed sea level in San Diego Bay, 1900-2010, (from ICLEI, 2012)

Despite uncertainty, global climate experts have used greenhouse gas emissions scenarios and other methods to create a range of possible future sea level rise amounts. Figure 16 shows an estimated range of future global sea level rise trajectories from 7 different climate models. In California, the State is recommending the use of projections of between 4 and 24 inches (10.1 to 61 cm) in 2050 and of 31 to 69 inches (78 to 176 cm) in 2100. The restoration project will design for and evaluate sea level rise impacts based on State recommended projections for 2050. By the California State CAT-OPC guidance, sea level rise projections range between 4.68 and 24 inches (12 to 61 cm) by 2050. To calculate the tidal hydraulic responses of the restoration alternatives to these potential future sea levels, it is necessary to anticipate the tidal response inside San Diego Bay to these ranges of sea level rise on the open coastline. Two approaches are used. The first is linear superposition of the open ocean sea level rise on to the present 30 year time series of south San Diego Bay tides developed from spectral corrections to the NOAA Navy Pier tides detailed in Section 3.2. The second is to apply a spectral correction derived from the Navy's Bay tide model for sea level rise (ICLEI, 2012).

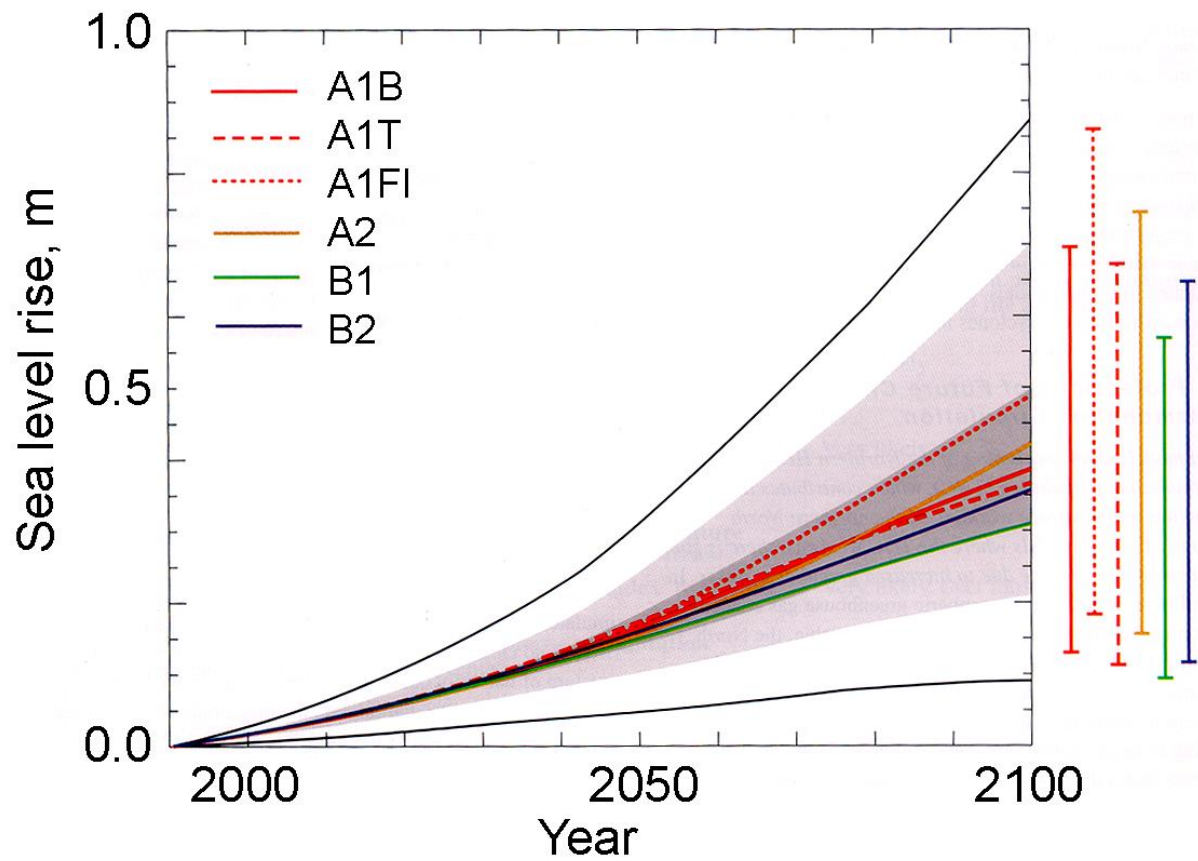


**Figure 16:** Range of sea level rise scenarios predicted out to year 2100 by seven separate global climate models (from IPCC, 2007)

Figure 17a shows a data snippet comparing tides at the mouth of the Otay River at present sea level (gray) versus the South Bay tidal response predicted for 2050 by the linear superposition method (red) and by the spectral correction method (blue). Obviously the higher-high and lower-low water levels will all be higher in 2050 based on the maximum CAT OPC guidance for sea level rise of 24 inches. The decisive issue is what the South Bay tidal range will be at these higher sea levels. The linear superposition method predicts the exact same tidal range as present, only oscillating around a 2 ft. higher sea level (Figure 17 a & b). The spectral correction method predicts the exact same higher high water levels as the linear superposition method, but yields a larger tidal range (Figure 17a & c). This is due to the fact that the 2050 tidal spectra derived from the Navy's Bay tide model predicts principle spectral peaks with a diminished second harmonic of the K1 lunar-solar diurnal tidal constituent at the mouth of the

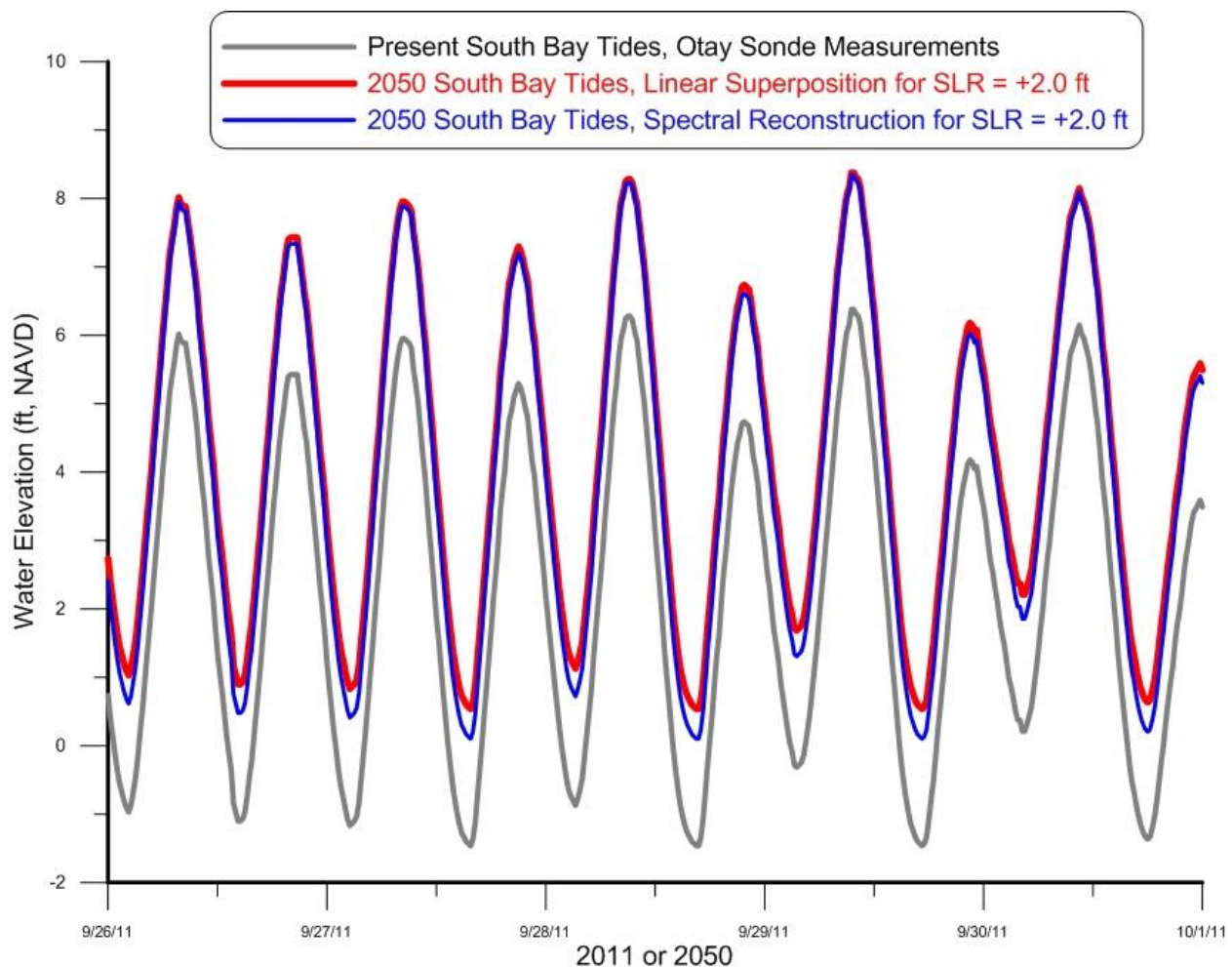


**Figure 17a:** Comparison of South San Diego Bay tides for present sea level (gray) versus South Bay tidal response on 2050 by the linear superposition method (red) and the spectral correction method (blue).

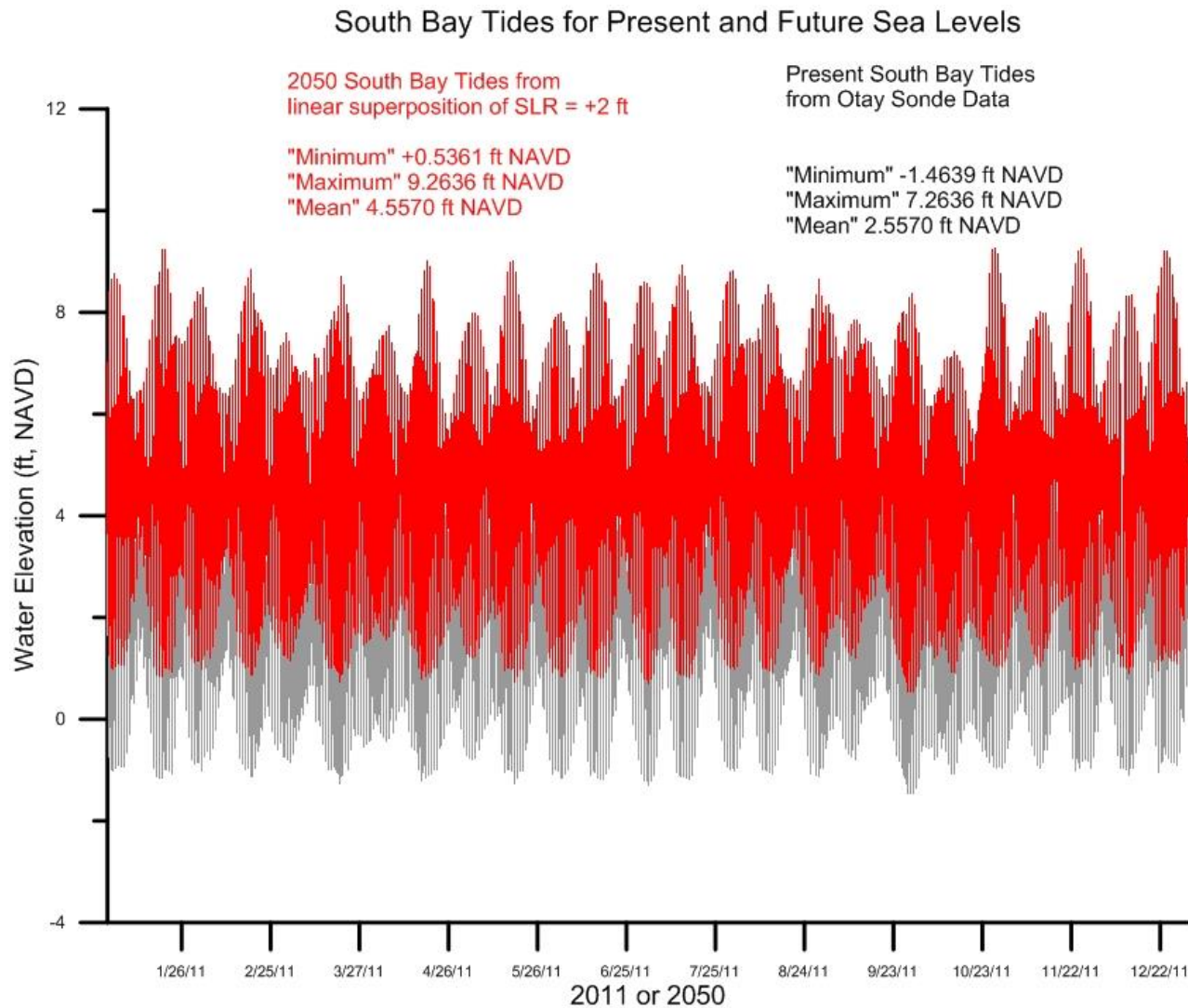


**Figure 17b:** Comparison of a typical year of South San Diego Bay tides for present sea level (gray) versus South Bay tidal response on 2050 by the linear superposition method (red).

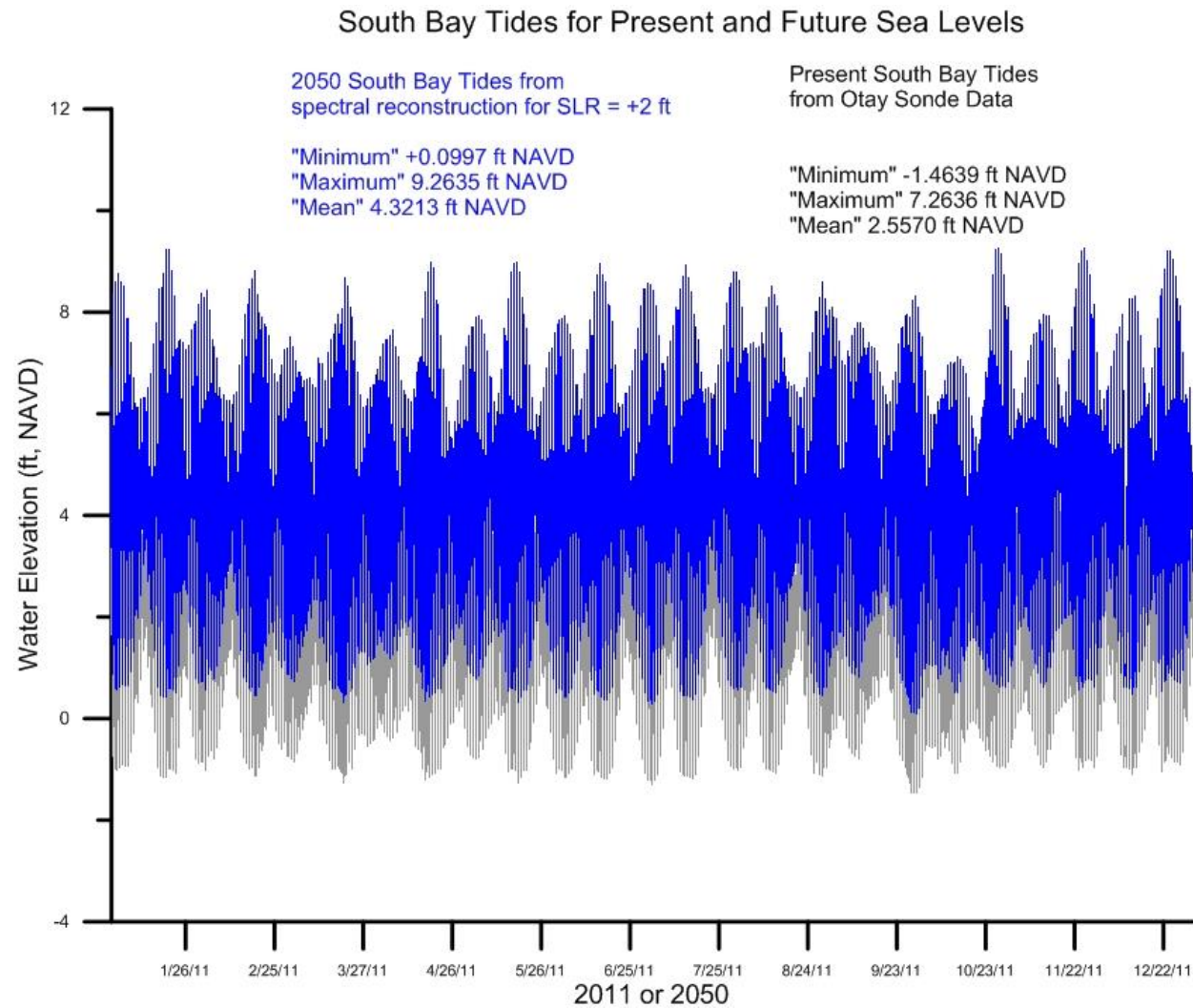


**Figure 17c:** Comparison of a typical year of South San Diego Bay tides for present sea level (gray) versus South Bay tidal response on 2050 by the spectral correction method (blue).

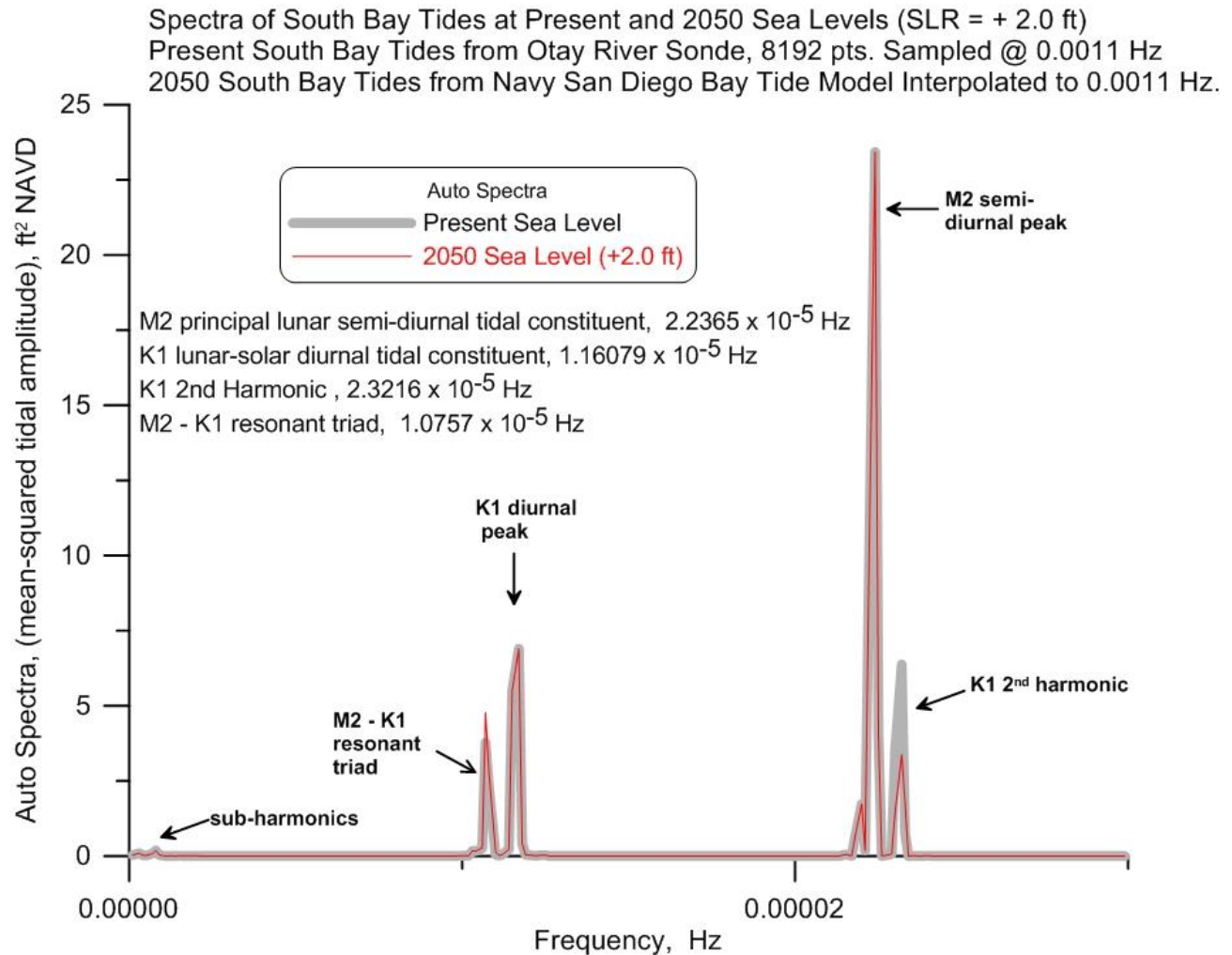


**Figure 18:** Comparison of spectra South San Diego Bay tides for present sea level (gray) versus South Bay tidal response for maximum estimated sea level rise in 2050 (red).

Otay River, (Figure 18), indicating diminished bottom friction over the South Bay Shelf due to feet of additional water depth at higher sea level. Also there is further enhancement of resonant triad sub-harmonic in Figure 18, (difference frequency) between the K1 lunar-solar diurnal tidal constituent and the M2 principal lunar semi-diurnal tidal constituent measured at the mouth of the Otay River, indicating bathymetrically trapped tidal oscillations on the South Bay Shelf has intensified in the presence of deeper water and diminished bottom friction.

Inundation refers to a condition when land that was once dry becomes permanently wet. Sea level rise could result in certain currently dry locations around the San Diego Bay being inundated by daily high tides. This potential future inundation in the Bay at 2050 is projected in Figure 19. Inspection of this figure reveals significant inundation impacts in South San Diego



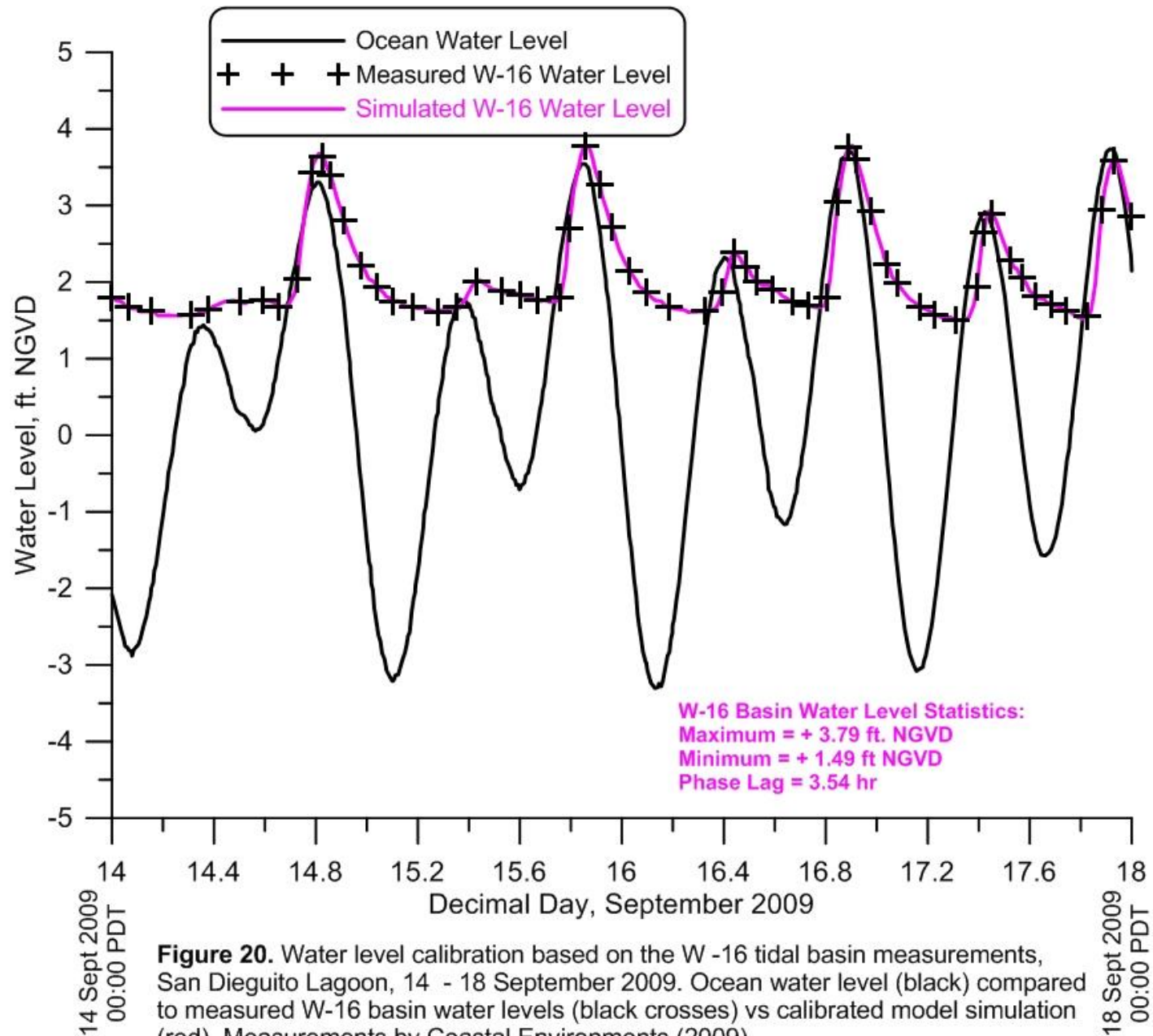
**Figure 19:** Projected Inundation impact areas in San Diego Bay due to 2050 sea level rise, (from ICLEI, 2012).

Bay by projected 2050 sea level rise. The Chula Vista Wildlife Reserve, and nearly all of the Pond #12 - #28 complex will be completely inundated, as well as most of Pond #10a. In addition to the clear threats inundation poses to the built environment, this impact is also predicted to impact natural systems or ecosystems in several key ways. Inundation is expected to cause the landward migration of intertidal and upland natural environments, such as marshes, tidal flats, and dunes. However, if there is nowhere for these features to migrate due to adjacent development, then inundation could result in the complete loss or fracturing of these systems. The loss of these intertidal habitats would be highly destructive to the many species that rely heavily on their existence.

**3.5) Model Calibration:** We use monitoring data for the newly completed San Dieguito Lagoon Restoration Project to calibrate the TIDE\_FEM tidal hydraulics model; and then use that calibration to simulate tidal inundation of the three wetland restoration alternatives in the Otay River flood plain. The San Dieguito Lagoon monitoring data was collected by Coastal Environments (2009) during September 2009. We select the W-16 tidal basin at San Dieguito Lagoon as a proxy for the proposed tidal basin in the Otay River floodplain because of morphologic similarities between the two cases: in particular both have a long “goose-neck” feeder channel connecting source water to interior tidal basins of comparable acreage and distance from the source water.

Spring, neap and mean tidal range simulations of the tidal hydraulics of San Dieguito Lagoon were performed using astronomic tidal forcing functions at = 2 sec time step intervals for the period 1980-2007. Computed water surface elevations and depth averaged velocities from the global solution matrix were converted to lagoon waterline contours and flow trajectories. Calibrations for determining the appropriate Manning factors and eddy viscosities were performed by running the TIDE\_FEM model on the San Dieguito bathymetry file and comparing calculated water surface elevations in the W-16 tidal basins against water level measurements by Coastal Environments (2009) during the monitoring period of 14-18 September 2009. Iterative selection of Manning factor  $n_0 = 0.0261$  and an eddy viscosity of  $\varepsilon = 7.129 \text{ ft}^2/\text{sec}$  gave calculations of water surface elevation and inlet that reproduced the measured values to within 2% over the 2009 monitoring period at San Dieguito Lagoon.

Figure 20 provides a quantitative assessment of predictive skill of the calibrated model using water level measurements in the newly created W-16 Tidal Basin located east of I-5 off the north bank of the San Dieguito River. Here we compare W-16 Tidal Basin water level variations predicted by the model (purple trace) with the water level measurements (black crosses) during the post-construction monitoring of the Edison Plan by Coastal Environments, (2005). The W-16 Basin water level variations are found to lag the ocean water levels by as much as 3.79 hr during the mid-range tides of the monitoring period. High tide water levels equal or exceed those in the ocean due to trapping of higher harmonics of the K1 lunar-solar diurnal tidal constituent and the M2 principal lunar semi-diurnal tidal constituent, similar to what occurs in San Diego Bay. However, low tide water levels in the W-16 basin never drop below + 1.49 ft NGVD and are well above ocean low tide water levels due to frictional impedance and depth limiting travel time of the tidal wave propagation in the long sinuous feeder channels that connect the W-16 tidal basin



with the ocean. Low tide levels in W-16 could fall no lower than +0.23 ft NGVD due to the present elevation of the hard channel bottom under the I-5 bridge. The amplitudes and degree of non-linearity in the W-16 Basin water level time series are accurately simulated by the model and closely duplicate those features observed in the measured lagoon tides.

#### 4.0) Tidal Hydraulics of the Existing Otay River Floodplain

The TIDE\_FEM bathymetric computational mesh was initialized for the updated Otay River Floodplain bathymetry derived from the 2011 WRA precision GPS surveys (Figure 21). The TIDE\_FEM computational mesh is nested in the farfield of south San Diego Bay, and was subjected to 30 years of historic tidal forcing using the 1980-2009 period of record at the Navy Pier in San Diego Bay, after spectrally correcting that record to the mouth of the Otay River as detailed in Section 3.2 .

**4.1) Tidal Current Simulations:** Peak flooding currents during spring tides were simulated in the existing river channel in Figure 22, while ebbing currents during spring tides are found in Figure 23. These progressive vector diagrams show that flooding spring tidal currents are about 0.1 m/sec (0.33 ft/sec) at the river mouth and then accelerate to 0.18 m/sec (0.59 ft/sec) in the deeper sections of the inlet channel (north/south reach of the Otay River adjacent Ponds 10 and 11). Further up-river currents reach 0.15 m/sec (0.50 ft/sec) in the narrower east/west reach near the railroad bridge. Flood tide currents then decelerate to less than 0.01 m/sec (0.03 ft/sec) into the complex dendritic system of channels in the upper reaches of the flood plain.

The tidal currents calculated in the lower Otay River and feeder channel during spring tides (cf Figures 22 & 23) are compared against grain size data to estimate the potential for scour and erosion. A 2012 geotechnical investigation of the Otay River Floodplain was conducted by CalScience Environmental Laboratories, Inc. that included boring locations and some gradation curves in the lower Otay River channel. Figure 24a gives the grain size distribution from a composite sample of channel borings, indicating the river channel sediments are fairly well sorted (due to hydraulic sorting during river floods and perhaps relict wave action) with a median grain size of  $D_{50} = 0.3$  mm. Comparing this median grain size against the Hjulstrom Curve in Figure 24b indicates these river channel sediments have a threshold scour speed of 0.66 ft/sec (0.2 m/s). Tidal current speeds between 0.27 ft/sec (0.08 m/sec) and 0.66 ft/sec would lead to bed load transport but not erosion. Erosion and scour would only occur for tidal currents that exceed 0.66 ft/sec, while currents less 0.27 ft/sec would yield deposition. These transport thresholds of the native river bed sediments indicate that the only potentially problematic areas are the narrow, deep north-south reach of channel adjacent Ponds 10 and 11 and the two pinch points near the railroad bridge where a series of humps, shoals and scour holes are found in the river bathymetry. In the north/south reach adjacent to Ponds 10 and 11, the channel has already scoured to an equilibrium depth where maximum tidal currents reach but do not exceed the threshold scour speed of the channel sediments; and at the two pinch points near the railroad bridge maximum tidal currents approach but do not exceed the sediment incipient scour speeds. Under these conditions, tidal erosion does not occur since the sedimentary bed remains in a steady state of bed load transport. Thus a stable, quasi- equilibrium channel prevails, wherein there is incipient sediment transport without either erosion or deposition. One special attribute of

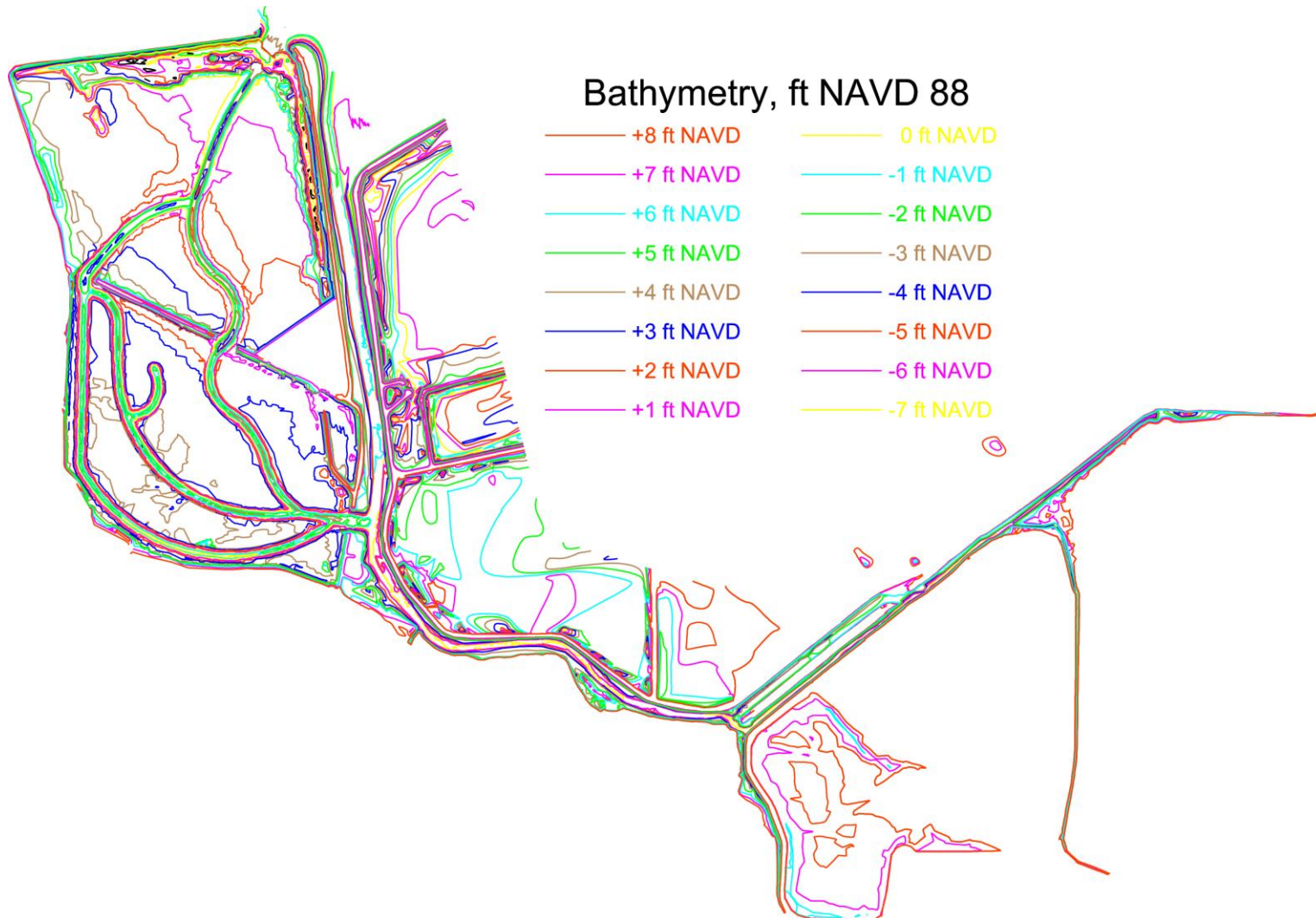


**Figure 21:** The updated Otay River Floodplain bathymetry derived from the 2011 WRA precision GPS survey.



**Figure 22:** Hydrodynamic simulation of progressive vector flow distribution at 30 min time integration during maximum flood flow during spring tides for the existing lower Otay River and salt pond system based on 2011 WRA bathymetric survey and the 1983-2001 tidal epoch for San Diego Bay tides.

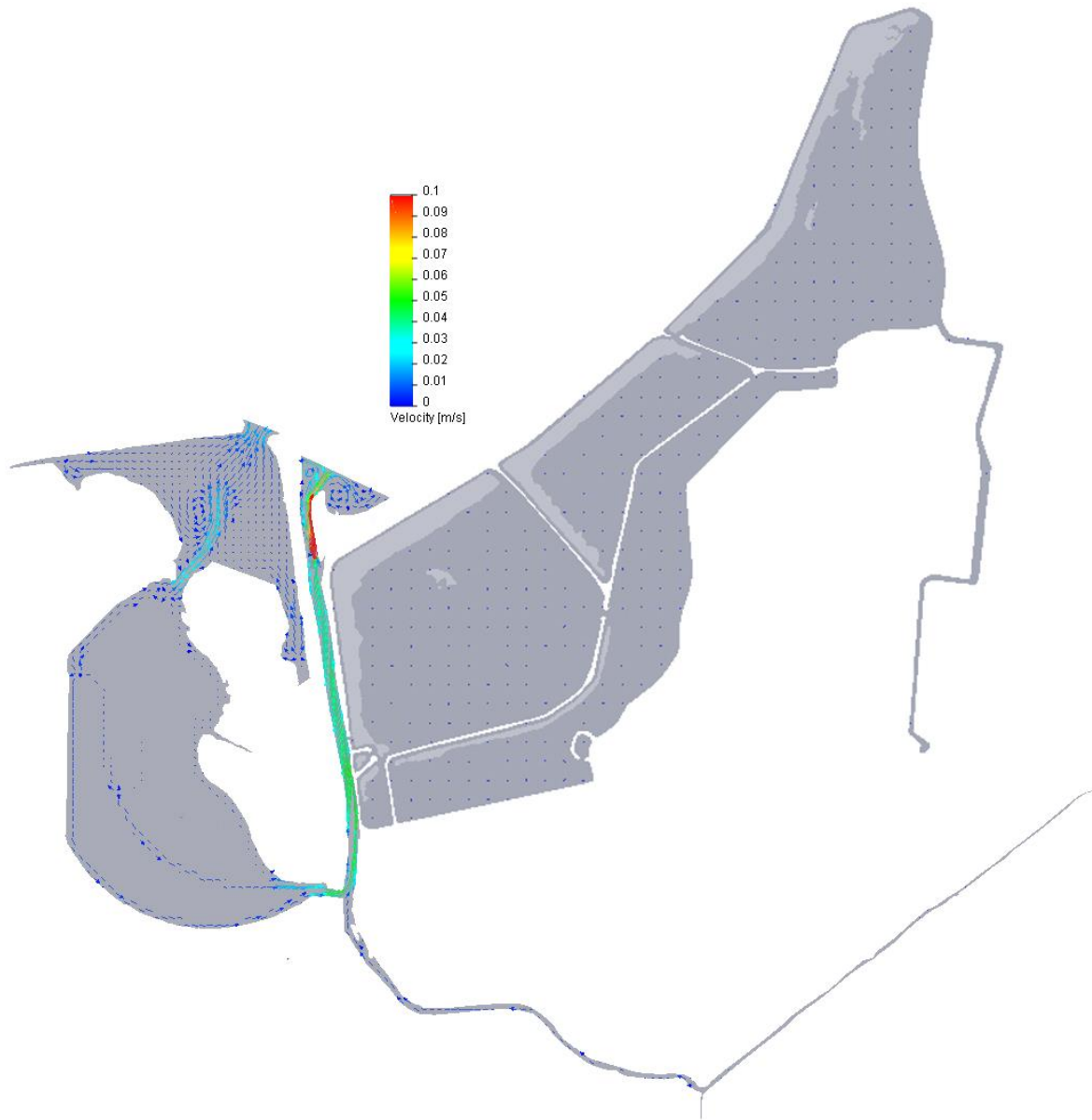


**Figure 23:** Hydrodynamic simulation of progressive vector flow distribution at 30 min time integration during maximum ebb flow during spring tides for the existing lower Otay River and salt pond system based on 2011 WRA bathymetric survey and the 1983-2001 tidal epoch for San Diego Bay tides.

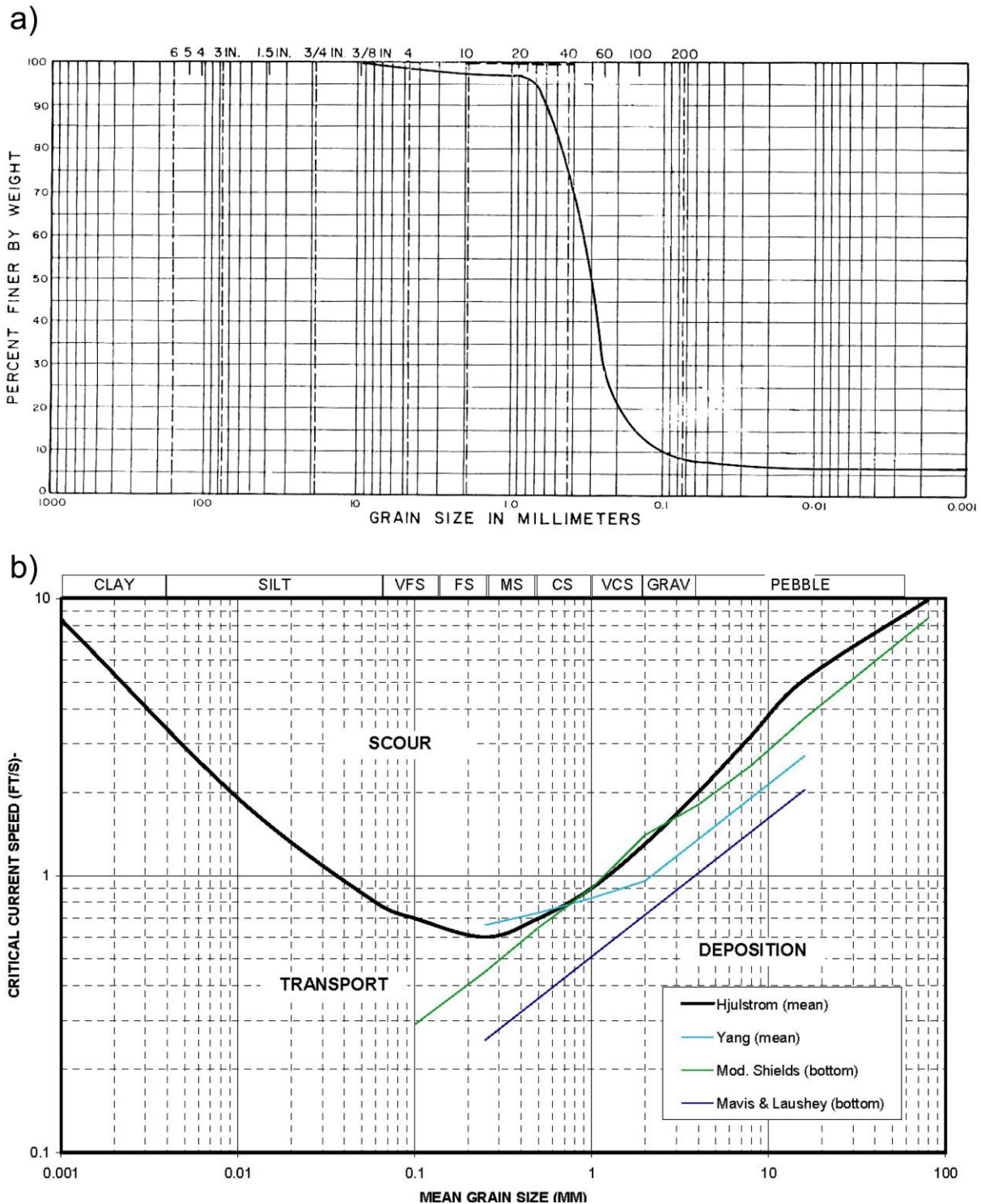


**Figure 24:** (a) Otay River channel grain size distribution from CalScience Environmental Laboratories, Inc., 15 May 2012. (b) Hjulstrom curve for critical current speeds of quartz sediment as a function of mean grain size, from Everest, (2007).

this site is that the inlet channel and the mouth of the Otay River are not subject to littoral transport by shoaling ocean waves, as south San Diego Bay provides complete sheltering from high energy shoaling swells. Consequently, the inlet channel is not likely to infill or close from sand influx in the source water, making the site significantly easier to maintain.

**4.2 Hydroperiod Simulations:** The hydroperiod function gives the percentage of exposure for each elevation throughout the full range of lagoon water level variation. This is the primary physical factor limiting the type of habitat that will thrive at a particular elevation in the wetland. These relationships are used later (Sections 4 & 5) to transpose tidal hydraulics model output into calculations of acreage of various wetland habitat types created by the two restoration alternatives.

The spectrally corrected San Diego Bay water levels for the 1980-2009 period of record were used to drive the TIDE\_FEM model at the mouth of the Otay River in order to solve for the time series of the water level variation in the existing Otay River floodplain. The computations involved  $N_o = 2,629,800$  time steps, each 6 minutes in length, in order to sweep the 30 year period of record. At each time step the average basin water elevation,  $\hat{\eta}$  was calculated from the ensemble average of the solutions at the nodes in the computational mesh. Conditional if statements and counting loops inserted into the TIDE\_FEM code would count the number time steps,  $N$ , for which the average lagoon water elevation was less than a particular elevation,  $Z_i$ . The percent time that elevation  $Z_i$  was exposed over the period of record was calculated as:

$$E_i = \frac{100\%}{N_o} \sum N(\hat{\eta} < Z_i) \quad (18)$$

The elevations dividing the various sub-tidal and intertidal habitat types are based on biological surveys conducted during the San Dieguito Lagoon Restoration Project by Josselyn & Whelchel (1999), and then later updated by vegetation surveys in the lower Otay River flood plain by Josselyn (2012). These surveys are mapped according to elevations and are used to develop functional relationships (referred to as a *hydroperiod function*) between habitat breaks and the exposure times computed from equation (18). From this procedure, the following exposure times were assigned to each habitat break:

**TABLE 2:** Exposure Levels for Hydroperiod Habitat Breaks

<b>Subtidal Exposure</b> < 0%;
0% < <b>Frequently Flooded Mud Flat Exposure</b> < 38%
38% < <b>Frequently Exposed Mud Flat Exposure</b> < 45%;
45% < <b>Low Salt Marsh Exposure</b> < 75%
75% < <b>Mid Salt Marsh Exposure</b> < 95%
95% < <b>High Salt Marsh Exposure</b> < 99.6%
99.6% < <b>Transitional Exposure</b> < 100%

Figure 25 below gives the hydroperiod function that was determined by this analysis the existing Otay River flood plain, and which is subsequently applied to the grading plans of the proposed restoration alternatives to determine the numbers of restored acres of each wetland habitat type. While the shape of this curve may vary with the particular restoration alternatives, the percent exposure times will determine the elevations on at which a particular habitat break occurs, and those elevations will in turn map into the grading design to determine the amount of acreage of each habitat type.

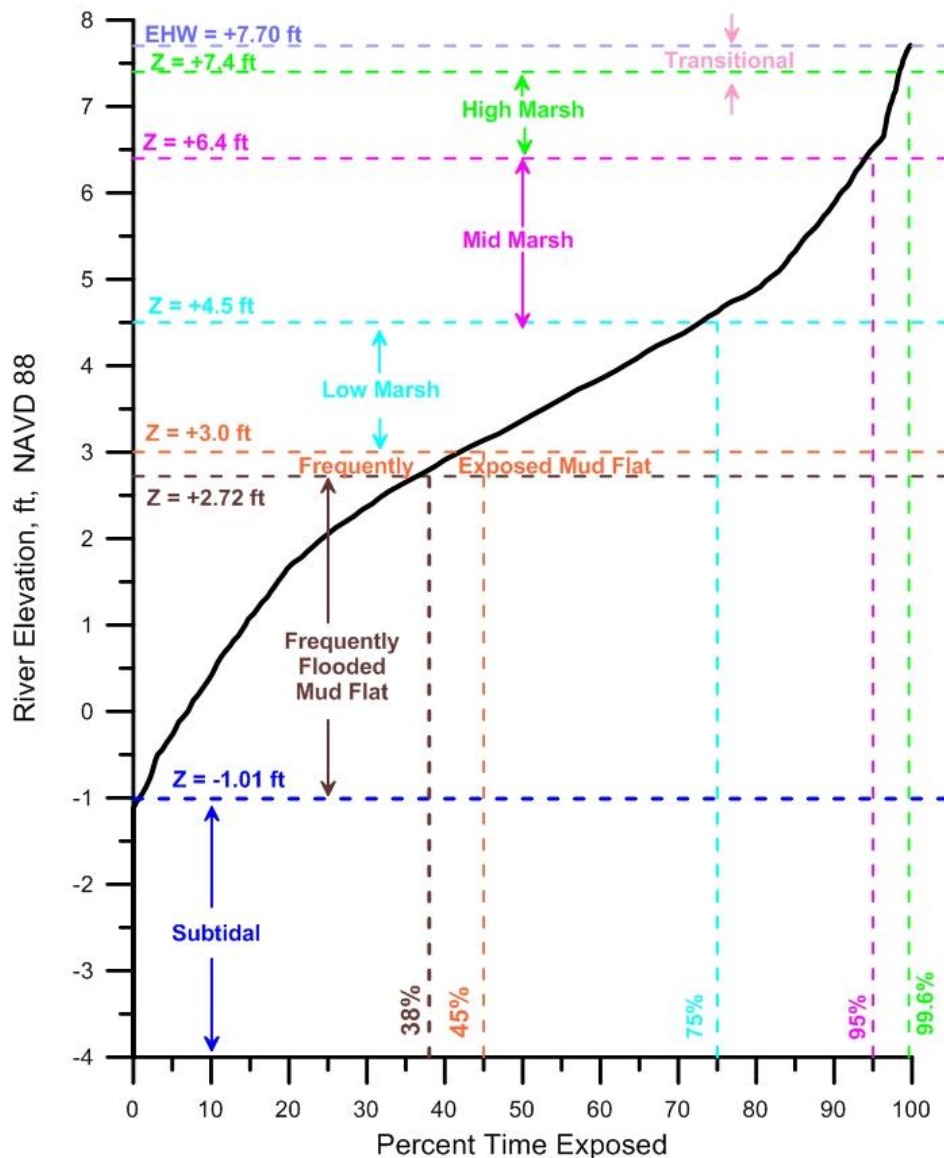


**Figure 25.** Hydroperiod function of the existing Otay River floodplain based on WRA 2011 bathymetric survey applied to water level data from NOAA tide gage #941-0170, for tidal epoch 1983-2001, with spectral correction from Otay River Sonde. Mannings roughness:  $n_0 = 0.0261$

## 5.0 Analysis of the Intertidal Alternative:

The model, analysis methods, and supporting data bases used herein are the same as those utilized in the Environmental Impact Report/Environmental Impact Statement (EIR/EIS) for the San Dieguito Wetland Restoration Project, (EIR/EIS, 2000), and for the preparation of the San Dieguito Wetlands Restoration Project, Final Restoration Plan, (SCE, 2005). Monitoring data for the newly completed San Dieguito Lagoon Restoration Project was also used to calibrate tidal hydraulics model. San Dieguito Lagoon was selected as a proxy for the restoration alternatives because of morphologic similarities: in particular, both restoration sites have a long “goose-neck” feeder channel connecting source water to interior tidal basins of comparable acreage and distance from the source water. Habitat surveys conducted during the San Dieguito Lagoon Restoration Project by Josselyn & Whelchel (1999), and then later updated by vegetation surveys in the lower Otay River flood plain by Josselyn (2012), were used to develop functional relationships between habitat breaks and amounts of time for wetting and drying (hydroperiod functions). These relationships were used to transpose tidal hydraulics model output into calculations of acreage of various wetland habitat types created by the *Intertidal* restoration plan. Calculations of habitat creation were based on long-term tidal hydraulics simulations using tidal forcing at the mouth of the Otay River, derived from a spectral correction applied to the NOAA tide gage #941-0170 located at the Navy Pier (cf. Section 3.2)

**5.1 Bathymetric Input for the Intertidal Alternative:** Grading contours for the Intertidal Alternative were provided in 0.5 ft intervals between -4.0 ft NAVD and + 10 ft NGVD by KTU+A. The TIDE\_FEM tidal hydraulics model presented in Jenkins and Inman (1999) was gridded for a computational mesh of the Intertidal Alternative built off the bathymetry in Figures 4 and 5. Figure 4 details the elevation grading contours of the Intertidal Alternative tidal basin in the Otay River floodplain merged with the Otay River bathymetry; while Figure 5 gives the elevation contours resulting from cut and fill of the Pond-15 tidal basin for the Intertidal Alternative. Of particular interest to the finite element mesh is the *hydraulic friction slope coefficient*,  $S_{ff}$ , providing tidal muting effects. Two separate formulations are used. One is given for the 3-node triangular elements situated in the interior of the mesh which do not experience successive wetting and drying during each tide cycle. The other formulation is for the elements situated along the wet and dry boundaries of the lagoon. These have been formulated as 3-node triangular elements with one curved side based upon the cubic-spline matrices developed by Weiyan (1992). These two sets of elements were assembled into a computational mesh of the restoration whose upper boundary conforms to the + 10 ft. NGVD contours in Figures 4 and 5. The + 10 ft. NGVD contour was chosen to allow sufficient computational domain to evaluate tidal inundation at 2050 sea levels that are as much as + 2.0 ft above present sealevel. The wet-dry boundary coordinates of the curved waterline,  $(x', y')$ , are linearly interpolated for any given water elevation from the contours stored in the bathymetry file.

Aside from gridding the TIDE\_FEM tidal model, storage rating functions were calculated from the bathymetric contours of Figures 4 and 5. Figure 26 gives the storage rating function of the floodplain tidal basin merged with the tidally influenced lower reach of the Otay River; while Figure 27 gives the storage rating function for the Pond 15 tidal basin as configured for the

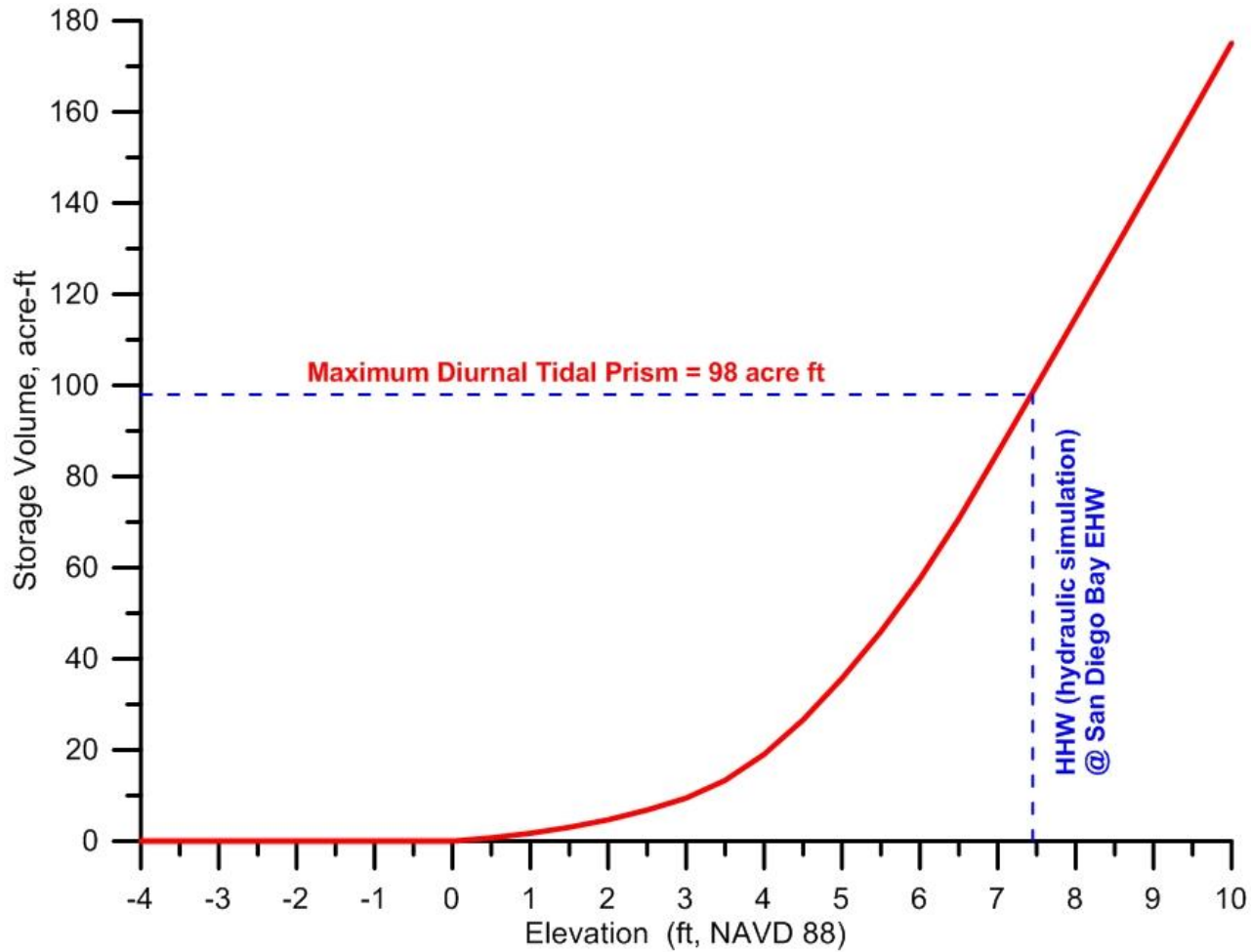


**Figure 26:** Storage rating function of the tidal basin in the Otay River floodplain for the Intertidal Alternative with no dredging of the existing river channel. Maximum diurnal tidal prism shown for extreme high-water event in San Diego Bay, 27 January 1983.

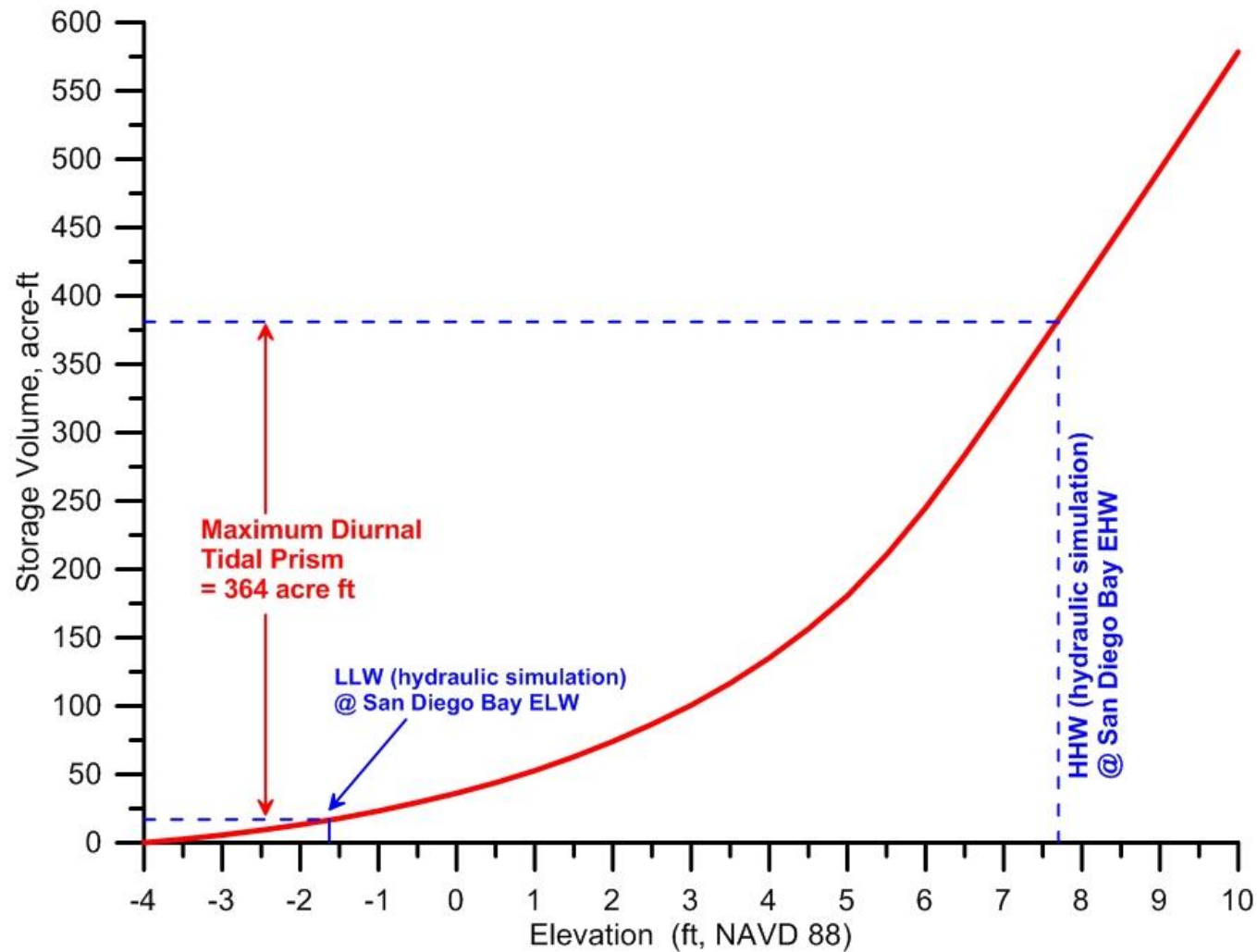


**Figure 27:** Storage rating function of the Pond 15 tidal basin for the Intertidal Alternative. Maximum diurnal tidal prism shown for extreme high-water event in San Diego Bay, 27 January 1983.

Intertidal Alternative. The storage rating functions are used in the initialization of the TIDE\_FEM tidal hydraulics model in order to enforce mass conservation in the tidal inundation simulations (see Jenkins and Inman, 1999). The initialization involves fitting a series of high-order polynomials to the volumes of the storage rating function in Figure 26 & 27. To accommodate possible future sea level rise the polynomial fits were carried up to a daylight contour chosen at +10.0 ft NGVD, even though the tidal inundation in San Diego Bay has never been observed above +7.71 ft NGVD. A fifth-order polynomial was fitted to the storage rating functions in Figures 26 & 27 with a coefficient of determination of  $r^2 = 0.998$ .

For tidal inundation up to the historic extreme high water level of San Diego Bay (EHW = +7.71 ft NGVD, (upper dashed blue line in Figure 26), the maximum volume of San Diego Bay water that is exchanged with the Intertidal Alternative floodplain tidal basin is 98 acre-ft. The maximum potential diurnal tidal prism of the Pond 15 tidal basin of the Intertidal Alternative is 364 acre ft for an extreme high water event at present sea level.

**5.2 Tidal Inundation Simulations of the Intertidal Alternative:** Figure 28 gives the flow trajectories and depth averaged tidal currents for the Intertidal Alternative computed by the calibrated TIDE\_FEM model during spring flooding tides on 18 September 2009. Velocities of tidal currents are portrayed according to the color coded velocity scale appearing in the lower left corner of the figure. Maximum flooding spring tidal currents at the mouth of the Otay River (in the neighborhood of the Otay Sonde) are about 0.10 m/sec (0.33 ft/sec), and then accelerate in the narrower north/south reach of the channel adjacent to Ponds 10 & 11 to 0.2 m/sec (0.66 ft/sec) where the channel has scoured under existing conditions to equilibrium depths on the order of -2.0 ft NAVD. After passing Pond 10, currents decelerate and then increase to 0.17 m/sec (0.55 ft/sec) near the two pinch points at the railroad bridge, before entering the floodplain tidal basin; where tidal currents entering the tidal basin initially form a well-defined jet at the west bank with speeds of about 0.08 m/s (0.26 ft/sec). This entry jet quickly diverges into a complex set of clockwise rotating eddies that populate the interior of the tidal basin. Eddy speeds in the tidal basin are on the order of 0.02 m/sec (0.07 ft/sec), insufficient to transport fine sand but an important stirring mechanism for mixing the tidal basin water mass to maintain high oxygen levels and to sustain fine silt and clay sized sediment particles in suspension. Maximum flooding spring tidal currents in the inlet channel to Pond #15 are about 0.07 m/sec (0.22 ft/sec), and then decelerate as a weak entry jet with speeds of about 0.05 m/s (0.16 ft/sec). This entry jet also quickly diverges into a complex set of counter rotating eddies that populate the interior of the tidal basin. Eddy speeds in the Pond #15 tidal basin are on the order of 0.01 m/sec (0.03 ft/sec), again insufficient to transport fine sand or cohesive silts, but also providing a stirring mechanism for mixing the Pond #15 water mass to maintain high oxygen levels and to sustain suspension of fine silt and clay sized sediment particles.

Figure 29 gives the flow trajectories and depth averaged tidal currents for the Intertidal Alternative computed by the TIDE\_FEM model during spring ebbing tides on 18 September 2009. The wetted area of the floodplain tidal basin is significantly reduced relative to the flood tide area in Figure 28, due to the fact that the grading plan allows for almost complete drainage at mean low water tidal stages. In Figure 29, creeping flow drains from the remnant dendritic channel of the floodplain basin, forming a feeder current in the upper river channel with speeds

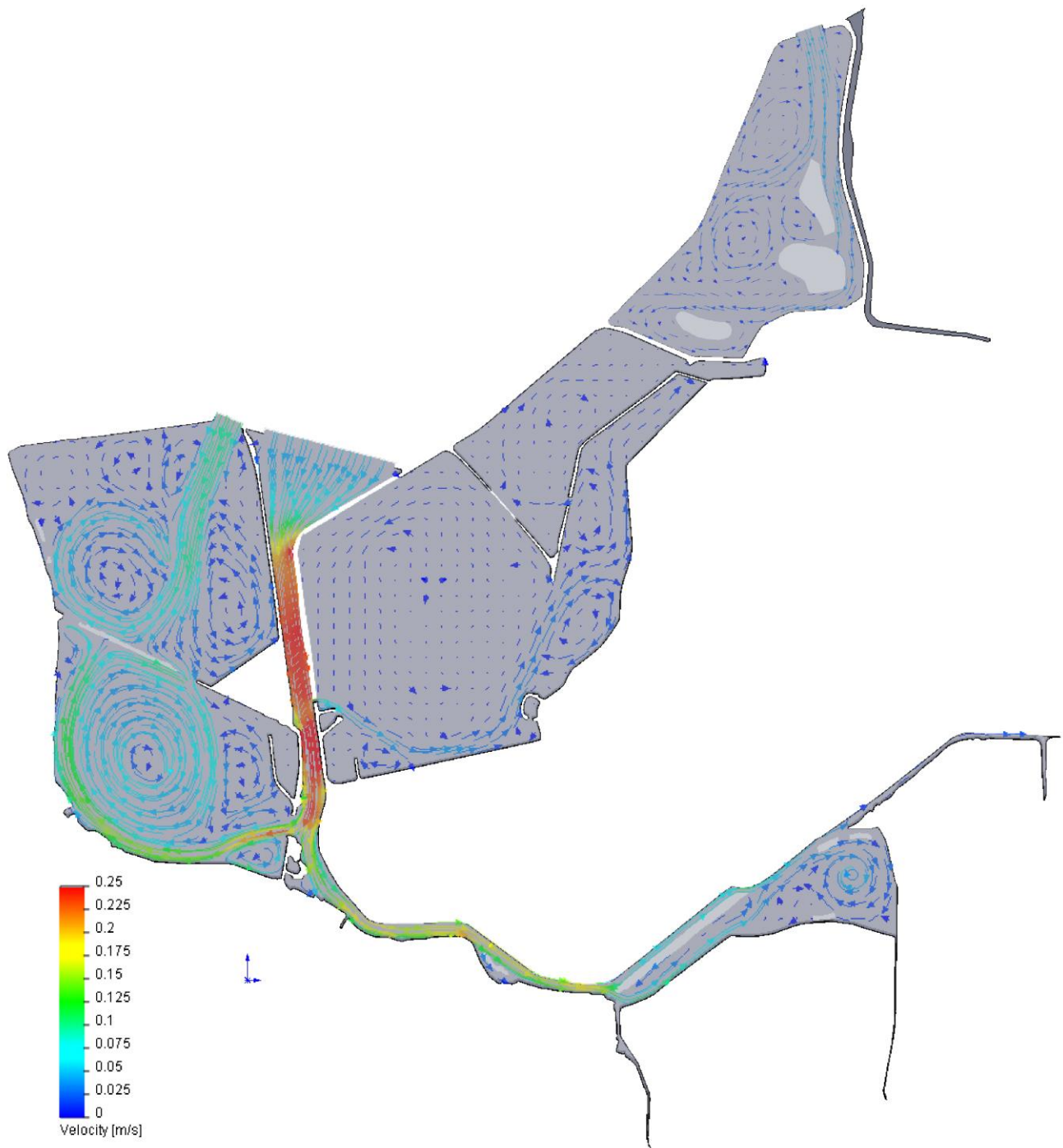


**Figure 28:** Intertidal Alternative flood tide progressive vector flow simulation at Mean High Water (MHW), where vector trajectories are plotted over 30 minute time integrations.

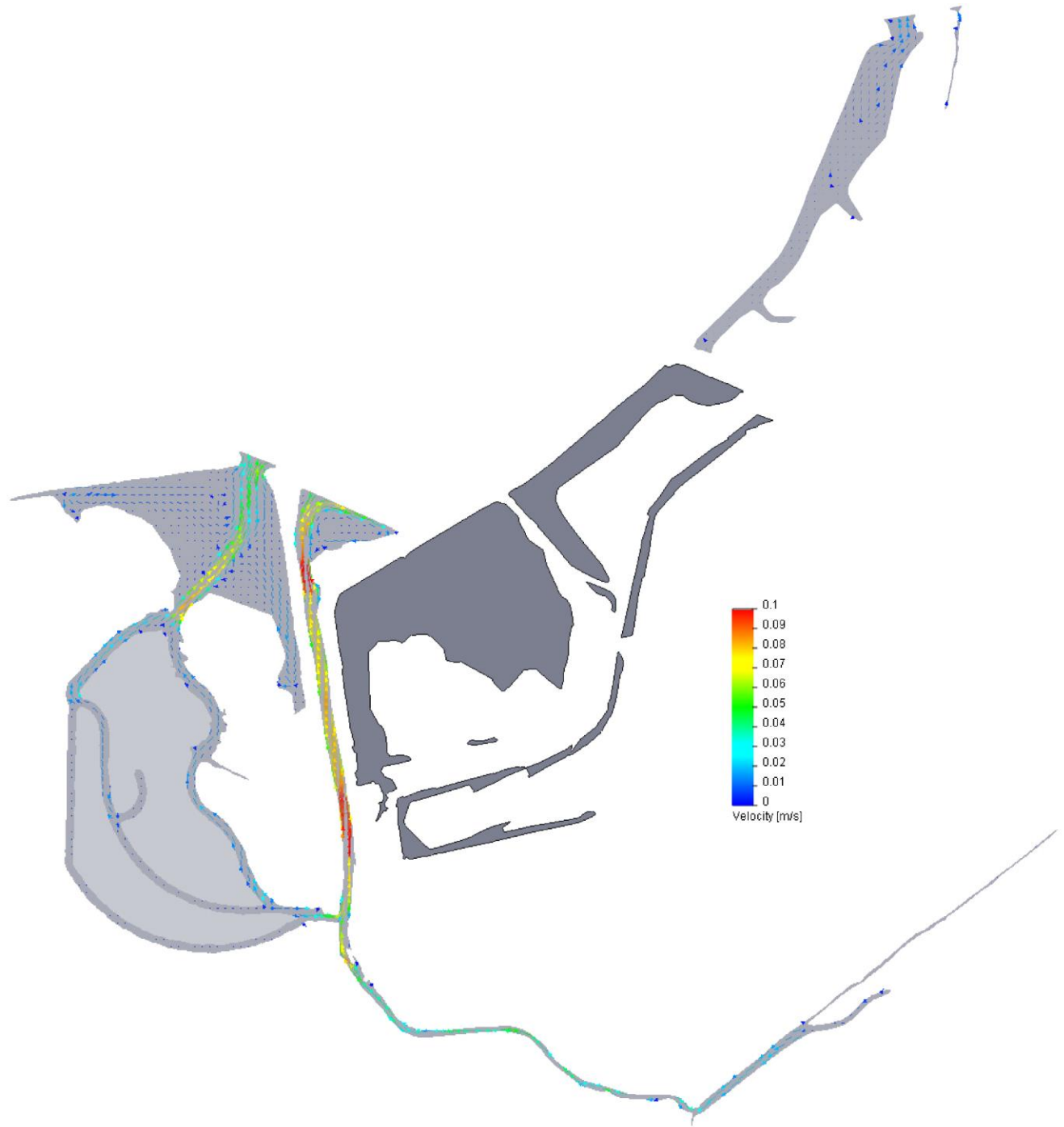


**Figure 29:** Intertidal Alternative ebb tide progressive vector flow simulation at Mean Low Water (MLW), where vector trajectories are plotted over 30 minute time integrations.

on the order of  $-0.01$  m/sec, or  $(-0.03$  ft/sec). This feeder current evacuates the tidal basin and then accelerates to  $-0.05$  m/sec  $(-0.16$  ft/sec) as it passes through the pinch point under the railroad bridge in the narrow east/west reach of channel. (We adopt the convention of negative velocities for ebb tide flows and positive velocities for flood tide flows). Ebb flow in the channel then accelerates further to  $-0.09$  m/sec  $(-0.289$  ft/sec) in the deeper north/south reach before discharging into San Diego Bay. In Pond #15 during ebb tide flow at mean low water level, the eastern half of the basin is completely drained and exposed, while a weak feeder current evacuates the western half with ebb flow of about  $-0.02$  m/sec  $(-0.07$  ft/sec). This feeder current accelerates to about  $0.06$  m/sec  $(0.20$  ft/sec), as it flows out the inlet of Pond #15, and is far below the threshold scour speed of the sediments along the bank of the Chula Vista Wildlife Reserve.

In Figure 30, tidal current speeds at the mouth of the Otay River for the Intertidal Alternative are simulated throughout an entire spring-neap tidal. These currents (plotted in red) are compared the threshold scour speeds for native river bed channel sediments as derived from the Hjulstrom Curve in Figure 24b based on grain size data in Figure 24a. These thresholds of incipient scour appear as red dashed lines for flood (positive) and ebb flow (negative) velocity sign conventions. It is apparent that ebb and flood flow velocities throughout a spring/neap cycle never reach the thresholds of incipient scour, where maximum flood flow velocity at the mouth of the Otay River is  $+0.329$  ft./sec, while maximum ebb flow velocity reaches only  $-0.289$  ft./sec under the Intertidal Alternative. These flood and ebb flow maximums are consistent with the progressive vector simulations in Figures 28 & 29. Figure 31 gives the corresponding spring/neap velocity time series at the inlet to Pond 15 of the Intertidal Alternative. Because of the large non-equilibrium cross section engineered for this inlet, velocities are considerably less than at the mouth of the Otay River. For Pond 15, maximum flood flow velocity at the inlet is  $+0.224$  ft./sec, while maximum ebb flow velocity reaches only  $-0.196$  ft./sec, well below the threshold scour speeds for the native sediments estimated to be  $\pm 0.66$  ft./sec from the the Hjulstrom Curve in Figure 24b. Tidal current speeds between  $0.27$  ft/ sec  $(0.08$  m/sec) and  $0.66$  ft/sec would lead to bed load transport but not erosion. Erosion and scour would only occur for tidal currents that exceed  $0.66$  ft/sec, while currents less  $0.27$  ft/sec would yield deposition. Therefore the mouth of the Otay River would be in steady state equilibrium that is neither depositional nor erosional under the Intertidal Alternative. However, the inlet to Pond 15 under the Intertidal Alternative could be depositional if there is an active sediment source nearby. However no such source appears to exist, other than perhaps very minimal and undocumented sediment yield from the Palomar Ditch during occasional El Nino floods. Littoral sediment transport by waves is generally de minimis due to the limited fetch across South San Diego Bay, and the inlet to Pond 15 is sheltered from direct wave exposure by the causeway of the Chula Vista Nature Reserve (cf. Figure 1).

Therefore, we conclude both source water inlets to the tidal basins of the Intertidal Alternative are stable and immune to closure or restriction by sedimentation under dry weather tidal exchange. (Wet-weather conditions are addressed in a companion study, Everest, 2014). Inlet sedimentation due to influxes of wave driven long-shore transport of sand (as occurs on the open coast), does not occur in the fetch limited environment of South San Diego Bay. The mouth of the Otay River that supplies source water to the floodplain tidal basin is in a dynamic steady-

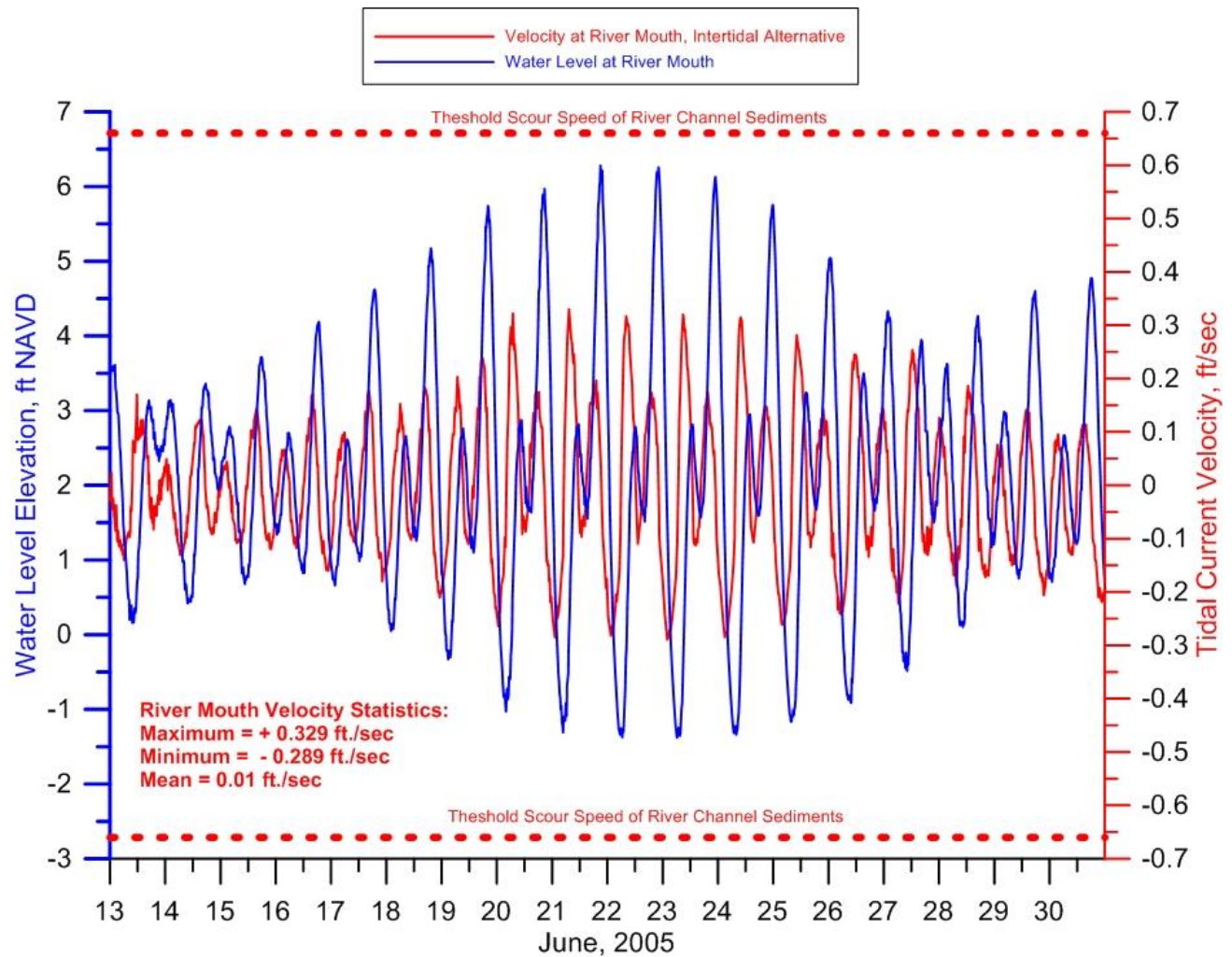


**Figure 30:** Tidal current speeds at the mouth of the Otay River as computed in red for the Intertidal Alternative throughout a spring-neap tidal cycle shown in blue. Threshold scour speeds for native river bed channel sediments shown as red dashed lines for flood and ebb flow conditions.

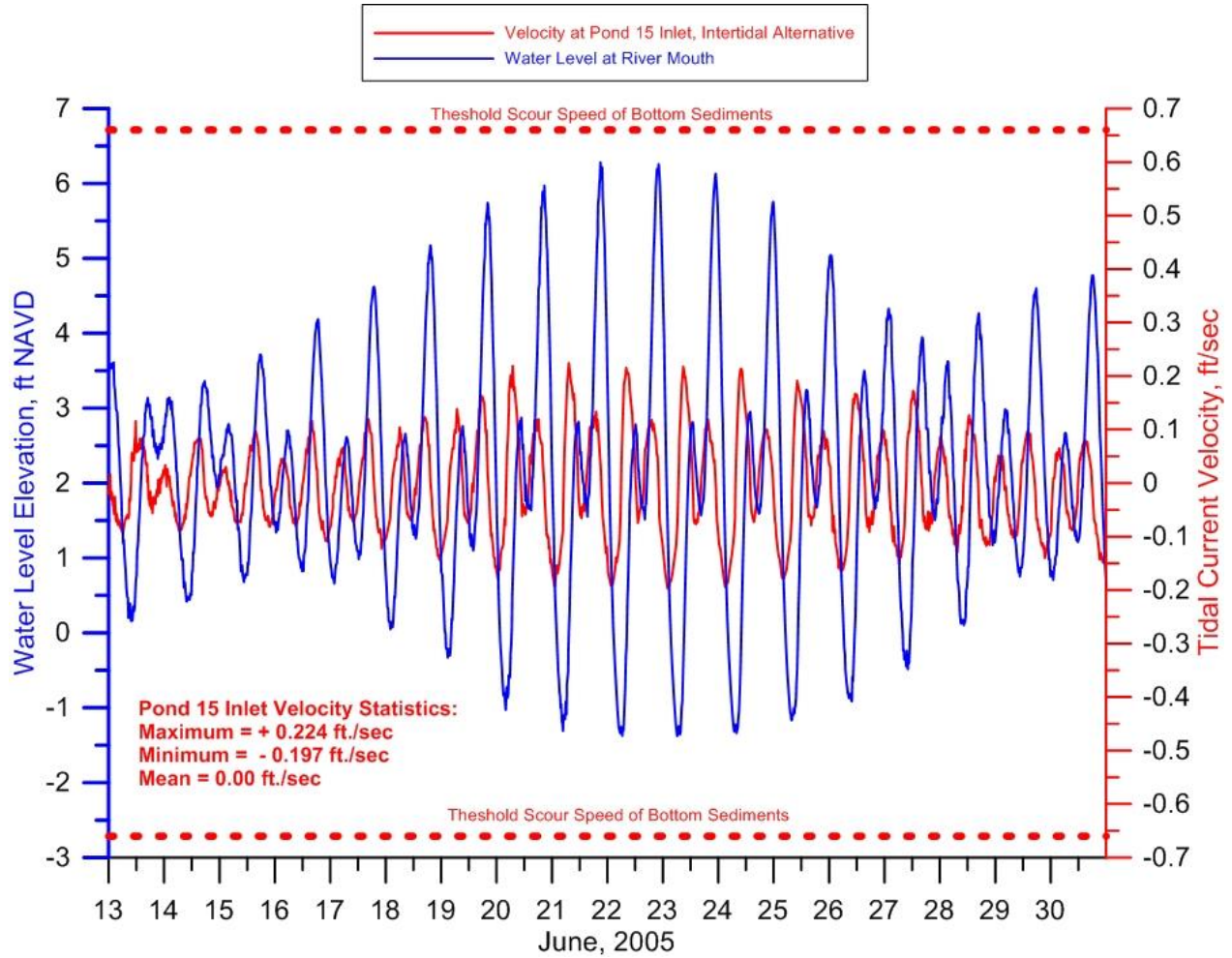


**Figure 31:** Tidal current speeds at the inlet to Pond 15 as computed in red for the Intertidal Alternative throughout a spring-neap tidal cycle shown in blue. Threshold scour speeds for native river bed channel sediments shown as red dashed lines for flood and ebb flow conditions.

state equilibrium that is neither depositional nor erosional, while the inlet to Pond 15 will remain in a non-equilibrium stationary state (as-built) in the absence of a local sediment sources or adequate fluid forcing by waves and currents that might otherwise import sediment from more distant sources.

Water elevations in the Intertidal Alternative floodplain basin are shown in Figure 32 for spring tides that occurred during 14-18 September, 2009, the same time period used for the model calibration with the proxy tidal system at San Dieguito Lagoon in Figure 20. Figure 32 provides a comparison between the water levels in the Intertidal Alternative floodplain tidal basin as predicted by the model (red trace) versus the actual San Diego Bay water level measurements (blue) reported by the Otay Sonde. The Intertidal Alternative floodplain tidal basin water level variations in red are found to lag the Bay water levels by as much as 27 minutes at higher high water (HHW) levels on flooding tides while this phase lag averages 2.46 hours at lower low water (LLW) level during ebb tides. These phase lags are an unavoidable consequence to frictional impedance and depth limited tidal propagation speeds down the 7,000 ft long channel that connects the floodplain tidal basin with the Bay. Lower low water levels in the Intertidal Alternative floodplain tidal basin are as much as 1.20 ft above South Bay water levels at the mouth of the Otay River due to the grading design which allows the floodplain basin to fully drain at LLW.

Higher high water levels in the Intertidal Alternative floodplain tidal basin sometimes exceed those in the South Bay at the river mouth by as much as +0.31 ft, (Figure 32), due to a trapped tidal modes (standing wave) typical of lagoons with large tidal basins and multiple choke point linkages to the ocean tides (Lamb, 1932; LeBlond & Mysak, 1978). Figure 33 shows these trapped modes are higher harmonics of the K1 lunar-solar diurnal tidal constituent and the M2 principal lunar semi-diurnal tidal constituent. Figure 14b plots the auto spectra of the Alternative-1 tidal basin tides and shows the predominant energy is centered on a diurnal frequency of the K1 lunar-solar diurnal tidal constituent at  $f_{K1} = 1.16079 \times 10^{-5}$  Hz and the M2 principal lunar semi-diurnal tidal constituent,  $f_{M2} = 2.2365 \times 10^{-5}$  Hz. The higher harmonics that lead to elevated basin high tide levels are a baroclinic *resonance* formed by a *triad* at the sum of the frequencies of the K1 and M2 barotropic tides, ie a diurnal third harmonic at a frequency  $f_3 = f_{K1} + f_{M2} = 3.3973 \times 10^{-5}$  Hz. This diurnal third harmonic is a baroclinic tide excited by the barotropic K1 and M2 tides interacting with the bottom topography, principally the long inlet channel to the Intertidal Alternative floodplain tidal basin. Another baroclinic resonance apparent in the spectra of the ocean tides in Figure 33 is a second harmonic of the barotropic M2 tide appearing at a frequency of  $2f_{M2} = 4.4730 \times 10^{-5}$  Hz. An additional non-linear resonance appears as a triad formed by the sum of the K1 barotropic mode and the baroclinic second harmonic of the M2 tide,  $f_{K1} + 2f_{M2} = 5.6338 \times 10^{-5}$  Hz. Apparently this mode is excited by non-linear tidal interaction with the tidal basin and channel bathymetry.

The hydroperiod function (used to calculate the habitat acreage creation of the Intertidal Alternative) is calculated by the model for both present and future extremes of sea level in the year 2050 from estimates of both maximum and minimum sea level rise. Using the methods detailed in Sections 3.2 and 3.4 for providing long-term, locally relevant tidal forcing for the model, the hydroperiod functions are calculated at present and future sea levels for the Intertidal

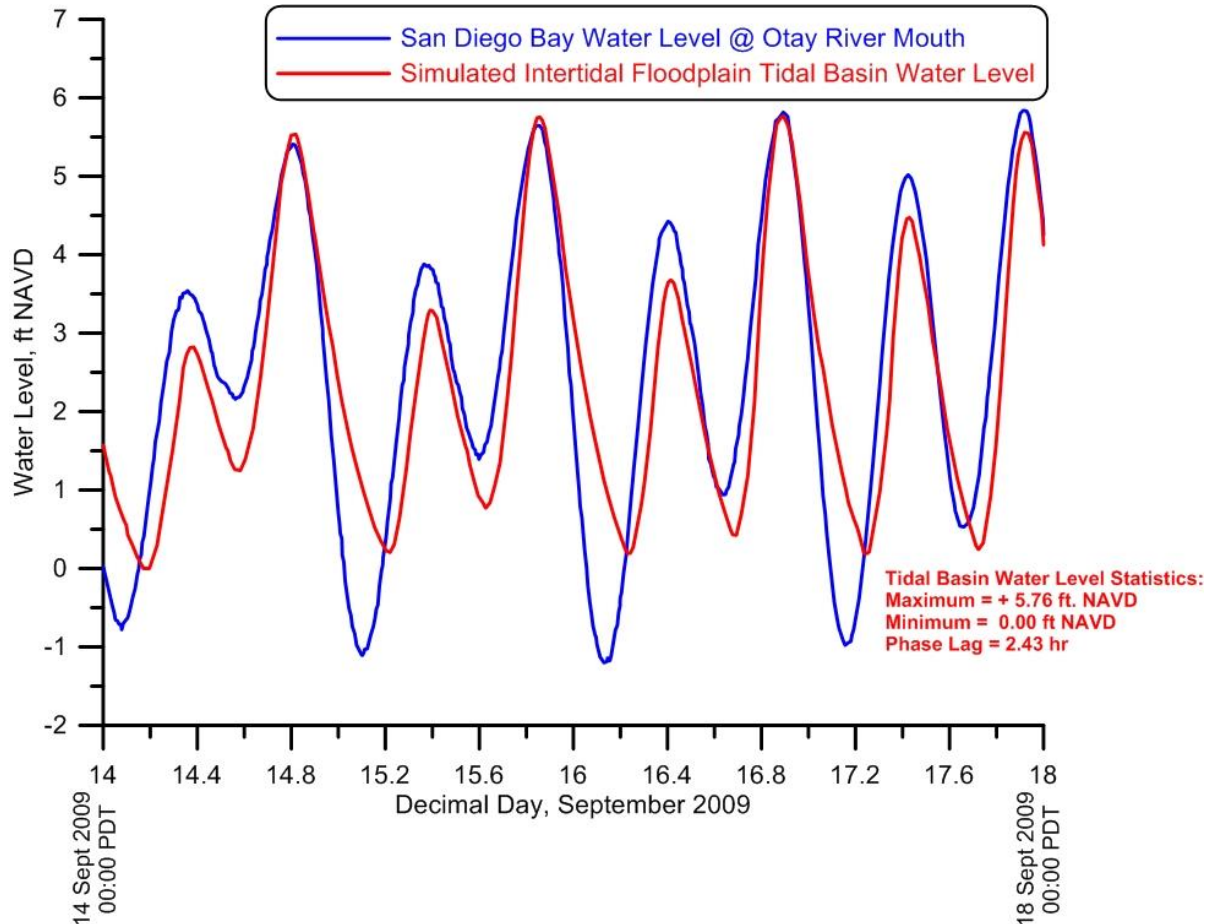


**Figure 32:** Water level elevations at the mouth of the Otay River (blue) compared to model simulation of Intertidal Alternative floodplain basin water levels (red) during spring tides, 14-18 September 2009.

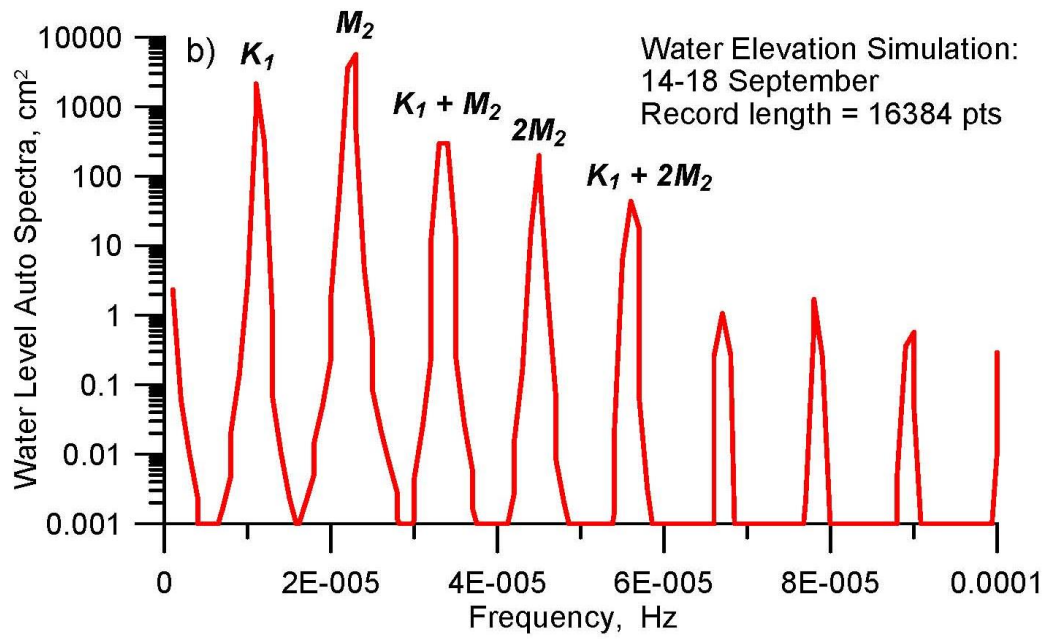


**Figure 33:** Auto spectra of water level elevations in the at the floodplain basin of the Intertidal Alternative during spring tides, 14-18 September 2009.

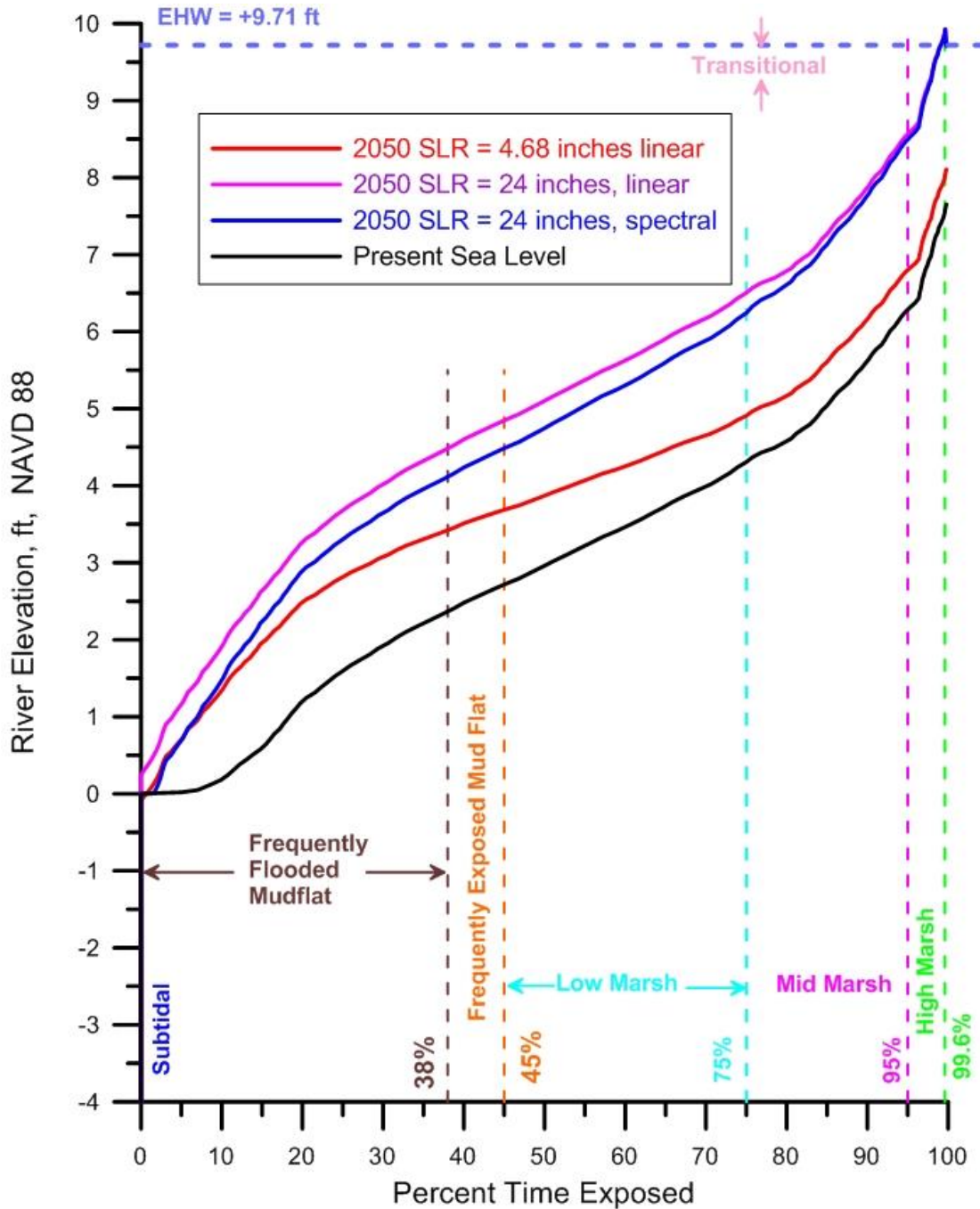


**Figure 34:** Hydroperiod Function for Intertidal Alternative, Otay Floodplain Tidal Basin for present sea level and 2050 sea level rise per CAT OPC guidance. Based on Otay Habitat Survey Data Evaluated By Josselyn (2012) and water level data from NOAA tide gage #941-0170, with spectral correction from Otay River Sonde. Manning's roughness,  $n = 0.0261$

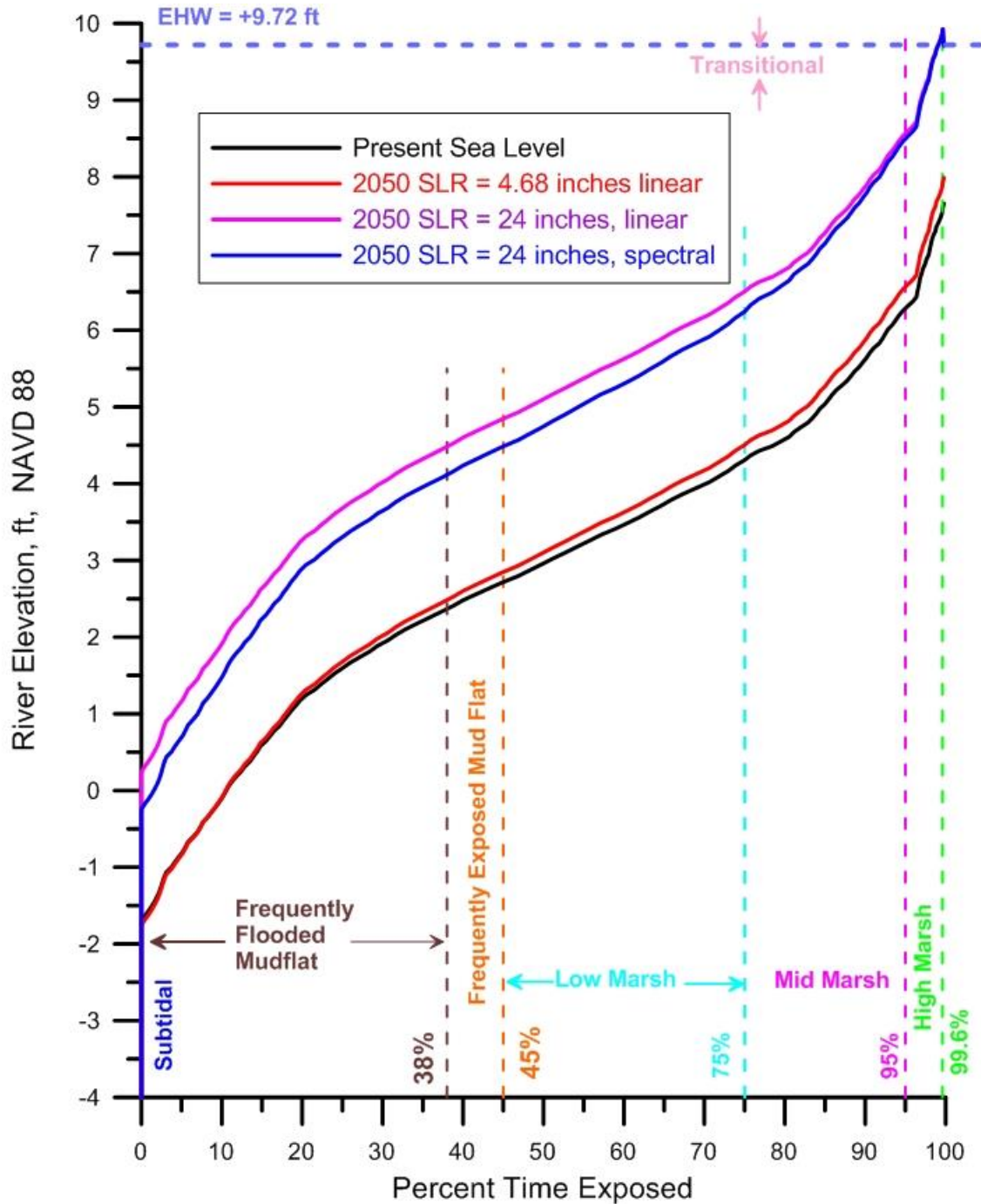


**Figure 35:** Hydroperiod Function for the Intertidal Alternative Pond #15 Tidal Basin for present sea level and 2050 sea level rise per CAT OPC guidance. Based on Otay Habitat Survey Data Evaluated By Josselyn (2012) and water level data from NOAA tide gage #941-0170, with spectral correction from Otay River Sonde. Manning's roughness,  $n0 = 0.0261$ .

Plan floodplain basin in Figure 34 and for the Pond #15 basin in Figure 35. The elevation breaks (zonation) between the different wetland habitat types from the hydroperiod curves are summarized in Tables 3 and Tables 4. The elevations for the habitat breaks in these figures and tables are applied to the KTUA grading designs and yield the acreages of habitat creation listed in Table 5 at present sea level, and at 2050 sea levels in Table 6.

**Table 3:** Elevations of Upper Limits of Habitat Breaks in the Intertidal Plan Floodplain Basin

Elevation of Habitat Breaks (Units of ft. NAVD 88)	@ Present Sea Level	@ 4.68 in. linear Sea Level Rise	@ 24 in. linear Sea Level Rise	@ 24 in. spectral Sea Level Rise
Sub-tidal	0.00 ft.	0.00 ft.	0.25 ft.	0.00 ft.
Frequently Flooded Mud Flat	2.40 ft.	3.40 ft.	4.50 ft.	4.10 ft.
Frequently Exposed Mud Flat	2.70 ft.	3.70 ft.	4.85 ft.	4.45 ft.
Low Marsh	4.30 ft.	4.90 ft.	6.55 ft.	6.25 ft.
Mid Marsh	6.30 ft.	6.80 ft.	8.55 ft.	8.50 ft.
High Marsh	7.55 ft.	8.05 ft.	9.71 ft.	9.71 ft.

**Table 4:** Elevations of Upper Limits of Habitat Breaks in the Intertidal Plan Pond 15 Basin

Elevation of Habitat Breaks (Units of ft. NAVD 88)	@ Present Sea Level	@ 4.68 in. linear Sea Level Rise	@ 24 in. linear Sea Level Rise	@ 24 in. spectral Sea Level Rise
Sub-tidal	-1.65 ft.	-1.70 ft.	0.25 ft.	-0.25 ft.
Frequently Flooded Mud Flat	2.40 ft.	2.50 ft.	4.50 ft.	4.10 ft.
Frequently Exposed Mud Flat	2.70 ft.	2.85 ft.	4.85 ft.	4.45 ft.
Low Marsh	4.30 ft.	4.50 ft.	6.50 ft.	6.25 ft.
Mid Marsh	6.30 ft.	6.55 ft.	8.55 ft.	8.50 ft.
High Marsh	7.50 ft.	7.90ft.	9.72 ft.	9.72 ft.

For all possible sea level scenarios, the elevation limit of subtidal habitat in the floodplain basin (Figure 34) is limited by the grading design (Figure 4) and by existing bars and channel bottom features at the inlet and inside the branch channel into this basin that create an inlet sill at 0.0 ft NAVD 88. The Intertidal Alternative calls for no construction dredging of the existing Otay River channel so as not to disrupt existing habitat residing down-river from the inlet to the proposed floodplain basin. That existing down-river habitat consists of additional mud flat residing below – 0.0 ft NAVD 88 and subtidal habitat below -1.01 ft NAVD 88 (cf. Section 4). Low tide drainage of the Pond # 15 (Figure 35) is constrained by the tidal muting of the South Bay Shelf (cf. Sections 3.2 & 3.4), which varies with sea level. At present sea level, Pond # 15 will not drain below – 1.65 ft. NAVD 88, producing the subtidal footprint shown in Figure 29. However, with a moderate amount of sea level rise, the linear SLR = 4.68 in. solution indicates a moderate improvement in drainage to – 1.70 ft NAVD 88. If sea level were to rise by 2 ft. according to the maximum sea level rise prediction in 2050, the available tidal range is not sufficient to prevent a rise in subtidal elevations in Pond # 15. This amount of sea level rise will raise the elevations of the zonation of all habitat types (Figure 35). This upward displacement of

**Table 5:** Intertidal Alternative Predicted Habitat Distribution, acres 2018

Vegetation Community to be Created	Otay River Floodplain Site Acres	Pond 15 Site
SubTidal	0.00	9.53
Mudflat – Frequently Flooded	4.45	16.36
Mudflat – Frequently Exposed	0.70	1.57
Low Marsh	10.34	15.73
Mid Marsh	10.99	34.47
High Marsh	3.23	5.61
Total Marsh	29.26	80.68
Transitional	0.45	2.59
<b>Total Created Habitat</b>	<b>29.71</b>	<b>83.27</b>

**Table 6:** Intertidal Alternative Predicted Habitat Distribution, acres 2050

Vegetation Community to be Created	Otay River Floodplain Site Acres	Pond 15 Site
SubTidal	0	9.35
Mudflat – Frequently Flooded	8.84	17.06
Mudflat – Frequently Exposed	2.21	1.85
Low Marsh	7.91	17.32
Mid Marsh	10.36	35.38
High Marsh	0.52	2.87
<b>Total Created Habitat</b>	<b>29.84</b>	<b>83.83</b>

wetland zonation is largest for the linear superposition scenario, because the spectral correction scenario predicts a larger tidal range of about 1.0 ft. Under the 24 in. spectral sea level rise scenario at 2050, intertidal wetland habitat would begin at an elevation of -0.25 ft NAVD, and the mud flat habitat would reside about 0.4 ft to 0.5 ft. lower than under the linear super-position scenario; while the low marsh habitat would reside about 0.25 ft. lower than under the linear super-position scenario. Therefore there is some apparent differences between the habitat mix predictions of these two sea-level rise prediction methods; although both give the same estimate of the maximum elevation of high salt marsh wetland zonation in both of the proposed basins of the Intertidal Plan (cf. Tables 3 & 4).

**5.3) Residence Time of the Intertidal Alternative:** Residence time refers to the average amount of time source water spends in a particular tidal system. Residence time begins from the moment a *material element of water* (a parcel that contains the same collection of water molecules) enters a tidal system on flooding tide and ends when that same element leaves the system on ebbing tide. At lowest order, the residence time in a particular tidal system can be approximated by *removal time*, which is a ratio of the storage capacity of that system at mean

higher high water to the rate of tidal exchange during a mean diurnal tidal period (Horikawa, 1988; Schwartz, 2005), or :

$$\bar{\tau} = \frac{V_s}{V_p} T$$

Where  $\bar{\tau}$  is the removal time;  $V_s$  is the storage capacity of a particular restoration alternative at mean higher high water (including both the inlet channel and tidal basin);  $V_p$  is the mean diurnal tidal prism of a particular restoration alternative, and  $T$  is a diurnal tidal period equal to 1.0347 days (24 hours and 50 minutes). From this simple relation the removal time varies between each restoration alternative according to the ratio of storage capacity to diurnal tidal prism,  $V_s/V_p$ .

However, removal time is only a simple algebraic proxy for residence time because the mean diurnal tidal prism for each of the basins is less than the storage capacity of those basins at MHHW, and it takes a number of tide cycles to completely replace all of the *old water* in each of those systems. Old water is defined here as water that remains in the tidal system (including both the inlet channel and tidal basin) after water outflow during ebb tide. As new water comes into the inlet channel and tidal basin, the old water becomes more diluted with each tidal cycle until all the old water is eventually replaced by new water. We utilize the mass conservation and transport algorithms of the TIDE\_FEM model to solve for this progressive dilution of old water in each of the restoration alternatives. To facilitate comparisons of residence time calculations performed at other coastal lagoons, we adopt the convention of assigning residence time as the time required for old water to dilute to less than 2% of the storage capacity of the system (Elwany, et. al., 2005; Coastal Environments, 2009).

Figure 36 gives the TIDE\_FEM hydrodynamic simulations of the time for dilution of old water in each of the tidal systems (inlet channel + tidal basin) of the Intertidal Alternative. Figure 36 presents the model results of residence time of South Bay water in the tidal basins of the Intertidal Alternative for the Otay River floodplain basin (blue) and the Pond #15 basin (red). Residence time of South Bay water is 2 days in the floodplain basin and 3 days in the Pond#15 basin. Residence time is less in the floodplain basin because its maximum storage volume at higher-high water level is only 98 acre ft. (4.27 million cubic ft.) and nearly completely drains at mean lower low water levels; whereas the maximum storage volume of the Pond #15 basin is 3.6 times greater at 15.9 million cubic ft., and about 700 hundred thousand cubic ft. of water fail to drain after one diurnal tidal cycle. Regardless, the residence time numbers for the restoration are rather good for marginalizing potential dissolve oxygen depletion, although the DO of South Bay water can become quite low during evaporative summer time conditions (cf. Section 3.3). Maximum diurnal tidal prisms at present sea levels are 98 acre ft. (4.3 million cubic ft.) for the proposed Otay River floodplain basin; and 364 acre ft. (15.9 million cubic ft.) for the proposed Pond #15 basin.

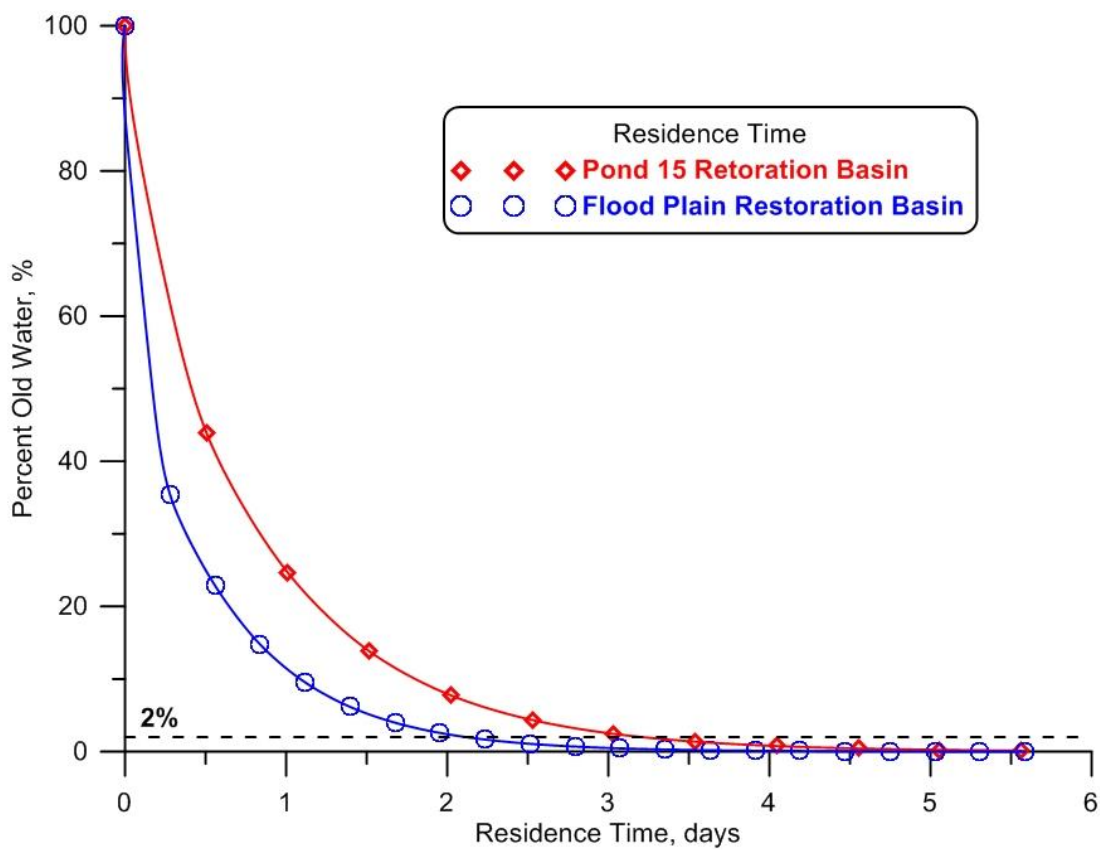


**Figure 36:** Residence time of South Bay water in the tidal basins of the Intertidal Alternative: Otay River floodplain basin (blue); Pond #15 basin (red).

## 6.0 Analysis of the Subtidal Alternative

The model, analysis methods, and supporting data bases used herein are the same as those utilized in the Environmental Impact Report/Environmental Impact Statement (EIR/EIS) for the San Dieguito Wetland Restoration Project, (EIR/EIS, 2000), and for the preparation of the San Dieguito Wetlands Restoration Project, Final Restoration Plan, (SCE, 2005). Monitoring data for the newly completed San Dieguito Lagoon Restoration Project was also used to calibrate tidal hydraulics model. San Dieguito Lagoon was selected as a proxy for the restoration alternatives because of morphologic similarities: in particular, both restoration sites have a long “goose-neck” feeder channel connecting source water to interior tidal basins of comparable acreage and distance from the source water. Habitat surveys conducted during the San Dieguito Lagoon Restoration Project by Josselyn & Whelchel (1999), and then later updated by vegetation surveys in the lower Otay River flood plain by Josselyn (2012), were used to develop functional relationships between habitat breaks and amounts of time for wetting and drying (hydroperiod functions). These relationships were used to transpose tidal hydraulics model output into calculations of acreage of various wetland habitat types created by the *Subtidal* restoration plan. Calculations of habitat creation were based on long-term tidal hydraulics simulations using tidal forcing at the mouth of the Otay River, derived from a spectral correction applied to the NOAA tide gage #941-0170 located at the Navy Pier (cf. Section 3.2)

**6.1 Bathymetric Input for the Subtidal Alternative:** Grading contours for the Subtidal Alternative were provided in 0.5 ft intervals between -4.0 ft NAVD and + 10 ft NGVD by KTU+A. The TIDE\_FEM tidal hydraulics model presented in Jenkins and Inman (1999) was gridded for a computational mesh of the Subtidal Alternative built off the bathymetry in Figures 4 and 5. Figure 4 details the elevation grading contours of the Subtidal Alternative tidal basin in the Otay River floodplain merged with the Otay River bathymetry; while Figure 5 gives the elevation contours resulting from cut and fill of the Pond-15 tidal basin for the Subtidal Alternative. Of particular interest to the finite element mesh is the *hydraulic friction slope coefficient*,  $S_{ff}$ , providing tidal muting effects. Two separate formulations are used. One is given for the 3-node triangular elements situated in the interior of the mesh which do not experience successive wetting and drying during each tide cycle. The other formulation is for the elements situated along the wet and dry boundaries of the lagoon. These have been formulated as 3-node triangular elements with one curved side based upon the cubic-spline matrices developed by Weiyan (1992). These two sets of elements were assembled into a computational mesh of the restoration whose upper boundary conforms to the + 10 ft. NGVD contours in Figures 4 and 5. The + 10 ft. NGVD contour was chosen to allow sufficient computational domain to evaluate tidal inundation at 2050 sea levels that are as much as + 2.0 ft above present sealevel. The wet-dry boundary coordinates of the curved waterline,  $(x', y')$ , are linearly interpolated for any given water elevation from the contours stored in the bathymetry file.

Aside from gridding the TIDE\_FEM tidal model, storage rating functions were calculated from the bathymetric contours of Figures 4 and 5. Figure 37 gives the storage rating function of the floodplain tidal basin merged with the tidally influenced lower reach of the Otay River; while Figure 38 gives the storage rating function for the Pond 15 tidal basin as configured for the

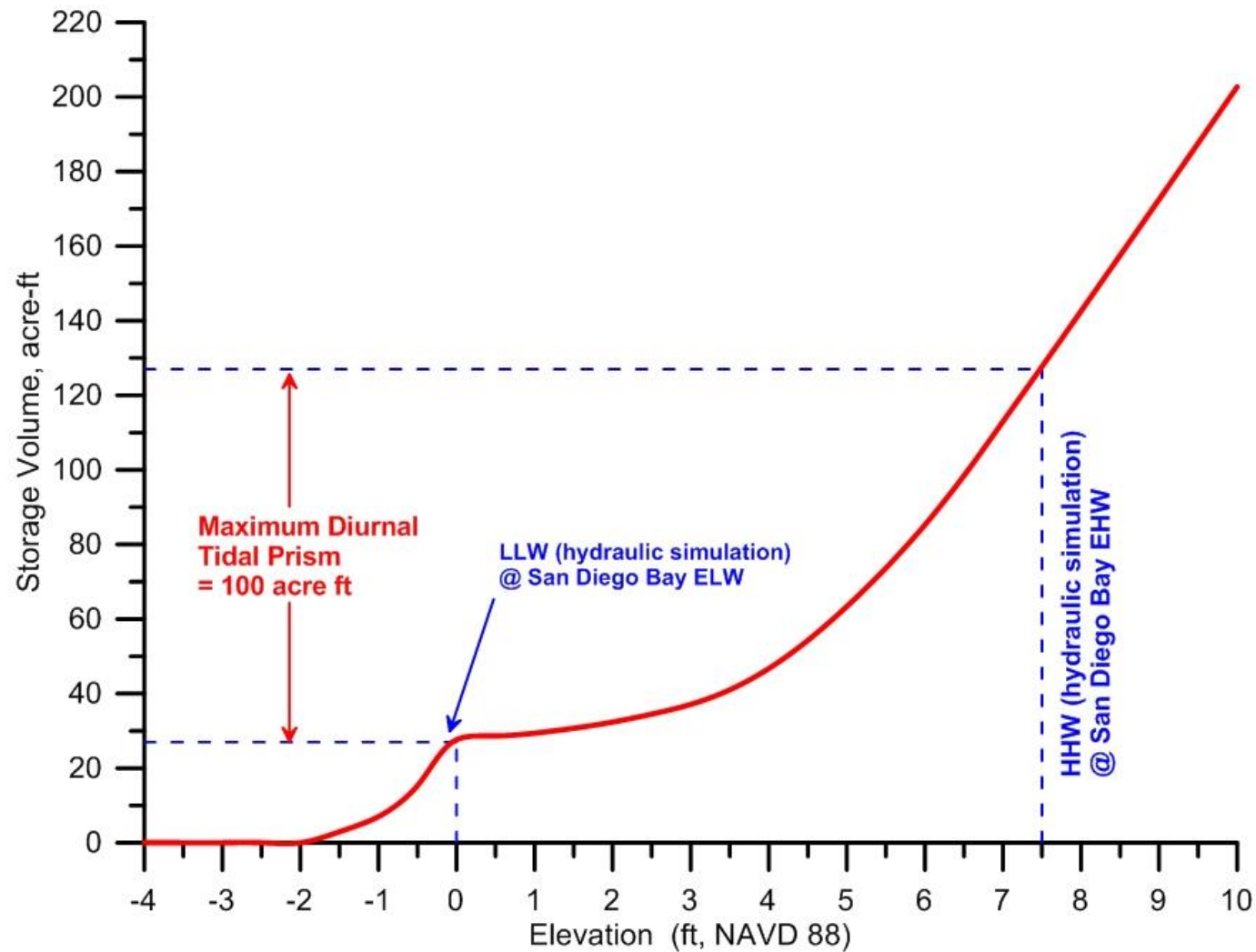


**Figure 37:** Storage rating function of the tidal basin in the Otay River floodplain for the Subtidal Alternative with no dredging of the existing river channel. Maximum diurnal tidal prism shown for extreme high-water event in San Diego Bay, 27 January 1983.

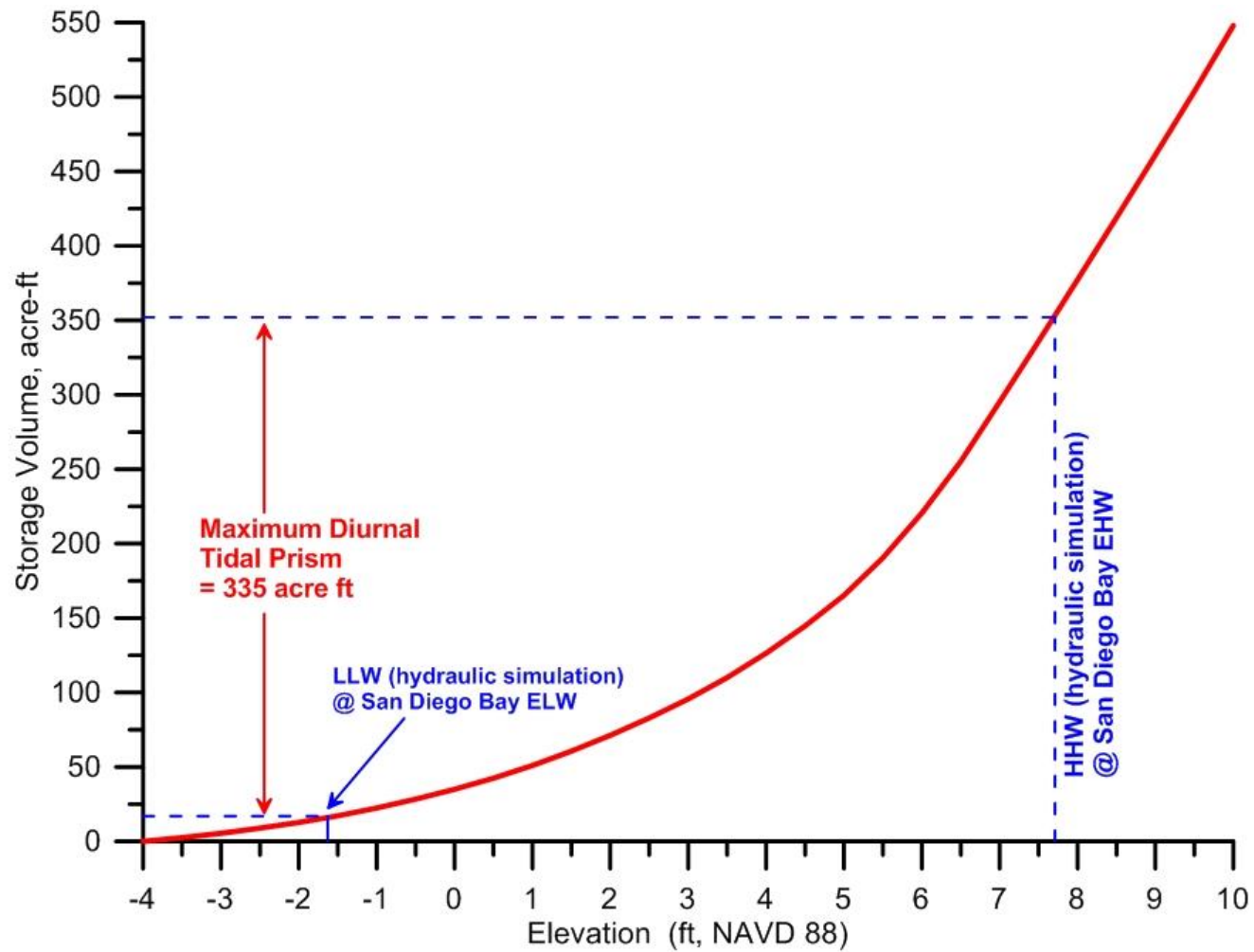
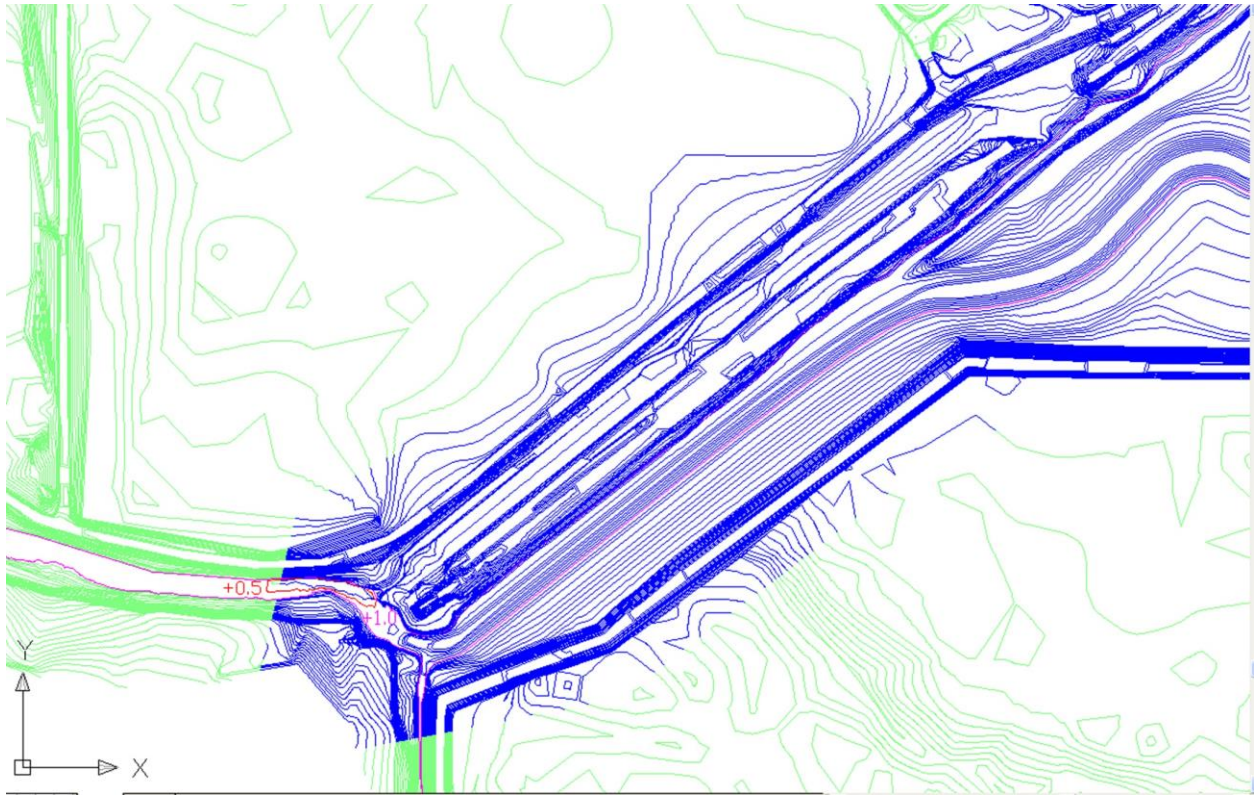


**Figure 38:** Storage rating function of the Pond 15 tidal basin for the Subtidal Alternative. Maximum diurnal tidal prism shown for extreme high-water event in San Diego Bay, 27 January 1983.

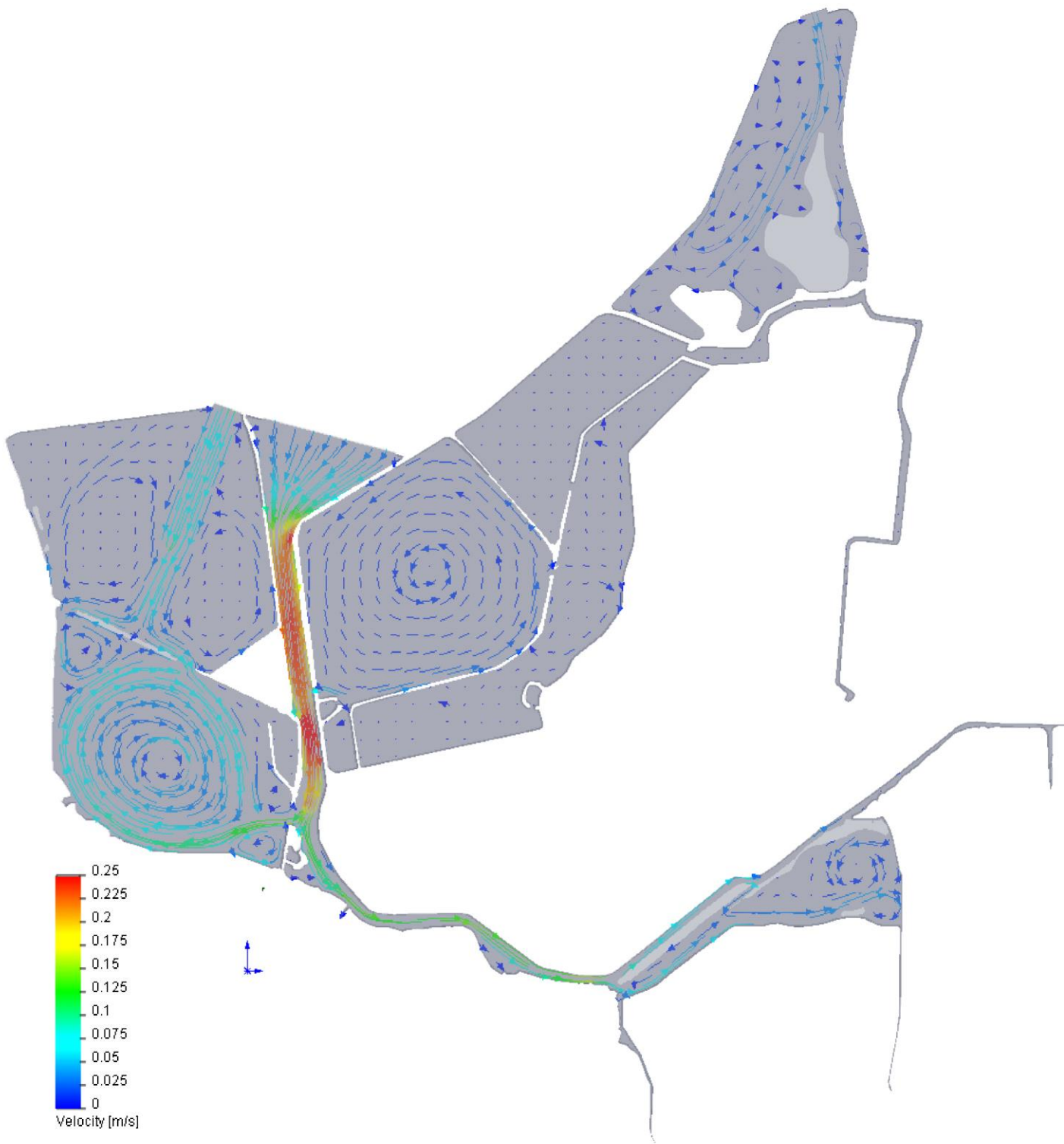
Subtidal Alternative. The storage rating functions are used in the initialization of the TIDE\_FEM tidal hydraulics model in order to enforce mass conservation in the tidal inundation simulations (see Jenkins and Inman, 1999). The initialization involves fitting a series of high-order polynomials to the volumes of the storage rating function in Figure 37 & 38. To accommodate possible future sea level rise the polynomial fits were carried up to a daylight contour chosen at +10.0 ft NGVD, even though the tidal inundation in San Diego Bay has never been observed above +7.71 ft NGVD. A seventh- order polynomial was fitted to the storage rating functions in Figures 37 & 38 with a coefficient of determination of  $r^2 = 0.996$ .

For tidal inundation up to the historic extreme high water level of San Diego Bay (EHW = +7.71 ft NGVD, (upper dashed blue line in Figure 37), the maximum volume of San Diego Bay water that is exchanged with the Subtidal Alternative floodplain tidal basin is 100 acre-ft. Although this basin has a subtidal channel graded down to -2.0 ft NAVD, it does not drain much below lower low water levels due to bars, hummocks, and shoals that form a sill near the confluence of the Subtidal Floodplain basin and the Otay River channel as delineated in red in Figure 39. The maximum potential diurnal tidal prism of the Pond 15 tidal basin of the Subtidal Alternative is 335 acre ft for an extreme high water event at present sea level. The Subtidal Alternative Pond-15 basin has about 29 acre ft. less potential diurnal tidal prism than the Intertidal Alternative Pond-15 basin due to the disposal of additional dredge fill derived from the subtidal channel of the Subtidal Alternative Floodplain tidal basin.

**6.2 Tidal Inundation Simulations of the Subtidal Alternative:** Figure 40 gives the flow trajectories and depth averaged tidal currents for the Subtidal Alternative computed by the calibrated TIDE\_FEM model during spring flooding tides on 18 September 2009. Velocities of tidal currents are portrayed according to the color coded velocity scale appearing in the lower left corner of the figure. Maximum flooding spring tidal currents at the mouth of the Otay River (in the neighborhood of the Otay Sonde) are about 0.10 m/sec (0.33 ft/sec), and then accelerate in the narrower north/south reach of the channel adjacent to Ponds 10 & 11 to 0.2 m/sec (0.66 ft/sec) where the channel has scoured under existing conditions to equilibrium depths on the order of -2.0 ft NAVD. After passing Pond 10, currents decelerate and then increase to 0.17 m/sec (0.55 ft/sec) near the two pinch points at the railroad bridge, before entering the floodplain tidal basin; where tidal currents entering the tidal basin initially form a well-defined jet at the west bank with speeds of about 0.08 m/s (0.26 ft/sec). This entry jet quickly diverges into a complex set of clockwise rotating eddies that populate the interior of the tidal basin. Eddy speeds in the tidal basin are on the order of 0.02 m/sec (0.07 ft/sec), insufficient to transport fine sand but an important stirring mechanism for mixing the tidal basin water mass to maintain high oxygen levels and to sustain fine silt and clay sized sediment particles in suspension. Maximum flooding spring tidal currents in the inlet channel to Pond #15 are about 0.06 m/sec (0.21 ft/sec), and then decelerate as a weak entry jet with speeds of about 0.05 m/s (0.16 ft/sec). This entry jet also quickly diverges into a complex set of counter rotating eddies that populate the interior of the tidal basin. Eddy speeds in the Pond #15 tidal basin are on the order of 0.01 m/sec (0.03 ft/sec), again insufficient to transport fine sand or cohesive silts, but also providing a stirring mechanism for mixing the Pond #15 water mass to maintain high oxygen levels and to sustain suspension of fine silt and clay sized sediment particles.



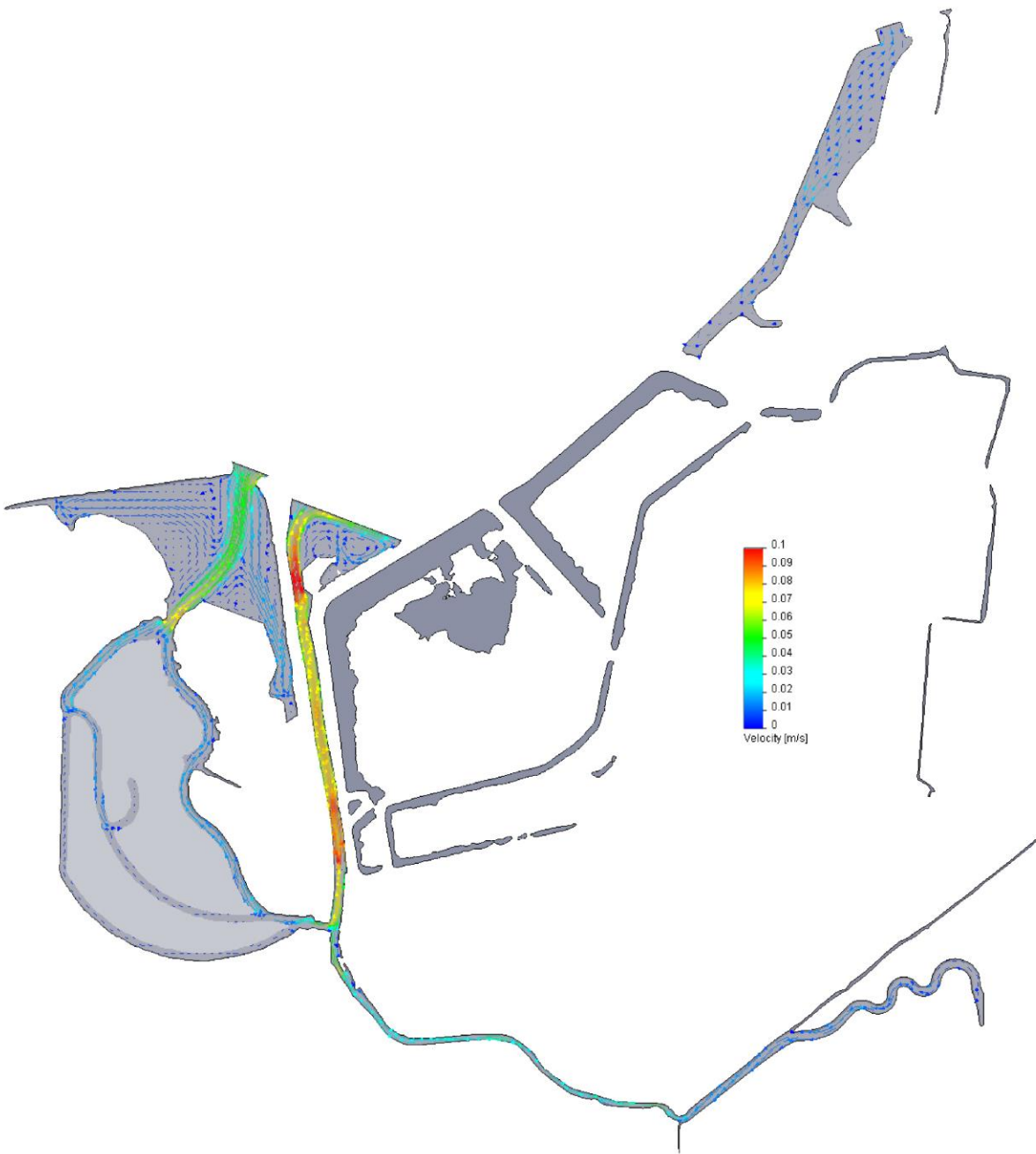
**Figure 39:** Existing Otay River channel bars and hummocks delineated in red limit drainage of Subtidal Floodplain Tidal Basin. Depth contours in ft. NAVD 88.



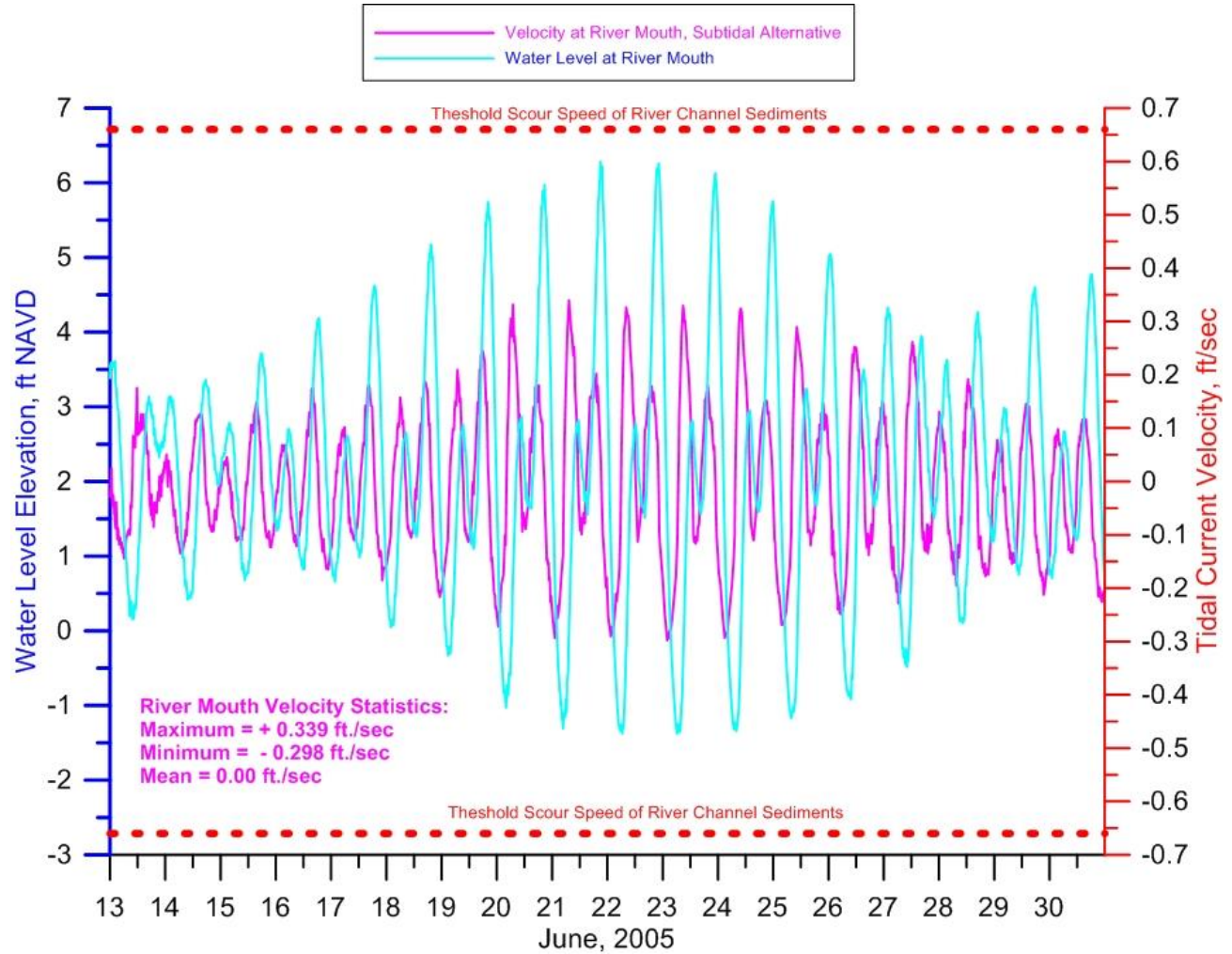
**Figure 40:** Subtidal Alternative flood tide progressive vector flow simulation at Mean High Water (MHW), where vector trajectories are plotted over 30 minute time integrations.

Figure 41 gives the flow trajectories and depth averaged tidal currents for the Subtidal Alternative computed by the TIDE\_FEM model during spring ebbing tides on 18 September 2009. The wetted area of the floodplain tidal basin is significantly reduced relative to the flood tide area in Figure 40, due to the fact that the grading plan allows for almost complete drainage at mean low water tidal stages. In Figure 41, creeping flow drains from the remnant dendritic channel of the floodplain basin, forming a feeder current in the upper river channel with speeds on the order of -0.01 m/sec, or (-0.03 ft/sec). This feeder current evacuates the tidal basin and then accelerates to -0.05 m/sec (-0.16 ft/sec) as it passes through the pinch point under the railroad bridge in the narrow east/west reach of channel. (We adopt the convention of negative velocities for ebb tide flows and positive velocities for flood tide flows). Ebb flow in the channel then accelerates further to -0.091 m/sec (-0.298 ft/sec) in the deeper north/south reach before discharging into San Diego Bay. In Pond #15 during ebb tide flow at mean low water level, the eastern half of the basin is completely drained and exposed, while a weak feeder current evacuates the western half with ebb flow of about -0.02 m/sec (-0.07 ft/sec). This feeder current accelerates to about 0.055 m/sec (0.181 ft/sec), as it flows out the inlet of Pond #15, and is far below the threshold scour speed of the sediments along the bank of the Chula Vista Wildlife Reserve.

In Figure 42, tidal current speeds at the mouth of the Otay River for the Subtidal Alternative are simulated throughout an entire spring-neap tidal. These currents (plotted in red) are compared the threshold scour speeds for native river bed channel sediments as derived from the Hjulstrom Curve in Figure 24b based on grain size data in Figure 24a. These thresholds of incipient scour appear as red dashed lines for flood (positive) and ebb flow (negative) velocity sign conventions. It is apparent that ebb and flood flow velocities throughout a spring/neap cycle never reach the thresholds of incipient scour, where maximum flood flow velocity at the mouth of the Otay River is +0.339 ft./sec, while maximum ebb flow velocity reaches only - 0.298 ft./sec under the Subtidal Alternative. These flood and ebb flow maximums are consistent with the progressive vector simulations in Figures 40 & 41. Figure 43 gives the corresponding spring/neap velocity time series at the inlet to Pond 15 of the Subtidal Alternative. Because of the large non-equilibrium cross section engineered for this inlet, velocities are considerably less than at the mouth of the Otay River. For Pond 15, maximum flood flow velocity at the inlet is +0.206 ft./sec, while maximum ebb flow velocity reaches only - 0.181 ft./sec, slightly less than the Pond-15 results of the Intertidal Alternative (due to smaller tidal prism), and well below the threshold scour speeds for the native sediments estimated to be +/- 0.66 ft./sec from the the Hjulstrom Curve in Figure 24b. Tidal current speeds between 0.27 ft/ sec (0.08 m/sec) and 0.66 ft/sec would lead to bed load transport but not erosion. Erosion and scour would only occur for tidal currents that exceed 0.66 ft/sec, while currents less 0.27 ft/sec would yield deposition. Therefore the mouth of the Otay River would be in steady state equilibrium that is neither depositional nor erosional under the Subtidal Alternative. However, the inlet to Pond 15 under the Subtidal Alternative could be depositional if there is an active sediment source nearby. However no such source appears to exist, other than perhaps very minimal and undocumented sediment yield from the Palomar Ditch during occasional El Nino floods. Littoral sediment transport by waves is generally de minimis due to the limited fetch across South San Diego Bay, and the inlet to Pond 15 is sheltered from direct wave exposure by the causeway of the Chula



**Figure 41:** Subtidal Alternative ebb tide progressive vector flow simulation at Mean Low Water (MLW), where vector trajectories are plotted over 30 minute time integrations.



**Figure 42:** Tidal current speeds at the mouth of the Otay River as computed in magenta for the Subtidal Alternative throughout a spring-neap tidal cycle shown in cyan. Threshold scour speeds for native river bed channel sediments shown as red dashed lines for flood and ebb flow conditions.

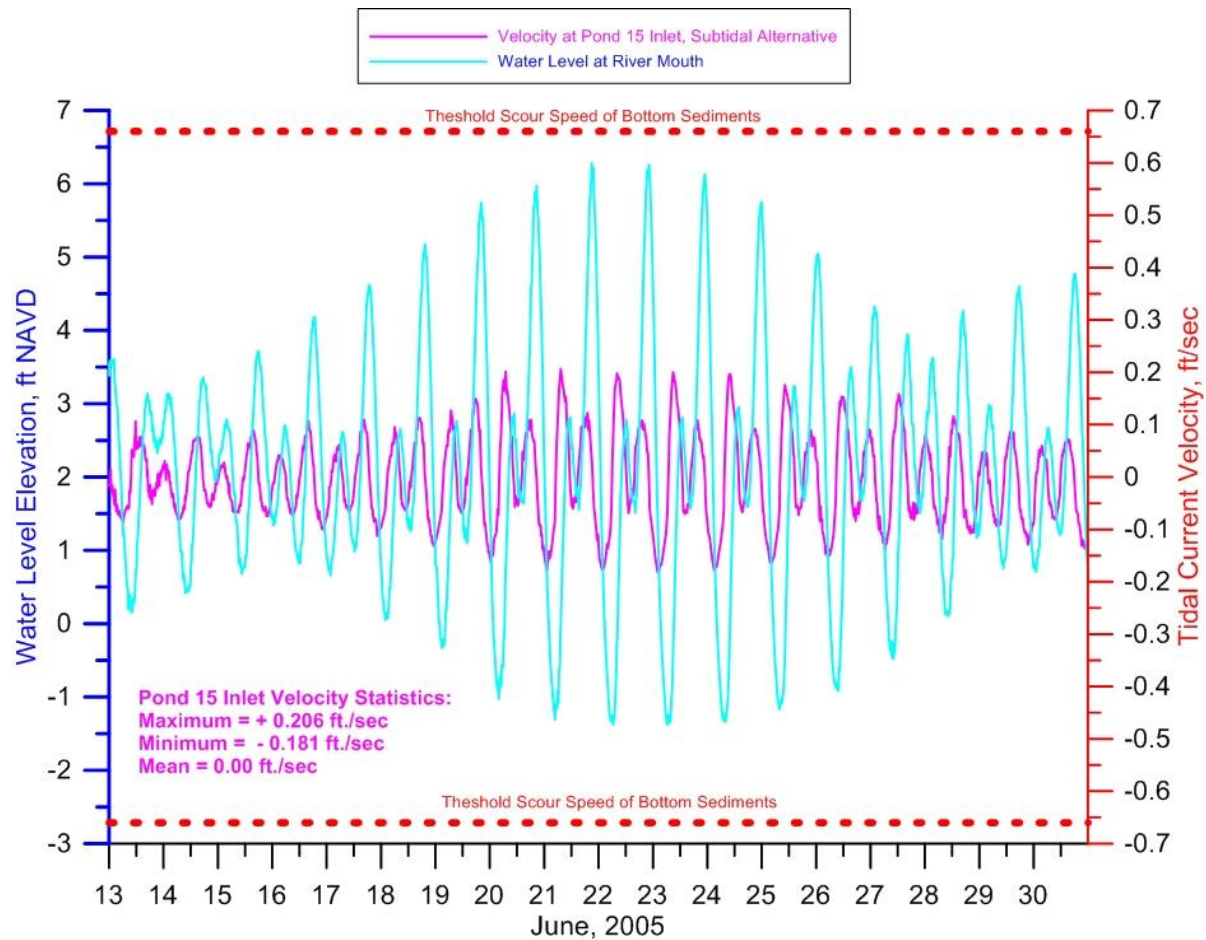


**Figure 43:** Tidal current speeds at the inlet to Pond 15 as computed in magenta for the Subtidal Alternative throughout a spring-neap tidal cycle shown in cyan. Threshold scour speeds for native river bed channel sediments shown as red dashed lines for flood and ebb flow conditions.

Vista Nature Reserve (cf. Figure 1).

Therefore, we conclude both source water inlets to the tidal basins of the Subtidal Alternative are stable and immune to closure or restriction by sedimentation under dry weather tidal exchange. Inlet sedimentation due to influxes of wave driven long-shore transport of sand (as occurs on the open coast), does not occur in the fetch limited environment of South San Diego Bay. The mouth of the Otay River supplying source water to the floodplain tidal basin is in a dynamic steady-state equilibrium that is neither depositional nor erosional, while the inlet to Pond 15 will remain in a non-equilibrium stationary state (as-built) in the absence of a local sediment sources or adequate fluid forcing by waves and currents to import sediment from more distant sources.

Water elevations in the Subtidal Alternative floodplain basin are shown in Figure 44 for spring tides that occurred during 14-18 September, 2009, the same time period used for the model calibration with the proxy tidal system at San Dieguito Lagoon in Figure 20. Figure 44 provides a comparison between the water levels in the Subtidal Alternative floodplain tidal basin as predicted by the model (magenta trace) versus the actual San Diego Bay water level measurements (cyan) reported by the Otay Sonde. The Subtidal Alternative floodplain tidal basin water level variations in red are found to lag the Bay water levels by as much as 26 minutes at higher high water (HHW) levels on flooding tides while this phase lag averages 2.42 hours at lower low water (LLW) level during ebb tides. These phase lags are an unavoidable consequence to frictional impedance and depth limited tidal propagation speeds down the 7,000 ft long channel that connects the floodplain tidal basin with the Bay. Lower low water levels in the Subtidal Alternative floodplain tidal basin are as much as 1.28 ft above South Bay water levels at the mouth of the Otay River due to the grading design which allows the floodplain basin to fully drain at LLW. The auto spectra of the water levels in the floodplain tidal basin of the Subtidal Alternative are nearly indistinguishable from the spectra found for the Intertidal alternative in Figure 33.

The hydroperiod function (used to calculate the habitat acreage creation of the Subtidal Alternative) is calculated by the model for both present and future extremes of sea level in the year 2050 from estimates of both maximum and minimum sea level rise. Using the methods detailed in Sections 3.2 and 3.4 for providing long-term, locally relevant tidal forcing for the model, the hydroperiod functions are calculated at present and future sea levels for the Subtidal Plan floodplain basin in Figure 45 and for the Pond #15 basin in Figure 46. The elevation breaks (zonation) between the different wetland habitat types from the hydroperiod curves are summarized in Tables 7 and Tables 8. The elevations for the habitat breaks in these figures and tables are applied to the KTUA grading designs and yield the acreages of habitat creation listed in Table 9 at present sea level, and at 2050 sea levels in Table 10. Comparing Table 5 from Section 5.2 with Table 9 below, it is apparent that the Intertidal Alternative creates an additional 1.37 acres of habitat in 2018 than does the Subtidal Alternative.

For all possible sea level scenarios, the elevation limit of subtidal habitat in the floodplain basin (Figure 45) is limited by existing bars, hummocks and other channel bottom features at the inlet and inside the branch channel into this basin that create an inlet sill at 0.0 ft NAVD 88. The Subtidal Alternative calls for no construction dredging of the existing Otay River channel so as not to disrupt existing habitat residing down-river from the inlet to the proposed floodplain basin.

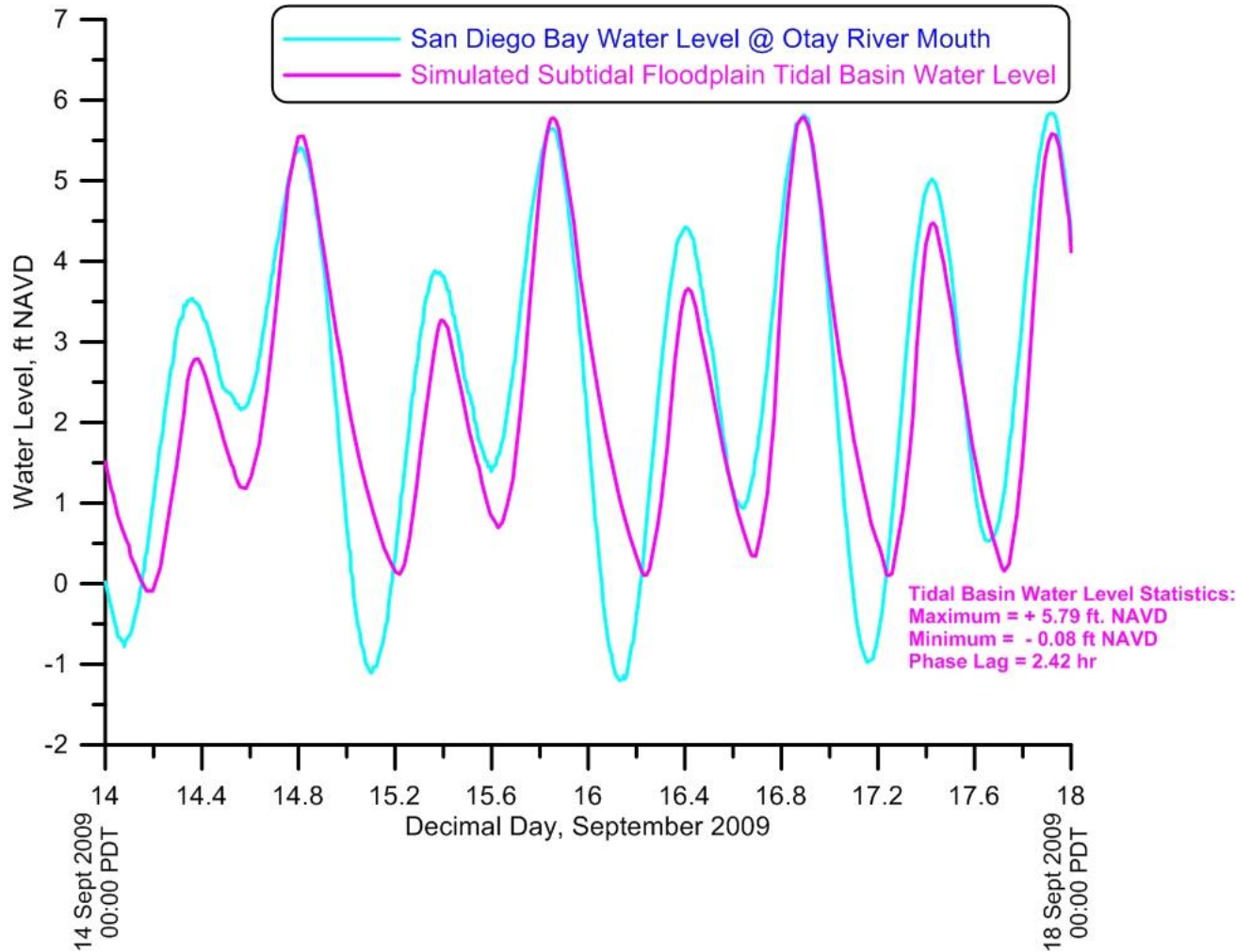


**Figure 44:** Water level elevations at the mouth of the Otay River (cyan) compared to model simulation of Subtidal Alternative floodplain basin water levels (magenta) during spring tides, 14-18 September 2009.

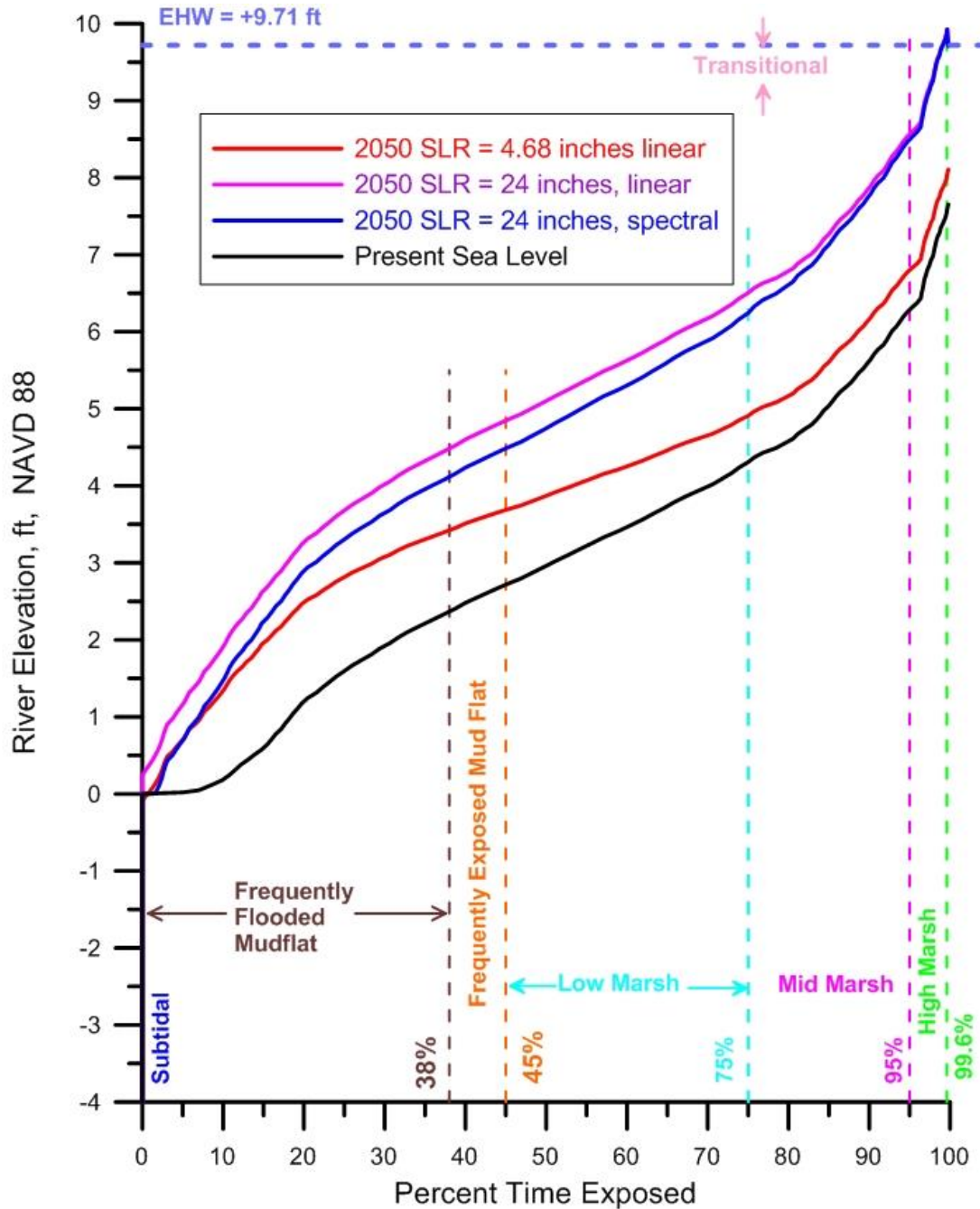


**Figure 45:** Hydroperiod Function for Subtidal Alternative, Otay Floodplain Tidal Basin for present sea level and 2050 sea level rise per CAT OPC guidance. Based on Otay Habitat Survey Data Evaluated By Josselyn (2012) and water level data from NOAA tide gage #941-0170, with spectral correction from Otay River Sonde. Manning's roughness,  $n = 0.0261$

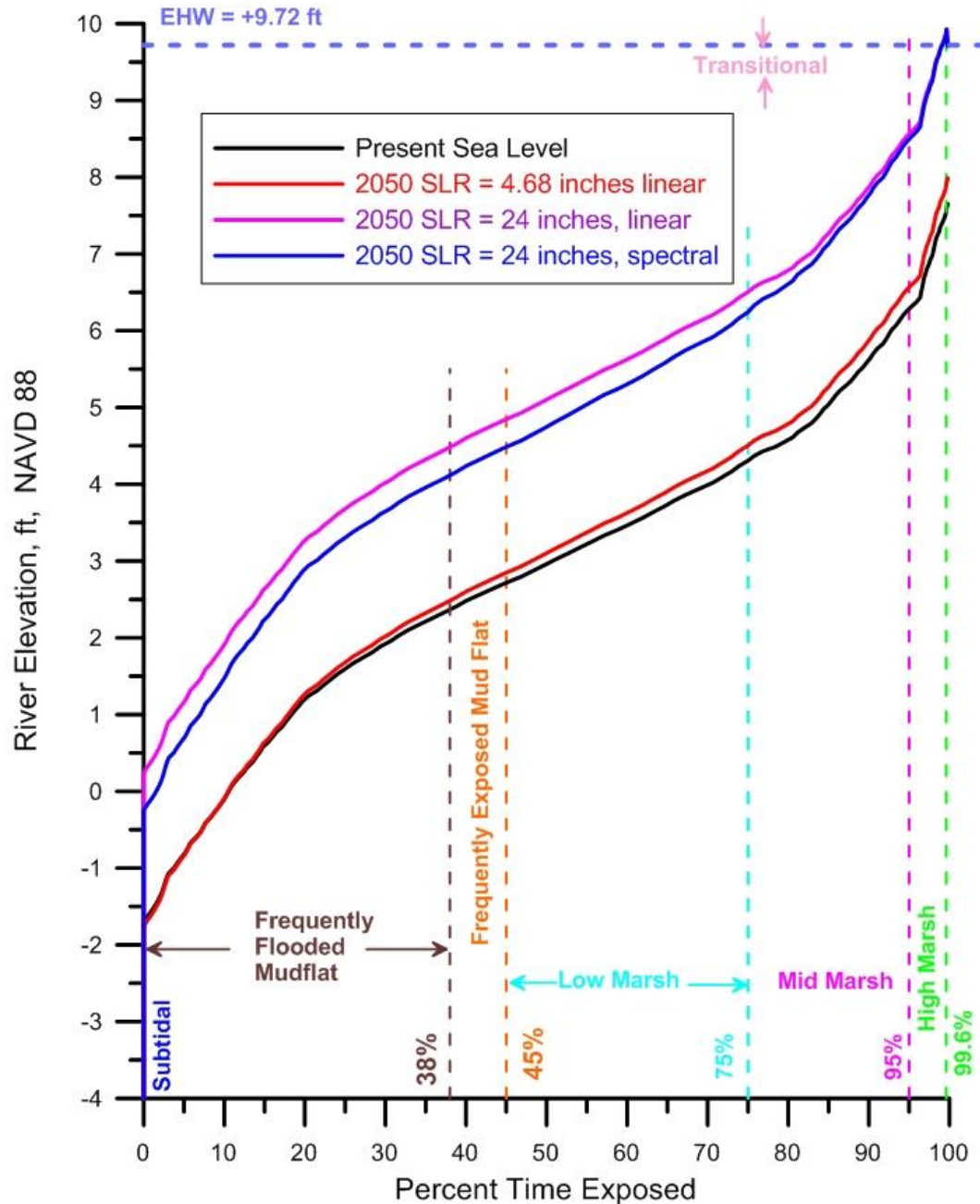


**Figure 46:** Hydroperiod Function for the Subtidal Alternative Pond #15 Tidal Basin for present sea level and 2050 sea level rise per CAT OPC guidance. Based on Otay Habitat Survey Data Evaluated By Josselyn (2012) and water level data from NOAA tide gage #941-0170, with spectral correction from Otay River Sonde. Manning's roughness,  $n0 = 0.0261$ .

**Table 7:** Elevations of Upper Limits of Habitat Breaks in the Subtidal Plan Floodplain Basin

Elevation of Habitat Breaks (Units of ft. NAVD 88)	@ Present Sea Level	@ 4.68 in. linear Sea Level Rise	@ 24 in. linear Sea Level Rise	@ 24 in. spectral Sea Level Rise
Sub-tidal	0.00 ft.	0.00 ft.	0.25 ft.	0.00 ft.
Frequently Flooded Mud Flat	2.38 ft.	3.40 ft.	4.50 ft.	4.15 ft.
Frequently Exposed Mud Flat	2.70 ft.	3.70 ft.	4.85 ft.	4.50 ft.
Low Marsh	4.30 ft.	4.90 ft.	6.52 ft.	6.25 ft.
Mid Marsh	6.27 ft.	6.80 ft.	8.55 ft.	8.50 ft.
High Marsh	7.55 ft.	8.10 ft.	9.71 ft.	9.71 ft.

**Table 8:** Elevations of Upper Limits of Habitat Breaks in the Subtidal Plan Pond 15 Basin

Elevation of Habitat Breaks (Units of ft. NAVD 88)	@ Present Sea Level	@ 4.68 in. linear Sea Level Rise	@ 24 in. linear Sea Level Rise	@ 24 in. spectral Sea Level Rise
Sub-tidal	-1.65 ft.	-1.70 ft.	0.25 ft.	-0.20 ft.
Frequently Flooded Mud Flat	2.35 ft.	2.50 ft.	4.50 ft.	4.15 ft.
Frequently Exposed Mud Flat	2.70 ft.	2.85 ft.	4.85 ft.	4.50 ft.
Low Marsh	4.30 ft.	4.50 ft.	6.50 ft.	6.25 ft.
Mid Marsh	6.30 ft.	6.55 ft.	8.55 ft.	8.50 ft.
High Marsh	7.50 ft.	7.90ft.	9.72 ft.	9.72 ft.

**Table 9:** Subtidal Alternative Predicted Habitat Distribution, acres, 2018

Vegetation Community to be Created	Otay River Floodplain Site Acres	Pond 15 Site
Subtidal	4.48	9.17
Mudflat – Frequently Flooded	5.26	14.70
Mudflat – Frequently Exposed	1.79	1.32
Low Marsh	8.64	11.77
Mid Marsh	7.90	33.25
High Marsh	1.64	11.78
Total Salt Marsh	29.71	82.00
Transitional	0.45	2.15
<b>Total Created Habitat</b>	<b>29.26</b>	<b>79.85</b>

**Table 10:** Subtidal Alternative Predicted Habitat Distribution, acres, 2050

<b>Vegetation Community to be Created</b>	<b>Otay River Floodplain Site Acres</b>	<b>Pond 15 Site</b>
Subtidal	4.48	9.0
Mudflat – Frequently Flooded	110.01	15.28
Mudflat – Frequently Exposed	1.70	1.58
Low Marsh	5.43	12.68
Mid Marsh	6.71	41.20
High Marsh	0.52	3.06
<b>Total Created Habitat</b>	<b>29.85</b>	<b>82.80</b>

That existing down-river habitat consists of additional mud flat residing below – 0.0 ft NAVD 88 and subtidal habitat below -1.01 ft NAVD 88 (cf. Section 4). Low tide drainage of the Pond # 15 (see Figure 46) is constrained by the tidal muting of the South Bay Shelf (cf. Sections 3.2 & 3.4), which varies with sea level. At present sea level, Pond # 15 will not drain below – 1.65 ft. NAVD 88, producing the subtidal footprint shown in Figure 41. However, with a moderate amount of sea level rise, the linear SLR = 4.68 in. solution indicates a moderate improvement in drainage to – 1.70 ft NAVD 88. If sea level were to rise by 2 ft. according to the maximum sea level rise prediction in 2050, the available tidal range is not sufficient to prevent a rise in subtidal elevations in Pond # 15. This amount of sea level rise will raise the elevations of the zonation of all habitat types (Figure 46). This upward displacement of wetland zonation is largest for the linear superposition scenario, because the spectral correction scenario predicts a larger tidal range of about 1.0 ft. Under the 24 in. spectral sea level rise scenario at 2050, intertidal wetland habitat would begin at an elevation of -0.20 ft NAVD, and the mud flat habitat would reside about 0.4 ft. to 0.5 ft. lower than under the linear super-position scenario; while the low marsh habitat would reside about 0.25 ft. lower than under the linear super-position scenario. Therefore there are some apparent differences between the habitat mix predictions of these two sea-level rise prediction methods; although both give the same estimate of the maximum elevation of high salt marsh wetland zonation in both of the proposed basins of the Subtidal Alternative (cf. Tables 7 & 8).

**6.3) Residence Time of the Subtidal Alternative:** A discussion at the beginning of Section 5.3 details the calculus of residence time and how it represents the average amount of time source water spends in a particular tidal system. Figure 47 gives the TIDE\_FEM hydrodynamic simulations of the time for dilution of old water in each of the tidal systems (inlet channel + tidal basin) of the Subtidal Alternative. Figure 47 presents the model results of residence time of South Bay water in the tidal basins of the Subtidal Alternative for the Otay River floodplain basin (blue) and the Pond #15 basin (red). Residence time of South Bay water is 2.5 days in the floodplain basin and 3 days in the Pond#15 basin. Residence time in the floodplain basin is 0.5 days longer than for the Intertidal Alternative in Section 5.3 because a residual of 29 acre ft. in the subtidal channel of the Subtidal Alternative fails to drain at mean lower low water levels. Regardless, the residence time numbers for the Subtidal Alternative are

rather good for marginalizing potential dissolve oxygen depletion, although the DO of South Bay water can become quite low during evaporative summer time conditions (cf. Section 3,3). Maximum diurnal tidal prisms at present sea levels are 100 acre ft. ( 4.4 million cubic ft.) for the proposed Otay River floodplain basin; and 335 acre ft. (14.6 million cubic ft.) for the proposed Pond #15 basin.

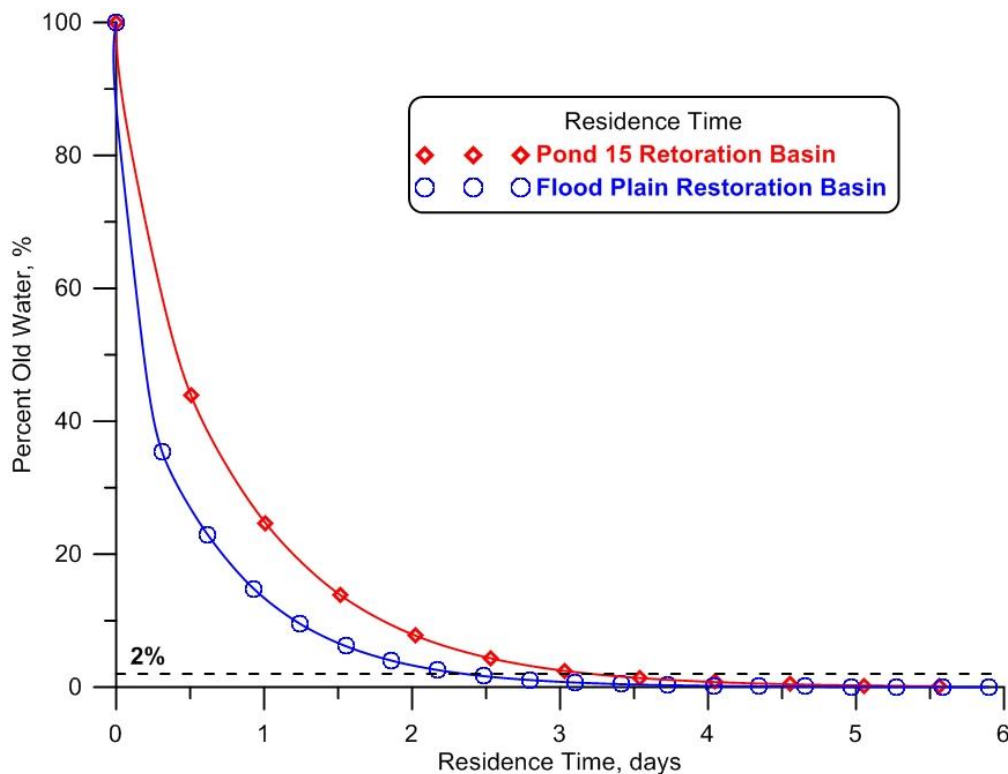


**Figure 47:** Residence time of South Bay water in the tidal basins of the Subtidal Alternative: Otay River floodplain basin (blue); Pond #15 basin (red).

## 7.0) Summary and Conclusions:

This study employs a well-tested and peer-reviewed hydrodynamic model to evaluate the tidal hydraulics the Intertidal Alternative and the Subtidal Alternative for the Otay River Estuary Restoration Project (ORERP). Both alternatives involve restoration of a portion of the Otay River Floodplain Site and Pond 15 Site to native habitat by lowering the existing ground elevations in the Otay River Floodplain Site and using the excavated soils from the Otay River Floodplain Site as fill material in the Pond 15 Site.

The model, analysis methods, and supporting data bases used herein are the same as those utilized in the Environmental Impact Report/Environmental Impact Statement (EIR/EIS) for the San Dieguito Wetland Restoration Project, (EIR/EIS, 2000), and for the preparation of the San Dieguito Wetlands Restoration Project, Final Restoration Plan, (SCE, 2005). The analysis is based on updated bathymetry provided by Wetlands Research Associates (WRA) and latest updates to San Diego Bay tides for the 1983-2001 tidal epoch supported by Otay Sonde tidal elevation measurements at the mouth of the Otay River. The computer models used in this study are 2-dimensional finite element types, built from some well-studied and proven computational methods and numerical architecture that have been successful in predicting shallow water tidal propagation. Monitoring data for the newly completed San Dieguito Lagoon Restoration Project was used to calibrate tidal hydraulics model. San Dieguito Lagoon was selected as a calibration proxy for the restoration alternatives because of morphologic similarities: in particular, both the San Dieguito and restoration sites have a long “goose-neck” feeder channel connecting source water to interior tidal basins of comparable acreage and distance from the source water. Habitat surveys conducted during the San Dieguito Lagoon Restoration Project by Josselyn & Whelchel (1999), and then later updated by vegetation surveys in the lower Otay River flood plain by Josselyn (2012), were used to develop functional relationships between habitat breaks and amounts of time for wetting and drying (hydroperiod functions). The hydroperiod functions were calculated by the model for both present and future extremes of sea level in the year 2050 from estimates of both maximum and minimum sea level rise. These relationships were used to transpose tidal hydraulics model output into calculations of acreage of various wetland habitat types created by the two restoration alternatives.

The elevation breaks (zonation) between the different wetland habitat types from the modeled hydroperiod curves are summarized below in Tables S-1 and S-2 for the Intertidal Alternative; and in Tables S-3 and S-4 for the Subtidal Alternative. The elevations for the habitat breaks in these tables are applied to the KTUA grading designs and yield the acreages of habitat creation listed in Table S-5 for the Intertidal Alternative at present sea level, and at 2050 sea levels in Table S-6. The companion set of habitat creation acres for the Subtidal Alternative are listed in Table S-7 at present sea level, and in Table S-8 at 2050 sea levels. Comparing Tables S-5 and S-7, it is apparent that the Intertidal Alternative creates an additional 1.37 acres of habitat in 2018 than does the Subtidal Alternative. For all possible sea level scenarios, the elevation limit of subtidal habitat in the floodplain basin of both restoration alternatives is limited by existing bars, hummocks and other channel bottom features at the inlet and inside the branch channel into this basin. These channel bottom features create an inlet sill at 0.0 ft NAVD 88. However, if sea level were to rise by 2 ft. according to the maximum sea level rise prediction in

2050, the available tidal range is not sufficient to prevent a rise in subtidal elevations in Pond # 15 of either restoration alternative. This amount of sea level rise will raise the elevations of the zonation of all habitat types. This upward displacement of wetland zonation is largest for the linear superposition scenario of sea level rise, because the spectral correction scenario predicts a larger tidal range of about 1.0 ft. Under the 24 in. spectral sea level rise scenario at 2050, intertidal wetland habitat would begin at an elevation of between -0.25 ft. and -0.20 ft NAVD, and the mud flat habitat would reside about 0.4 ft. to 0.5 ft. lower than under the linear superposition scenario; while the low marsh habitat would reside about 0.25 ft. lower than under the linear superposition scenario. Therefore there are some apparent differences between the habitat mix predictions of these two sea-level rise prediction methods; although both give the same estimate of the maximum elevation of high salt marsh wetland zonation in both of the proposed basins of the restoration alternatives.

From model simulations of tidal currents throughout complete spring-neap tidal cycles, it is concluded that both source water inlets to the tidal basins of the Intertidal and Subtidal Alternatives are stable and immune to closure or restriction by sedimentation under dry weather tidal exchange. (Wet-weather conditions are addressed in a companion study, Everest, 2014). Inlet sedimentation due to influxes of wave driven long-shore transport of sand (as occurs on the open coast), does not occur in the fetch limited environment of South San Diego Bay. The mouth of the Otay River that supplies source water to the floodplain tidal basin is in a dynamic steady-state equilibrium that is neither depositional nor erosional; while the inlet to Pond 15 will remain in a non-equilibrium stationary state (as-built) in the absence of a local sediment sources or adequate fluid forcing by waves and currents that might otherwise import sediment from more distant sources.

**Table S-1:** Elevations of Upper Limits of Habitat Breaks Intertidal Plan Floodplain Basin

Elevation of Habitat Breaks (Units of ft. NAVD 88)	@ Present Sea Level	@ 4.68 in. linear Sea Level Rise	@ 24 in. linear Sea Level Rise	@ 24 in. spectral Sea Level Rise
Sub-tidal	0.00 ft.	0.00 ft.	0.25 ft.	0.00 ft.
Frequently Flooded Mud Flat	2.40 ft.	3.40 ft.	4.50 ft.	4.10 ft.
Frequently Exposed Mud Flat	2.70 ft.	3.70 ft.	4.85 ft.	4.45 ft.
Low Marsh	4.30 ft.	4.90 ft.	6.55 ft.	6.25 ft.
Mid Marsh	6.30 ft.	6.80 ft.	8.55 ft.	8.50 ft.
High Marsh	7.55 ft.	8.05 ft.	9.71 ft.	9.71 ft.

**Table S-2:** Elevations of Upper Limits of Habitat Breaks in the Intertidal Plan Pond 15 Basin

Elevation of Habitat Breaks (Units of ft. NAVD 88)	@ Present Sea Level	@ 4.68 in. linear Sea Level Rise	@ 24 in. linear Sea Level Rise	@ 24 in. spectral Sea Level Rise
Sub-tidal	-1.65 ft.	-1.70 ft.	0.25 ft.	-0.25 ft.
Frequently Flooded Mud Flat	2.40 ft.	2.50 ft.	4.50 ft.	4.10 ft.
Frequently Exposed Mud Flat	2.70 ft.	2.85 ft.	4.85 ft.	4.45 ft.
Low Marsh	4.30 ft.	4.50 ft.	6.50 ft.	6.25 ft.
Mid Marsh	6.30 ft.	6.55 ft.	8.55 ft.	8.50 ft.
High Marsh	7.50 ft.	7.90ft.	9.72 ft.	9.72 ft.

**Table S-3:** Elevations of Upper Limits of Habitat Breaks in the Subtidal Plan Floodplain Basin

Elevation of Habitat Breaks (Units of ft. NAVD 88)	@ Present Sea Level	@ 4.68 in. linear Sea Level Rise	@ 24 in. linear Sea Level Rise	@ 24 in. spectral Sea Level Rise
Sub-tidal	0.00 ft.	0.00 ft.	0.25 ft.	0.00 ft.
Frequently Flooded Mud Flat	2.38 ft.	3.40 ft.	4.50 ft.	4.15 ft.
Frequently Exposed Mud Flat	2.70 ft.	3.70 ft.	4.85 ft.	4.50 ft.
Low Marsh	4.30 ft.	4.90 ft.	6.52 ft.	6.25 ft.
Mid Marsh	6.27 ft.	6.80 ft.	8.55 ft.	8.50 ft.
High Marsh	7.55 ft.	8.10 ft.	9.71 ft.	9.71 ft.

**Table S-4:** Elevations of Upper Limits of Habitat Breaks in the Subtidal Plan Pond 15 Basin

Elevation of Habitat Breaks (Units of ft. NAVD 88)	@ Present Sea Level	@ 4.68 in. linear Sea Level Rise	@ 24 in. linear Sea Level Rise	@ 24 in. spectral Sea Level Rise
Sub-tidal	-1.65 ft.	-1.70 ft.	0.25 ft.	-0.20 ft.
Frequently Flooded Mud Flat	2.35 ft.	2.50 ft.	4.50 ft.	4.15 ft.
Frequently Exposed Mud Flat	2.70 ft.	2.85 ft.	4.85 ft.	4.50 ft.
Low Marsh	4.30 ft.	4.50 ft.	6.50 ft.	6.25 ft.
Mid Marsh	6.30 ft.	6.55 ft.	8.55 ft.	8.50 ft.
High Marsh	7.50 ft.	7.90ft.	9.72 ft.	9.72 ft.

**Table S-5:** Intertidal Alternative Predicted Habitat Distribution, acres 2018

<b>Vegetation Community to be Created</b>	<b>Otay River Floodplain Site Acres</b>	<b>Pond 15 Site</b>
SubTidal	0.00	9.53
Mudflat – Frequently Flooded	4.45	16.36
Mudflat – Frequently Exposed	0.70	1.57
Low Marsh	10.34	15.73
Mid Marsh	10.99	34.47
High Marsh	3.23	5.61
Total Marsh	29.26	80.68
Transitional	0.45	2.59
<b>Total Created Habitat</b>	<b>29.71</b>	<b>83.27</b>

**Table S-6:** Intertidal Alternative Predicted Habitat Distribution, acres 2050

<b>Vegetation Community to be Created</b>	<b>Otay River Floodplain Site Acres</b>	<b>Pond 15 Site</b>
SubTidal	0	9.35
Mudflat – Frequently Flooded	8.84	17.06
Mudflat – Frequently Exposed	2.21	1.85
Low Marsh	7.91	17.32
Mid Marsh	10.36	35.38
High Marsh	0.52	2.87
<b>Total Created Habitat</b>	<b>29.84</b>	<b>83.83</b>

**Table S-7:** Subtidal Alternative Predicted Habitat Distribution, acres, 2018

<b>Vegetation Community to be Created</b>	<b>Otay River Floodplain Site Acres</b>	<b>Pond 15 Site</b>
Subtidal	4.48	9.17
Mudflat – Frequently Flooded	5.26	14.70
Mudflat – Frequently Exposed	1.79	1.32
Low Marsh	8.64	11.77
Mid Marsh	7.90	33.25
High Marsh	1.64	11.78
Total Salt Marsh	29.71	82.00
Transitional	0.45	2.15
<b>Total Created Habitat</b>	<b>29.26</b>	<b>79.85</b>

**Table S-8:** Subtidal Alternative Predicted Habitat Distribution, acres, 2050

<b>Vegetation Community to be Created</b>	<b>Otay River Floodplain Site Acres</b>	<b>Pond 15 Site</b>
Subtidal	4.48	9.0
Mudflat – Frequently Flooded	110.01	15.28
Mudflat – Frequently Exposed	1.70	1.58
Low Marsh	5.43	12.68
Mid Marsh	6.71	41.20
High Marsh	0.52	3.06
<b>Total Created Habitat</b>	<b>29.85</b>	<b>82.80</b>

## REFERENCES

- Batchelor, G. K., 1970, *An Introduction to Fluid Dynamics*, Cambridge at the University Press, 615 pp
- Boland, J. M., “Water quality monitoring of San Dieguito Lagoon”, prepared for *California Coastal Commission*, 15 pp.
- Chadwick, D.B. 1997. Tidal Exchange at the Bay-Ocean Boundary. Ph.D. diss., University of California, San Diego.
- Chadwick, D.B., J.L. Largier and R.T. Cheng. 1996. The role of thermal stratification in tidal exchange at the mouth of San Diego Bay. Proceedings of the 7th International Conference on the Physics of Estuaries and Coastal Seas, American Geophysical Union (submitted).
- Coastal Environments, 2009, “2009 Monitoring Program for San Dieguito Lagoon: Topography, Hydrology, and Water Quality Surveys”, submitted to Southern California Edison Company, 134 pp + app.
- Connor, J. J. and J. D. Wang, 1973, "Finite element modeling of two-dimensional hydrodynamic circulation," MIT Tech Rpt., #MITSG 74-4, p. 1-57.
- EIR/EIS, 2000, Environmental Impact Report/Environmental Impact Statement (EIR/EIS) for the San Dieguito Wetland Restoration Project.
- Elwany, M. H. S., R. E. Flick, M. White, and K. Goodell, 2005, “Agua Hedionda Lagoon Hydrodynamic Studies,” prepared for Tenera Environmental, 39 pp. + appens.
- Everest, 2014 “Fluvial Analysis of the Otay River Estuary Restoration Plan”, submitted to Poseidon Water, LLC, 75pp.
- Flick, R. E. & D. R. Cayan, 1984, “Extreme sea levels on the coast of California,” Coastal Engineering 1984, *Proc. 19<sup>th</sup> Int. Conf. (Houston)*, Amer. Soc. Civil Eng., New York, p. 886-96.
- Gallagher, R. H., 1981, *Finite Elements in Fluids*, John Wiley & Sons, New York, 290pp.
- ICLEI (2012), “Sea Level Rise Adaptation Strategy for San Diego Bay,” January 2012, prepared by *ICLEI-Local Governments for Sustainability USA*, 66 pp.
- Intergovernmental Panel on Climate Change (IPCC). 2007. *Climate Change 2007: Synthesis Report for the Fourth Assessment Report of the Intergovernmental Panel on Climate Change*. Available Online: [www.ipcc.ch/pdf/assessmentreport/ar4/syr/ar4\\_syr.pdf](http://www.ipcc.ch/pdf/assessmentreport/ar4/syr/ar4_syr.pdf)

Jenkins, S. A. & D. L. Inman, 1999, "Sand transport mechanics for equilibrium tidal inlets," *Shore & Beach* (Magoon Volume, Jan 99), v. 67, n. 1, p. 53–58.

Jenkins, S. A. & J. Wasyl, 1996, Wave Transport Corrections to the Inlet Closure Problem of the San Dieguito Lagoon CA., submitted to *Southern California Edison Co.*, 101 pp.

Jenkins, S. A. & J. Wasyl, 1998, Analysis of Coastal Processes Effects due to the San Dieguito Lagoon Restoration Project: Final Report, submitted to *Southern California Edison Co.*, 333 pp.

Jenkins, S. A. & J. Wasyl, 1999a, Performance and Optimization of the Mixed Habitat Plan in Long-Term Inundations Simulation, submitted to *Southern California Edison Co.*, 62 pp. + 8 appens.

Jenkins, S. A. & J. Wasyl, 1999b, Long-Term Inundation Simulations of Alternative Restoration Plans\* for the San Dieguito Lagoon, CA, submitted to *Southern California Edison Co.*, 57 pp.

Jenkins, S. A. & J. Wasyl, 1999c, Long-Term Tidal Inundation Frequency Analysis for Credit Evaluation of the San Dieguito Lagoon Restoration Alternatives, submitted to *Southern California Edison Co.*, 10 pp. + 8 appens.

Jenkins, S. A., M. Josselyn & J. Wasyl, 1999, Hydroperiod and Residence Time Functions for Habitat Mapping of Restoration Alternatives for San Dieguito Lagoon, submitted to *Southern California Edison Co.*, 30 pp. + 1 appen.

Jenkins, S. A. and J. Wasyl, 2005, "Coastal evolution model," Scripps Institution of Oceanography Tech. Rpt. No. 58, 179 pp. + appendices.  
<http://repositories.cdlib.org/sio/techreport/58/>

Jenkins, S. A. and J. Wasyl, 20101, "Tidal Hydraulics of Wetlands Restoration Alternatives in the Otay River Flood Plain, Carlsbad Desalination Project Marine Life Mitigation Plan" submitted to Poseidon Resources Corp., 75pp.

Josselyn, M. & A. Whelchel, 1999, Determining the Upper Extent of Tidal Marsh Habitat San Dieguito Lagoon, submitted to *Southern California Edison Co.*, 16 pp.

Josselyn, M., 2012, "TECHNICAL MEMORANDUM ELEVATIONS OF INTERTIDAL VEGETATION PROJECTIONS FOR ORERP" WRA, submitted Poseidon Resources, Corp, 17 February, 2012, 5pp.

Largier, J. , 1995, "A study of the circulation of water in San Diego Bay for the purpose of assessing, monitoring and managing the transport and potential accumulation of pollutants and sediment in San Diego Bay", submitted to California Water Resources Control Board, 19 pp. + app.

Longuet-Higgins, M.S., 1953, "Mass transport in water waves", *Phil. Trans. R. Soc. Lond.*, v. A245, pp535-581.

SCE, 2005, " San Dieguito Wetlands Restoration Project, Final Restoration Plan" submitted to California Coastal Commission, prepared by Southern California Edison Company, November, 2005, 265 pp.

NOAA, 2013, "Verified/Historical Water Level Data"  
<http://tidesonline.nos.noaa.gov>

USACE, 1991, State of the Coast Report, San Diego Region, Coast of California Storm and Tidal Waves Study, *U. S. Army Corps of Engineers*, Los Angeles District, Chapters 1-10, Appen. A-I, 2 v.

Wang, P. F., Cheng, R. T., Richter, K., Gross, E. S., Sutton, D., and Gartner, J. W. (1998). "Modeling Tidal Hydrodynamics of San Diego Bay, California." *J. Amer. Water Res. Assoc.*, 34 (5), 1123-1140.

Weiyan, T., 1992, *Shallow Water Hydrodynamics*, Water & Power Press, Hong Kong, 434 pp.

Zedler, J. B. & G. W. Cox, 1985, "Characterizing wetland boundaries: a Pacific Coast example," *Wetlands*, 4, p. 43-55.

## **Technical Note on Possible Tidal Hydraulics Impacts of the Otay River Estuary Restoration Plan (ORERP) on Nestor Creek and the Upper Otay River Intertidal Zone**

by: Scott A. Jenkins, Ph. D

**ABSTRACT:** The output of tidal hydraulics modeling results detailed in Appendix D of the draft EIR were re-evaluated to consider potential project impacts on areas outside the project boundaries, specifically Nestor Creek and the upper reach of the Otay River intertidal zone up-river from the Bayshore Bikeway Bridge. Based on comparisons of hydroperiod functions pre- and post-project, it is concluded that either restoration alternative under the ORERP (the *Intertidal* or *Subtidal Alternatives*) have a negligible effect on tidal inundation in the upper reach of the Otay River; and result in a slight reduction of tidal muting and improvement in high water tidal inundation of Nestor Creek.

**1.0) Introduction:** This technical note is a response to the following comment (4.3.1) on the draft EIR for the Otay River Estuary Restoration Plan (ORERP) that was made by the U.S. Army Corps of Engineers (USACE).

*4.3.1 Impacts on Habitat and Vegetation Communities; direct impacts; Habitat and Vegetation Communities/Jurisdictional Waters; What about the indirect impacts to Nestor Creek or the Otay River based on altering the elevations and hydrology near these areas? Will there be a hydrologic change that could alter the functioning of waters?*

Responses to this comment are based on numerical tidal hydraulics modeling in the existing Otay River floodplain and on modeling of the tidal exchange in the floodplain after construction of either of two restoration alternatives for the ORERP, namely: *The Intertidal Plan*, and *The Subtidal Plan*. The details of the tidal hydraulics modeling are found in Appendix-D of the draft EIR. Appendix-D is entitled, “Tidal Hydraulics Analysis of the Otay River Estuary Restoration Plan,” 113 pp. Because Nestor Creek and the intertidal reaches of the upper Otay River floodplain are outside the project boundaries of the ORERP, the discussion in the EIR Appendix-D did not explicitly discuss tidal exchange in these areas, although Nestor Creek and the upper Otay River were both included in the model domain. In the following sections we will re-visit those outer reaches of the model domain and elaborate on tidal exchange in the Nestor Creek and the intertidal reaches of the upper Otay River floodplain to provide a quantitative response to the USACE comment (4.3.1).

**2.0) Review of Methodology:** The EIR tidal hydraulics analysis (Appendix-D) employed a well-tested and peer-reviewed hydrodynamic model (TIDE\_FEM) to evaluate the tidal hydraulics of both the existing Otay River floodplain as well as the Intertidal Alternative and the Subtidal Alternative for the Otay River Estuary Restoration Project (ORERP). The model, analysis methods, and supporting data bases used were the same as those utilized in the Environmental Impact Report/Environmental Impact Statement (EIR/EIS) for the San Dieguito Wetland Restoration Project, (EIR/EIS, 2000), and for the preparation of the San Dieguito Wetlands Restoration Project, Final Restoration Plan, (SCE, 2005). The analysis of the existing Otay River floodplain was based on updated bathymetry provided by Wetlands Research Associates (WRA) and latest updates to San Diego Bay tides for the 1983-2001 tidal epoch after spectrally

correcting that record to the mouth of the Otay River using tidal elevation measurements from the Otay River Sonde. The TIDE\_FEM computer model used in this study are 2-dimensional finite element types, built from some well-studied and proven computational methods and numerical architecture that have been successful in predicting shallow water tidal propagation. Monitoring data for the newly completed San Dieguito Lagoon Restoration Project was used to calibrate the TIDE\_FEM tidal hydraulics model. San Dieguito Lagoon was selected as a calibration proxy for the restoration alternatives because of morphologic similarities: in particular, both the San Dieguito and restoration sites have a long “goose-neck” feeder channel connecting source water to interior tidal basins of comparable acreage and distance from the source water. Habitat surveys conducted during the San Dieguito Lagoon Restoration Project by Josselyn & Whelchel (1999), and then later updated by vegetation surveys in the lower Otay River flood plain by Josselyn (2012), were used to develop functional relationships between habitat breaks and amounts of time for wetting and drying (hydroperiod functions). The hydroperiod functions were calculated by the model for both present and future extremes of sea level in the year 2050 from estimates of both maximum and minimum sea level rise. These relationships were used to transpose tidal hydraulics model output into calculations of acreage of various wetland habitat types created by the two restoration alternatives.

### **3.0) Existing Conditions, Nestor Creek and Upper Otay River Intertidal Zone:**

The TIDE\_FEM bathymetric computational mesh was initialized for the updated Otay River Floodplain bathymetry derived from the 2011 WRA precision GPS surveys (Figure 1). The TIDE\_FEM computational mesh is nested in the farfield of south San Diego Bay, and was subjected to 30 years of historic tidal forcing using the 1980-2009 period of record at the Navy Pier in San Diego Bay, after spectrally correcting that record to the mouth of the Otay River as detailed in Section 3.2 of Appendix-D of the draft EIR. For the purposes of the present analysis, we select six nodal points in the computational mesh to serve as control points for evaluating the hydroperiod functions both pre- and post-project in Nestor Creek and the intertidal zone of the Otay River. These control points are shown by the stars in Figure 1, all of which are located upriver from the Bayshore Bikeway Bridge and feeder channel to the proposed Floodplain Basin of the ORERP.

Peak flooding currents during spring tides (using 18 September 2009 as a proxy) were simulated in the existing river channel in Figure 2, while ebbing currents during spring tides are found in Figure 3. These progressive vector diagrams show that flooding spring tidal currents are about 0.1 m/sec (0.33 ft/sec) at the river mouth and then accelerate to 0.18 m/sec (0.59 ft/sec) in the deeper sections of the inlet channel (north/south reach of the Otay River adjacent Ponds 10 and 11). Further upriver, currents reach 0.15 m/sec (0.50 ft/sec) in the narrower east/west reach near the railroad bridge. Flood tide currents then decelerate to less than 0.01 m/sec (0.03 ft/sec) into the complex dendritic system of channels in the upper reaches of the intertidal zone of the Otay River and Nestor Creek. During ebb spring tides, Figure 3 shows that Nestor Creek completely drains while limited tidal inundation remains in the shallow SW to NE subtidal reach of the upper Otay River floodplain immediately upriver from the Bayshore Bikeway Bridge.

The hydroperiod function is derived from large numbers of simulations like those in Figures 2 and 3 to find the percentage of exposure for each elevation potentially subjected to tidal inundation throughout the full range of South Bay water level variation. The hydroperiod function is used to discriminate pre- and post-project changes in the tidal inundation of the upper

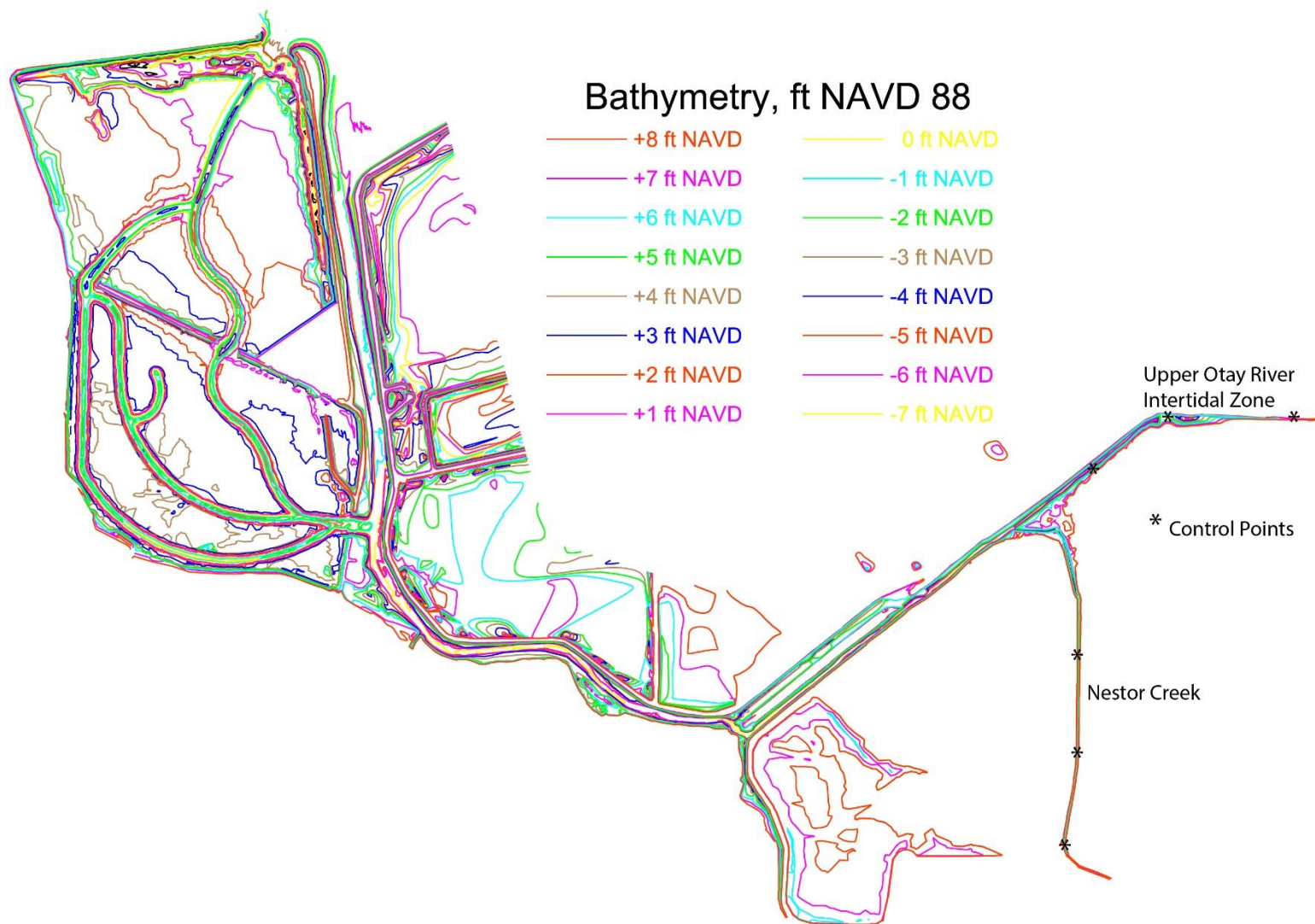


**Figure 1:** The updated Otay River Floodplain bathymetry derived from the WRA (2011) precision GPS survey. Control points for evaluating tidal exchange pre- and post-project in Nestor Creek and the tidally influenced upper Otay River are designated by stars.

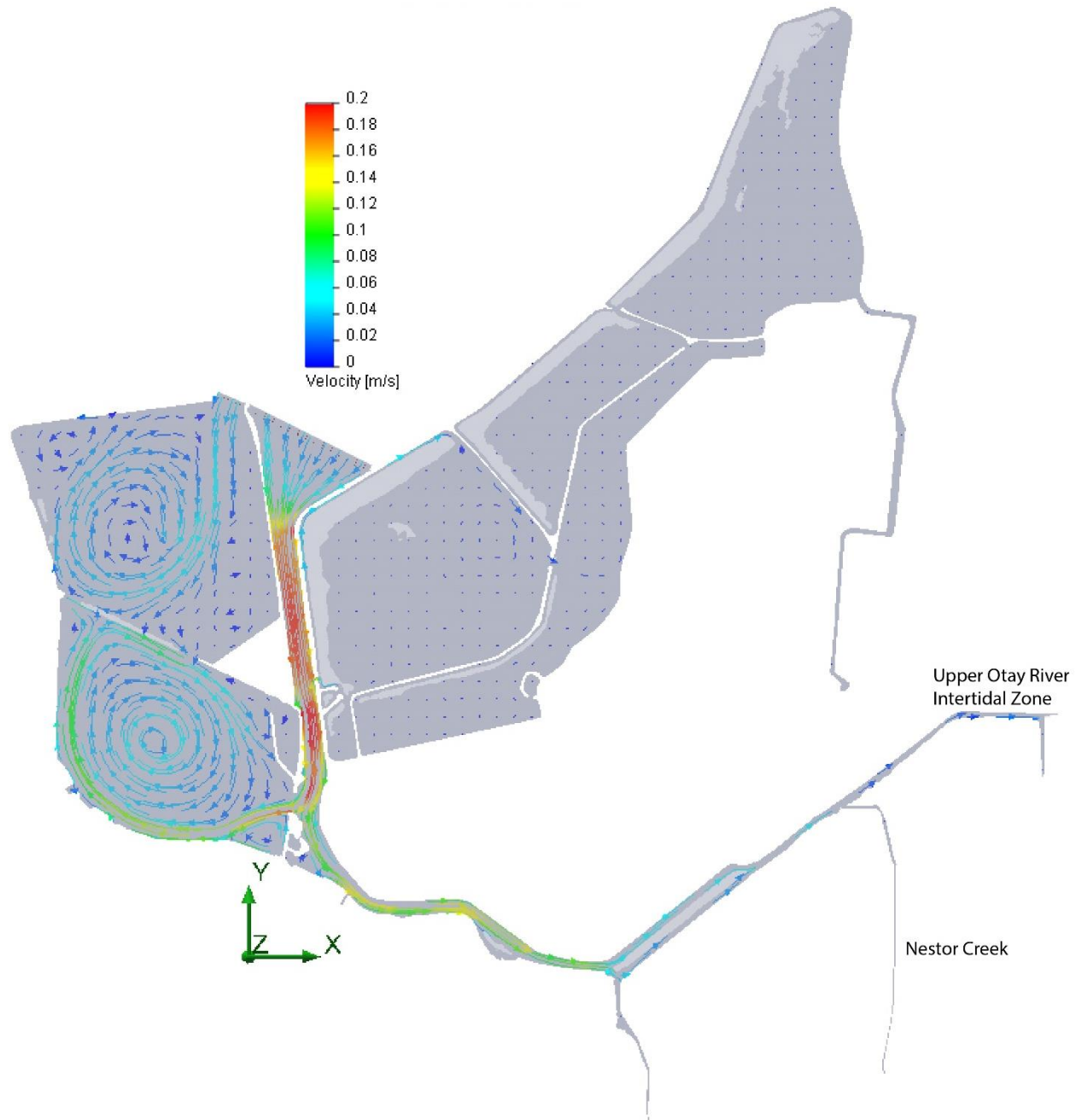


**Figure 2:** Hydrodynamic simulation of progressive vector flow distribution at 30 min time integration during maximum flood flow during spring tides for the existing lower Otay River and salt pond system based on 2011 WRA bathymetric survey and the 1983-2001 tidal epoch for San Diego Bay tides.

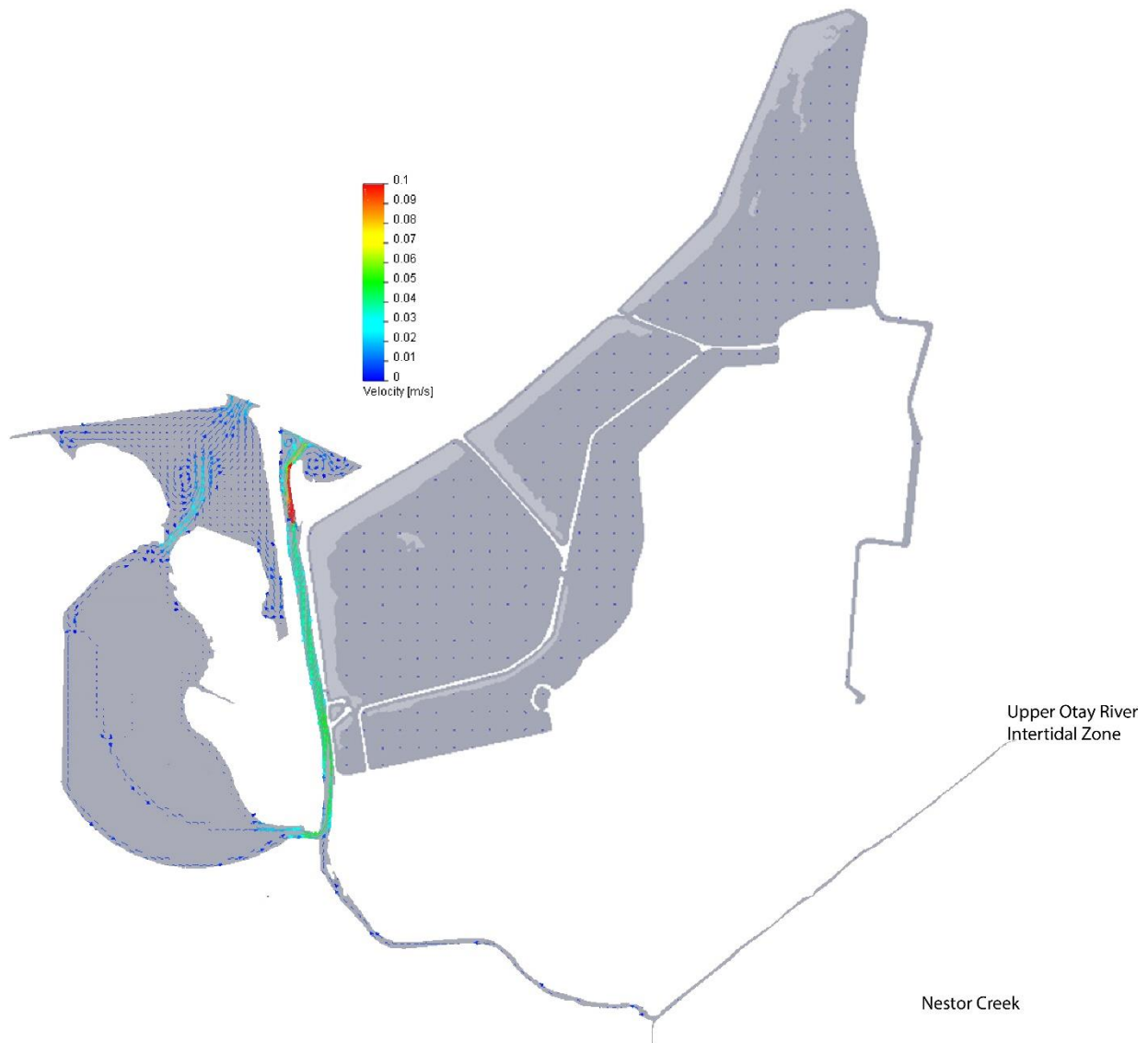


**Figure 3:** Hydrodynamic simulation of progressive vector flow distribution at 30 min time integration during maximum ebb flow during spring tides for the existing lower Otay River and salt pond system based on 2011 WRA bathymetric survey and the 1983-2001 tidal epoch for San Diego Bay tides.

Otay River and Nestor Creek. The computations involved  $N_o = 2,629,800$  time steps, each 6 minutes in length, in order to sweep the 30 year period of record of San Diego Bay water levels spectrally corrected to the mouth of the Otay River. At each time step the water elevations at the control points in Figure 1,  $\hat{\eta}$ , were calculated. Conditional if statements and counting loops inserted into the TIDE\_FEM code would count the number time steps,  $N$ , for which the average lagoon water elevation was less than a particular elevation,  $Z_i$ . The percent time that elevation  $Z_i$  was exposed over the period of record was calculated as:

$$E_i = \frac{100\%}{N_o} \sum N(\hat{\eta} < Z_i) \quad (1)$$

Equation (1) gives the hydroperiod function at each control point in Figure 1. These are ensemble averaged and the elevations divided among the various sub-tidal and intertidal habitat types based on biological the surveys biological surveys discussed in Section 2 above. The various degrees of exposure for each of these habitat types were determined to be:

**TABLE 1:** Exposure Levels for Hydroperiod Habitat Breaks

<b>Subtidal Exposure</b> < 0%;
0% < <b>Frequently Flooded Mud Flat Exposure</b> < 38%
38% < <b>Frequently Exposed Mud Flat Exposure</b> < 45%;
45% < <b>Low Salt Marsh Exposure</b> < 75%
75% < <b>Mid Salt Marsh Exposure</b> < 95%
95% < <b>High Salt Marsh Exposure</b> < 99.6%
99.6% < <b>Transitional Exposure</b> < 100%

Figure 4 below gives the hydroperiod functions that were determined by this analysis for the existing upper and lower reaches of the Otay River flood plain, and for Nestor Creek. Here the lower reach of the Otay River extends from the mouth of the Otay River to the Bayshore Bikeway Bridge, site of the legacy railroad bridge where the inlet to the feeder channel of the proposed ORERP Floodplain Basin is located. The upper reach extends from the Bayshore Bikeway Bridge upriver to the furthest point of high water tidal inundation. Comparing the black and red curves in Figure 4 reveals a small degree of high-water tidal muting occurs in the upper reaches in the existing Otay River relative to the lower reach; with extreme high water inundation (EHW) in the upper reach occurring at +7.45 ft NAVD 88, or about 0.25 ft lower than in the lower reach below the Bayshore Bikeway Bridge. Close inspection of Figure 1 reveals that this is attributable to hydraulic control exerted by the Bayshore Bikeway Bridge, whose abutments and channel hardening create a choke point with an associated complex sand bars immediately up-river from Bayshore Bikeway Bridge. These bars create a sill at 0.0 ft NAVD 88 which also limits drainage of the upper reach. Consequently, intertidal habitat in the upper reach does not extend below 0.0 ft NAVD under existing conditions; whereas in the lower reach, intertidal mud flat resides below – 0.0 ft NAVD and subtidal habitat below -1.01 ft NAVD. High water tidal inundation in Nestor Creek is further muted with EHW reaching only 7.0 ft NAVD 88 under existing conditions. This muting begins with the choke point and sand bars at

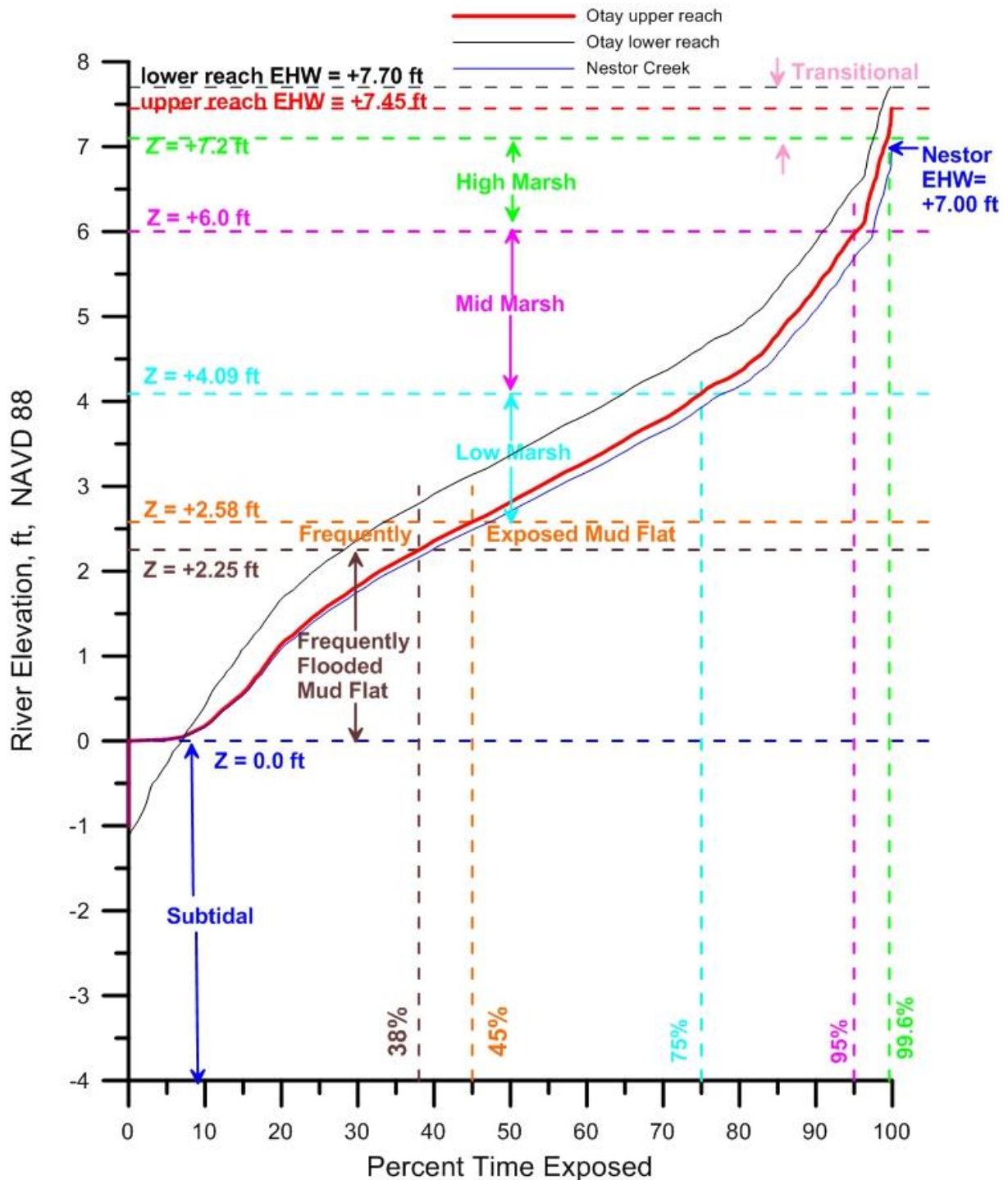


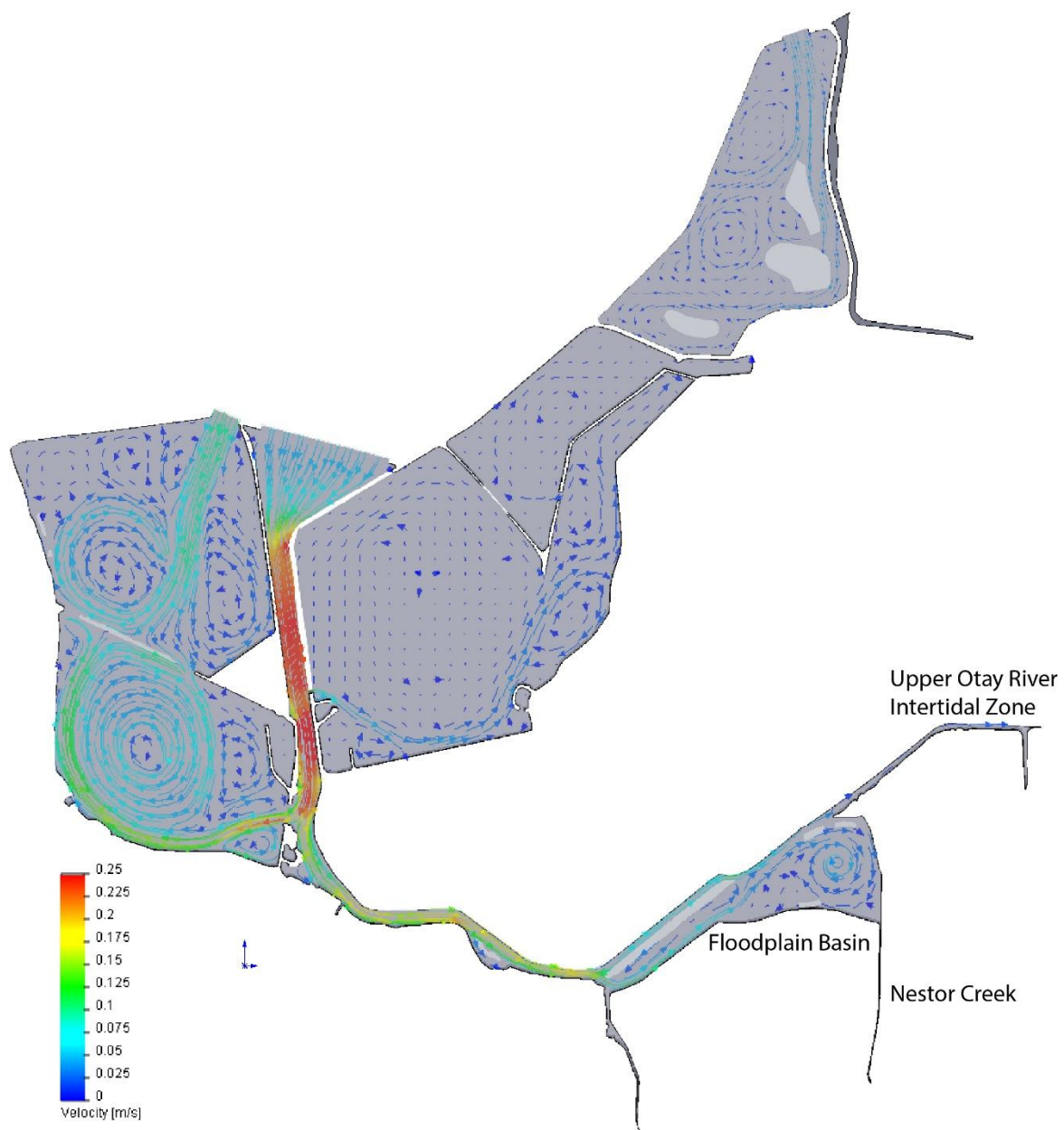
**Figure 4.** Hydroperiod functions of the existing Otay River lower reach (black), existing Otay River upper reach (red), and existing Nestor Creek (blue) based on WRA 2011 bathymetric survey applied to water level data from NOAA tide gage #941-0170, for tidal epoch 1983-2001, with spectral correction from Otay River Sonde. Mannings roughness:  $n_0 = 0.0261$

the Bayshore Bikeway Bridge and is further exacerbated by the narrow, shallow channel of Nestor Creek which does not extend below 0.0 ft NAVD 88 under existing conditions and is as high as + 1.0 ft NAVD 88 in its backwater reaches. Consequently Nestor Creek completely drains during most ebb tide cycles.

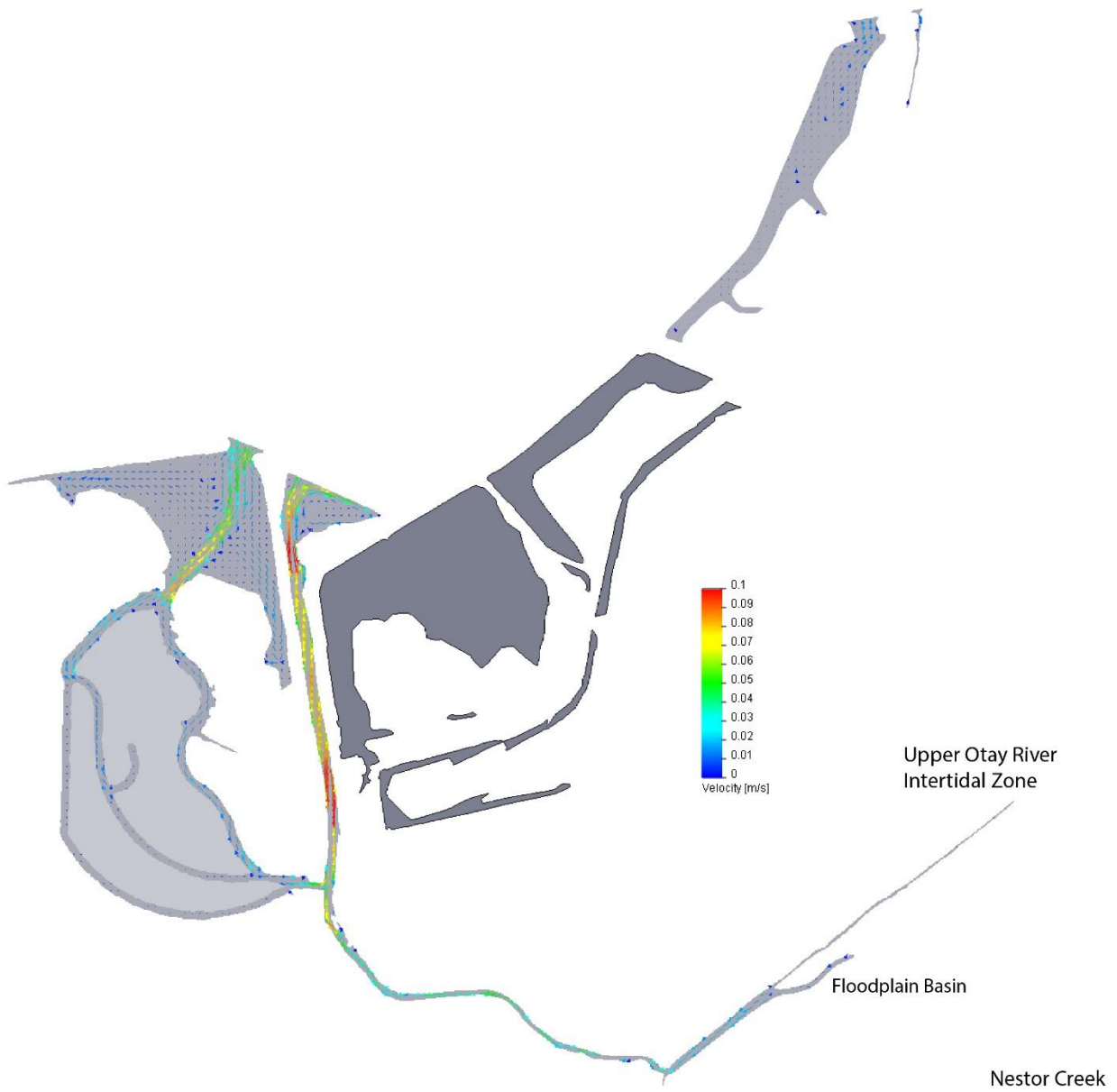
#### **4.0) Post-Project Conditions, Nestor Creek and Upper Otay River Intertidal Zone:**

Figure 5 gives the flow trajectories and depth averaged tidal currents for the Intertidal Alternative computed by the calibrated TIDE\_FEM model during spring flooding tides, using 18 September 2009 as a proxy. Velocities of tidal currents are portrayed according to the color coded velocity scale appearing in the lower left corner of the figure. Maximum flooding spring tidal currents at the mouth of the Otay River (in the neighborhood of the Otay Sonde) are about 0.10 m/sec (0.33 ft/sec), and then accelerate in the narrower north/south reach of the channel adjacent to Ponds 10 & 11 to 0.2 m/sec (0.66 ft/sec) where the channel has scoured under existing conditions to equilibrium depths on the order of -2.0 ft NAVD. After passing Pond 10, currents decelerate and then increase to 0.17 m/sec (0.55 ft/sec) near the choke point at the Bayshore Bikeway Bridge, before entering the floodplain tidal basin; where tidal currents entering the tidal basin initially form a well-defined jet at the west bank with speeds of about 0.08 m/s (0.26 ft/sec). This entry jet quickly diverges into a complex set of clockwise rotating eddies that populate the interior of the tidal basin. Eddy speeds in the tidal basin are on the order of 0.02 m/sec (0.07 ft/sec), insufficient to transport fine sand but an important stirring mechanism for mixing the tidal basin water mass to maintain high oxygen levels and to sustain fine silt and clay sized sediment particles in suspension. The lower reach of Nestor Creek has been incorporated along the east bank of the Floodplain Basin, thereby widening the channel cross section of Nestor Creek by a factor of 35 to 52; while the upper reach extends beyond of the southeast corner of the Floodplain Basin. The high water footprint of the upper reach of Nestor Creek under the Intertidal Alternative in Figure 5 appears larger relative to existing conditions in Figure 2, suggesting an improvement in high water tidal inundation under post-project conditions. On the other hand, the high water footprint of the upper reach of the Otay River intertidal zone under the Intertidal Alternative in Figure 5 appears about the same as existing conditions in Figure 2. In the lower reach of the Otay River, flood tide currents are swifter post-project than existing conditions, but generally remain below the threshold scour speeds for the native sediments, based on estimates from the Hjulstrom Curve.

Figure 6 gives the flow trajectories and depth averaged tidal currents for the Intertidal Alternative computed by the TIDE\_FEM model during spring ebbing tides on 18 September 2009. The wetted area of the floodplain tidal basin is significantly reduced relative to the flood tide area in Figure 28, due to the fact that the grading plan allows for almost complete drainage at mean low water tidal stages. In Figure 6, creeping flow drains from the remnant dendritic channel of the floodplain basin, forming a feeder current in the upper river channel with speeds on the order of -0.01 m/sec, or (-0.03 ft/sec). This feeder current evacuates the tidal basin and then accelerates to -0.05 m/sec (-0.16 ft/sec) as it passes through the pinch point under the railroad bridge in the narrow east/west reach of channel. (We adopt the convention of negative velocities for ebb tide flows and positive velocities for flood tide flows). Ebb flow in the channel then accelerates further to -0.09 m/sec (-0.289 ft/sec) in the deeper north/south reach before discharging into San Diego Bay. Again, ebb tide currents in the lower reach of the Otay River, are swifter post-project than existing conditions, but generally remain below the threshold scour



**Figure 5:** Intertidal Alternative flood tide progressive vector flow simulation at Mean High Water (MHW), where vector trajectories are plotted over 30 minute time integrations.

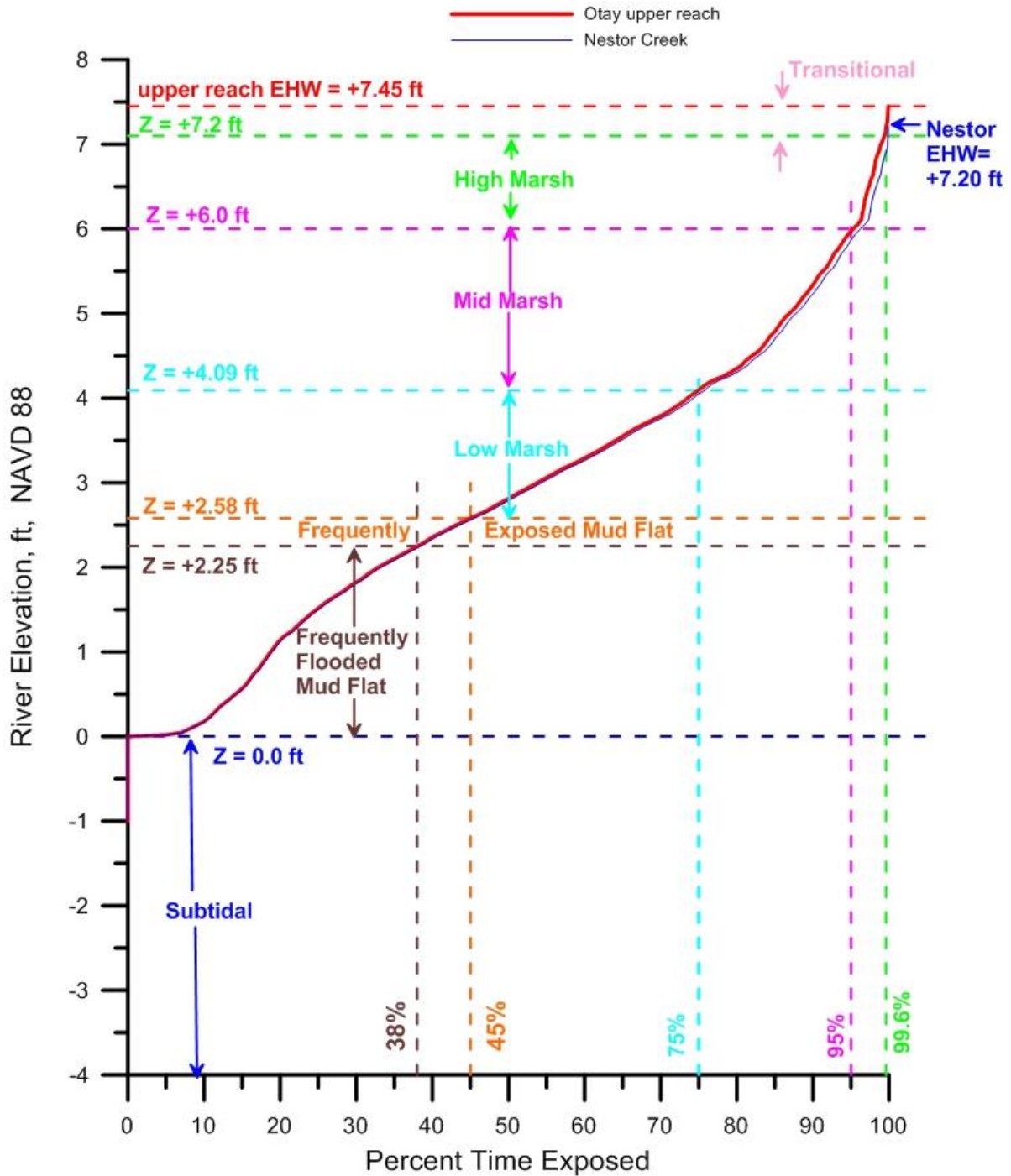


**Figure 6:** Intertidal Alternative ebb tide progressive vector flow simulation at Mean Low Water (MLW), where vector trajectories are plotted over 30 minute time integrations.

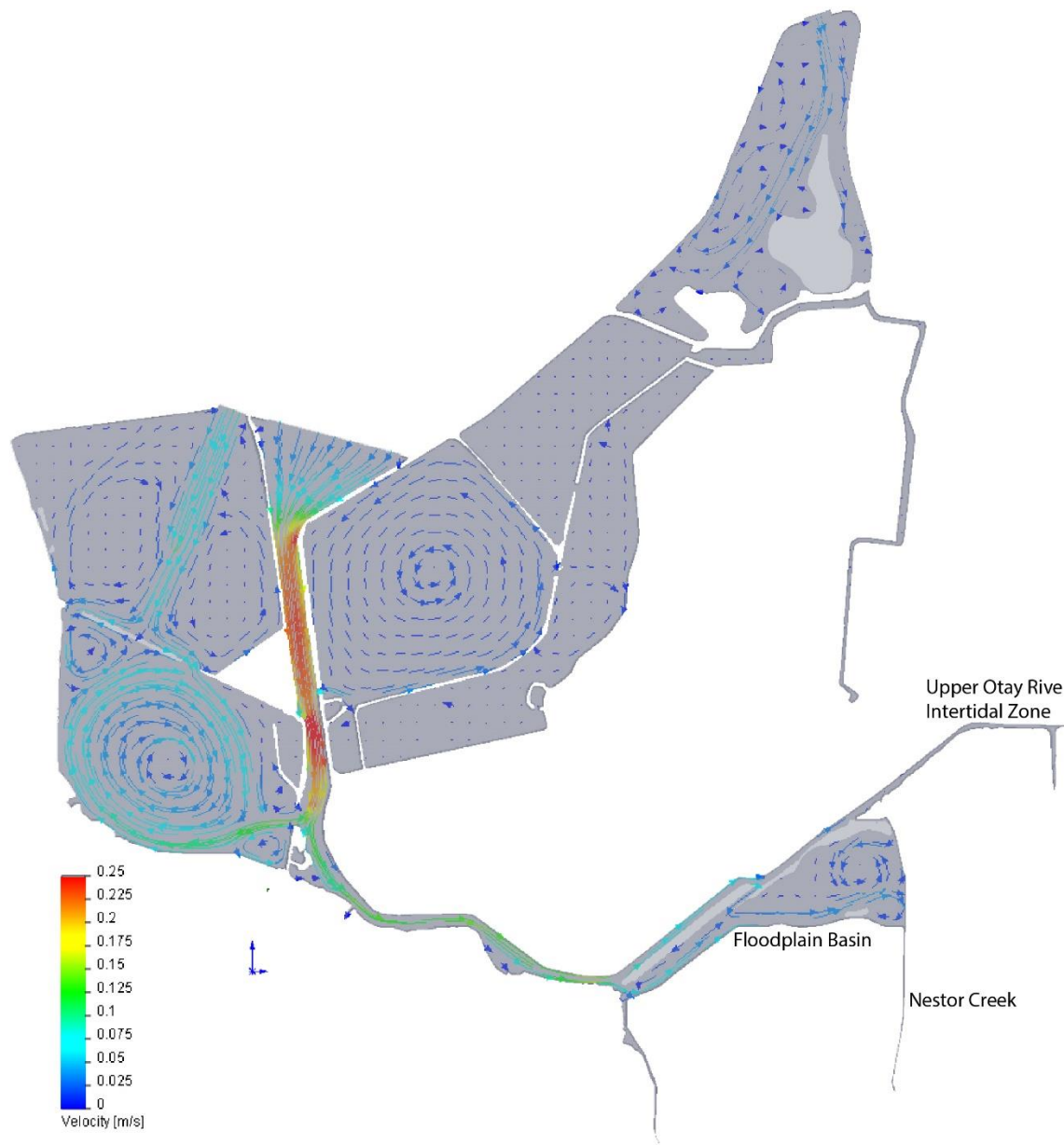
speeds for the native sediments, based on estimates from the Hjulstrom Curve. The low water footprint of Nestor Creek under the Intertidal Alternative in Figure 6 is completely vacated, the same as for existing conditions in Figure 3. The low water footprint of the upper reach of the Otay River under the Intertidal Alternative in Figure 6 is about the same as for existing conditions in Figure 3, other than for a slight widening at the merge with the feeder channel for the Floodplain Basin.

Figure 7 gives the hydroperiod functions for the upper Otay River intertidal zone and for Nestor Creek under the post-project conditions for the ORERP Intertidal Alternative, as calculated by the procedures reviewed in Section 3. At the resolution of the model, the hydroperiod function for the upper reach of the Otay River in Figure 7 is unchanged from that reported for existing conditions in Figure 4, where both pre- and post-project tidal inundation produce the same extreme high water levels at 7.45 ft. NAVD 88, and both have the same habitat zonations and basement levels of intertidal habitat at 0.0 ft NAVD 88. The reason for this is that hydraulic control for both pre- and post-project conditions in the upper reach is established by the choke point at the Bayshore Bikeway Bridge, a feature that is unchanged by post-project conditions, at least within the rigid-boundary approximations of the TIDE\_FEM model. On the other hand, the hydroperiod function for the Nestor Creek in Figure 7 reveals a small degree of reduction in high-tide muting as a result of the Intertidal Alternative, with post project EHW reaching 7.2 ft NAVD 88, or about 0.2 ft higher salt water inundation than existing conditions. The reason for this reduction in the high tide muting of Nestor Creek is that the post project conditions significantly increase its channel cross section, and thereby reduce the frictional damping of high water tidal elevations in Nestor Creek. Both pre- and post-project tidal inundation produce the same basement levels of intertidal habitat at 0.0 ft NAVD 88, while the post-project conditions increase the zonation elevation band for high marsh by about 0.3 ft.

Figure 8 gives the flow trajectories and depth averaged tidal currents for the Subtidal Alternative computed by the calibrated TIDE\_FEM model during spring flooding tides, using 18 September 2009 as a proxy. Velocities of tidal currents are portrayed according to the color coded velocity scale appearing in the lower left corner of the figure. Maximum flooding spring tidal currents at the mouth of the Otay River (in the neighborhood of the Otay Sonde) are about 0.10 m/sec (0.33 ft/sec), and then accelerate in the narrower north/south reach of the channel adjacent to Ponds 10 & 11 to 0.2 m/sec (0.66 ft/sec) where the channel has scoured under existing conditions to equilibrium depths on the order of -2.0 ft NAVD. After passing Pond 10, currents decelerate and then increase to 0.17 m/sec (0.55 ft/sec) near the choke point at the Bayshore Bikeway Bridge, before entering the floodplain tidal basin; where tidal currents entering the tidal basin initially form a well-defined jet at the west bank with speeds of about 0.08 m/s (0.26 ft/sec). This entry jet quickly diverges into a complex set of clockwise rotating eddies that populate the interior of the tidal basin. Eddy speeds in the tidal basin are on the order of 0.02 m/sec (0.07 ft/sec), insufficient to transport fine sand but an important stirring mechanism for mixing the tidal basin water mass to maintain high oxygen levels and to sustain fine silt and clay sized sediment particles in suspension. The lower reach of Nestor Creek has been incorporated along the east bank of the Floodplain Basin, thereby widening the channel cross section of Nestor Creek by a factor of 35 to 52; while the upper reach extends beyond of the southeast corner of the Floodplain Basin. The high water footprint of the upper reach of Nestor Creek under the Subtidal Alternative in Figure 8 appears larger relative to existing conditions in Figure 2, suggesting an improvement in high water tidal inundation under post-project conditions. On the other hand, the high water footprint of the upper reach of the Otay



**Figure 7.** Post-project hydroperiod functions of the Otay River upper reach (red) and Nestor Creek (blue) for the ORERP Intertidal Alternative based on WRA 2011 bathymetric survey applied to water level data from NOAA tide gage #941-0170, for tidal epoch 1983-2001, with spectral correction from Otay River Sonde. Mannings roughness:  $n_0 = 0.0261$

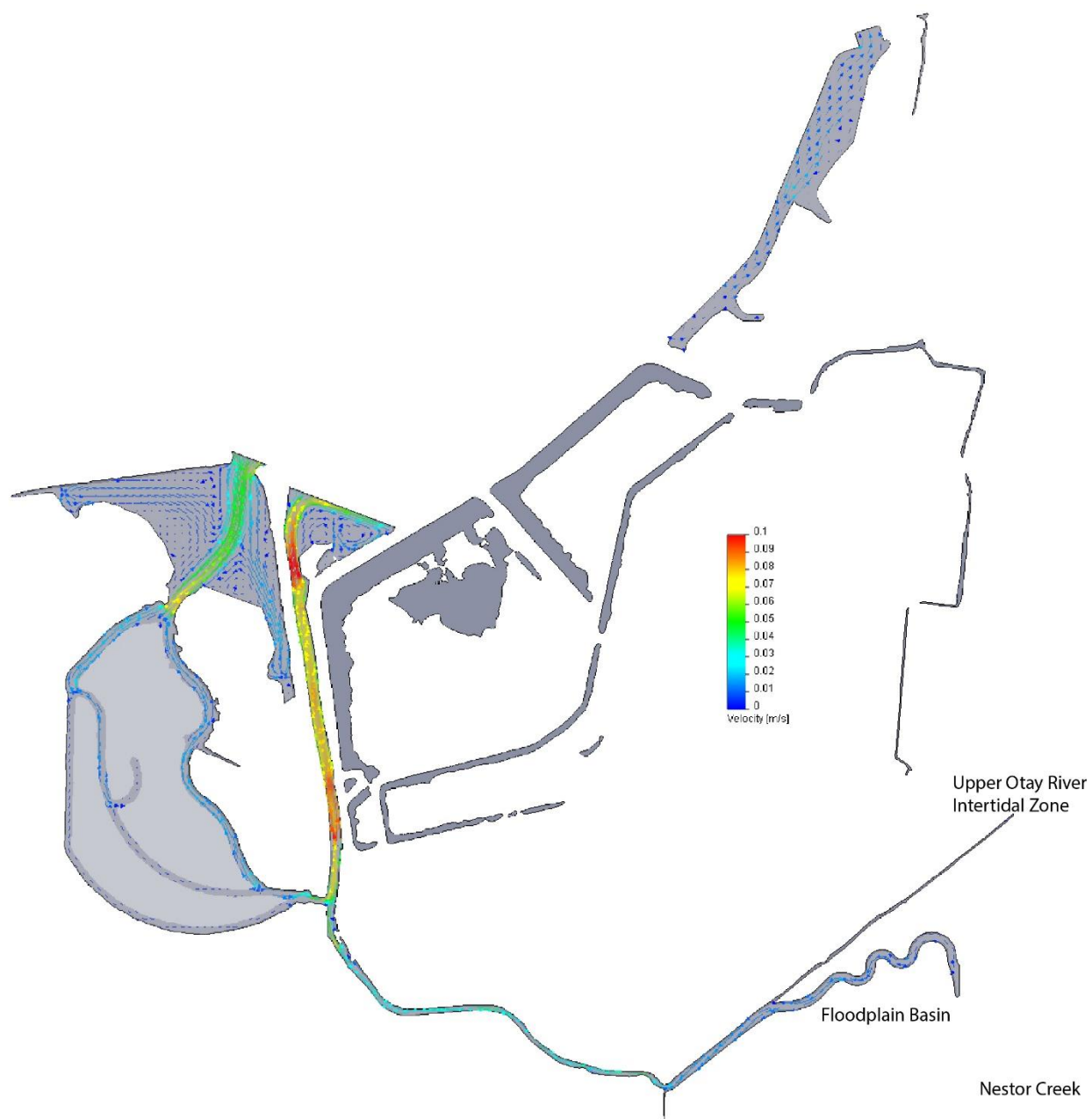


**Figure 8:** Subtidal Alternative flood tide progressive vector flow simulation at Mean High Water (MHW), where vector trajectories are plotted over 30 minute time integrations.

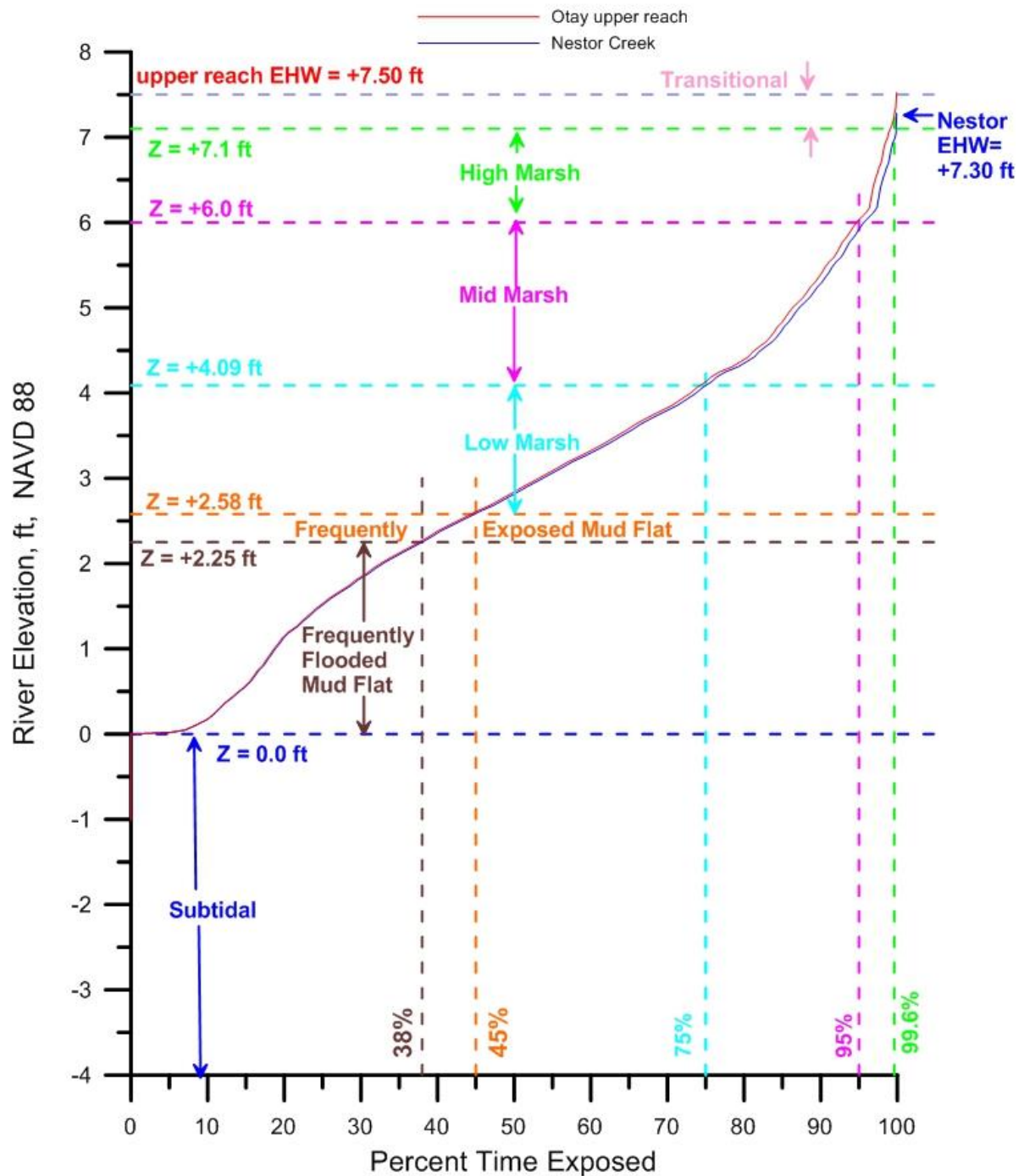
River intertidal zone under the Subtidal Alternative in Figure 8 appears about the same as existing conditions in Figure 2. In the lower reach of the Otay River, flood tide currents are swifter post-project than existing conditions, but generally remain below the threshold scour speeds for the native sediments, based on estimates from the Hjulstrom Curve.

Figure 9 gives the flow trajectories and depth averaged tidal currents for the Subtidal Alternative computed by the TIDE\_FEM model during spring ebbing tides on 18 September 2009. The wetted area of the floodplain tidal basin is significantly reduced relative to the flood tide area in Figure 9, due to the fact that the grading plan allows for almost complete drainage at mean low water tidal stages. In Figure 9, creeping flow drains from the remnant dendritic channel of the floodplain basin, forming a feeder current in the upper river channel with speeds on the order of -0.01 m/sec, or (-0.03 ft/sec). This feeder current evacuates the tidal basin and then accelerates to -0.05 m/sec (-0.16 ft/sec) as it passes through the pinch point under the railroad bridge in the narrow east/west reach of channel. (We adopt the convention of negative velocities for ebb tide flows and positive velocities for flood tide flows). Ebb flow in the channel then accelerates further to -0.09 m/sec (-0.289 ft/sec) in the deeper north/south reach before discharging into San Diego Bay. Again, ebb tide currents in the lower reach of the Otay River, are swifter post-project than existing conditions, but generally remain below the threshold scour speeds for the native sediments, based on estimates from the Hjulstrom Curve. The low water footprint of Nestor Creek under the Subtidal Alternative in Figure 9 is completely vacated, the same as for existing conditions in Figure 3. The low water footprint of the upper reach of the Otay River under the Subtidal Alternative in Figure 9 is about the same as for existing conditions in Figure 3, other than for a slight widening at the merge with the feeder channel for the Floodplain Basin.

Figures 8 and 9 indicate that flood and ebb velocities and inundation footprints in the Otay River and Floodplain Basin for the Subtidal Alternative are about the same as for the Intertidal Alternative in Figures 5 and 6. This is due to the fact that there is very little difference in the grading designs for the two alternatives, and neither alternative involves any dredging of the existing Otay River channel. The only difference in grading design is that the Subtidal Alternative has a subtidal channel graded down to -2.0 ft NAVD, but the tidal prisms of the two alternatives is about the same; 100 acre-ft. for the Subtidal Alternative as compared to 98 acre-ft. for the Intertidal Alternative. Consequently the hydroperiod functions for the upper Otay River intertidal zone and for Nestor Creek under the post-project conditions for the ORERP Subtidal Alternative in Figure 10 are essentially the same as those for the Intertidal Alternative in Figure 7. Under the Subtidal Alternative, the hydroperiod function for the upper reach of the Otay River in Figure 10 is unchanged from that reported for existing conditions in Figure 4, where both pre- and post-project tidal inundation produce the same extreme high water levels at 7.45 ft. NAVD 88, and both have the same habitat zonations and basement levels of intertidal habitat at 0.0 ft NAVD 88. Again, the reason for this is that hydraulic control for both pre- and post-project conditions in the upper reach is established by the choke point at the Bayshore Bikeway Bridge, a feature that is unchanged by post-project conditions. On the other hand, the hydroperiod function for the Nestor Creek in Figure 10 reveals a small degree of reduction in high-tide muting as a result of the Subtidal Alternative, with post project EHW reaching 7.2 ft NAVD 88, or about 0.2 ft higher salt water inundation than existing conditions. The reason for this reduction in the high tide muting of Nestor Creek is that the post project conditions significantly increase its channel cross section, and thereby reduce the frictional damping of high water tidal elevations in Nestor Creek. Both pre- and post-project tidal inundation produce the same basement levels of



**Figure 9:** Subtidal Alternative ebb tide progressive vector flow simulation at Mean Low Water (MLW), where vector trajectories are plotted over 30 minute time integrations.



**Figure 10.** Post-project hydroperiod functions of the Otay River upper reach (red) and Nestor Creek (blue) for the ORERP Subtidal Alternative based on WRA 2011 bathymetric survey applied to water level data from NOAA tide gage #941-0170, for tidal epoch 1983-2001, with spectral correction from Otay River Sonde. Mannings roughness:  $n_0 = 0.0261$

intertidal habitat at 0.0 ft NAVD 88, while the post-project conditions increase the zonation elevation band for high marsh by about 0.3 ft.

## **5.0) References:**

- Jenkins, S. A. & J. Wasyl, 1998, Analysis of Coastal Processes Effects due to the San Dieguito Lagoon Restoration Project: Final Report, submitted to *Southern California Edison Co.*, 333 pp.
- Jenkins, S. A. & D. L. Inman, 1999, "Sand transport mechanics for equilibrium tidal inlets," *Shore & Beach* (Magoon Volume, Jan 99), v. 67, n. 1, p. 53–58.
- Jenkins, S. A., M. Josselyn & J. Wasyl, 1999, Hydroperiod and Residence Time Functions for Habitat Mapping of Restoration Alternatives for San Dieguito Lagoon, submitted to *Southern California Edison Co.*, 30 pp. + 1 appen.
- Jenkins, S. A. and J. Wasyl, 2005, "Coastal evolution model," Scripps Institution of Oceanography Tech. Rpt. No. 58, 179 pp. + appendices.  
<http://repositories.cdlib.org/sio/techreport/58/>
- Jenkins, S. A., and J. Wasyl, 2014, "Tidal Hydraulics Analysis of the Otay River Estuary Restoration Plan," submitted to Poseidon Water LLC, 113 pp.
- Josselyn, M. & A. Whelchel, 1999, Determining the Upper Extent of Tidal Marsh Habitat San Dieguito Lagoon, submitted to *Southern California Edison Co.*, 16 pp.
- Josselyn, M., 2012, "TECHNICAL MEMORANDUM ELEVATIONS OF INTERTIDAL VEGETATION PROJECTIONS FOR ORERP" WRA, submitted Poseidon Resources, Corp, 17 February, 2012, 5pp.

